**Experimental Astronomy manuscript No.**
(will be inserted by the editor)

# Herschel celestial calibration sources

## Four large main-belt asteroids as prime flux calibrators for the far-IR/sub-mm range

**Thomas Müller · Zoltán Balog · Markus Nielbock · Tanya Lim · David Teyssier · Michael Olberg · Ulrich Klaas · Hendrik Linz · Bruno Altieri · Chris Pearson · George Bendo · Esa Vilenius**

Received: date / Accepted: date

**Abstract** Celestial standards play a major role in observational astrophysics. They are needed to characterise the performance of instruments and are paramount for photometric calibration. During the Herschel Calibration Asteroid Preparatory Programme approximately 50 asteroids have been established as far-IR/sub-mm/mm calibrators for Herschel. The selected asteroids fill the flux gap between the sub-mm/mm calibrators Mars, Uranus and Neptune, and the mid-IR bright calibration stars. All three Herschel instruments observed asteroids for various calibration purposes, including pointing tests, absolute flux calibration, relative spectral response function, observing mode validation, and cross-calibration aspects. Here we present newly established models for the four large and well characterized main-belt asteroids (1) Ceres, (2) Pallas, (4) Vesta, and (21) Lutetia which can be considered as new prime flux calibrators. The relevant object-specific properties (size, shape, spin-properties, albedo, thermal properties) are well established. The seasonal (distance to

T. Müller, E. Vilenius
Max Planck Institute for Extraterrestrial Physics, PO Box 1312, Giessenbachstrasse, 85741 Garching, Germany
Tel.: +49 89 30000-3499
E-mail: tmueller@mpe.mpg.de

Z. Balog, M. Nielbock, U. Klaas, H. Linz
Max Planck Institute for Astronomy, Königstuhl 17, 69117 Heidelberg, Germany

T. Lim, C. Pearson
Space Science and Technology Department, RAL, Didcot, OX11 0QX, Oxon UK

D. Teyssier, B. Altieri
European Space Astronomy Centre (ESAC), ESA, Villanueva de la Cañada, 28691 Madrid, Spain

M. Olberg
Onsala Space Observatory, Chalmers University of Technology, 43992 Onsala, Sweden

G. Bendo
UK ALMA Regional Centre Node, Jodrell Bank Centre for Astrophysics, Manchester M13 9PL, United Kingdom

Sun, distance to observer, phase angle, aspect angle) and daily variations (rotation) are included in a new thermophysical model setup for these targets. The thermophysical model predictions agree within 5% with the available (and independently calibrated) Herschel measurements. The four objects cover the flux regime from just below 1,000 Jy (Ceres at mid-IR N-/Q-band) down to fluxes below 0.1 Jy (Lutetia at the longest wavelengths). Based on the comparison with PACS, SPIRE and HIFI measurements and pre-Herschel experience, the validity of these new prime calibrators ranges from mid-infrared to about 700 $\mu$m, connecting nicely the absolute stellar reference system in the mid-IR with the planet-based calibration at sub-mm/mm wavelengths.

**Keywords** Herschel Space Observatory · PACS · SPIRE · HIFI · Far-infrared · Instrumentation · Calibration · Celestial standards · Asteroids

## 1 Introduction

With the availability of the full thermal infrared (IR) wavelength range (from a few microns to the millimetre range) through balloon, airborne and spaceborne instruments, it became necessary to establish new calibration standards and to develop new calibration strategies. Instruments working at mm-/cm-wavelengths were mainly calibrated against the planets Mars, Uranus and Neptune (e.g., [22, 44, 62, 72, 21]), while the mid-IR range was always tied to stellar models (e.g., [67, 24, 11, 12, 19, 20, 66, 82, 14]). For the far-IR/sub-mm regime no optimal calibrators were available right from the beginning: the stars are often too faint for calibration aspects which require high signal-to-noise (S/N) ratios or are problematic in case of near-IR filter leaks[1]. The planets are very bright and not point-like anymore. They are causing saturation or detector non-linearity effects. Between these two types of calibrators there remained a gap of more than two orders of magnitude in flux. This gap was filled by sets of well-known and well-characterized asteroids and their corresponding model predictions (e.g., [3, 48, 50, 75, 26, 53]). Figure 1 shows the flux-wavelength regime covered by the three types of objects typically used for calibration purposes at far-IR/sub-mm/mm wavelength range.

The idea of using asteroids for calibration purposes goes back to IRAS [3]. The IRAS 12, 25 and 60 $\mu$m bands were calibrated via stellar models and in that way connected to groundbased N- and Q-band measurements. But at 100 $\mu$m neither stellar model extrapolations nor planet models were considered reliable. Asteroids solved the problem. Models for a selected sample of large main-belt asteroids were used to "transfer" the observed IRAS 60 $\mu$m fluxes out to 100 $\mu$m and calibrate in that way the IRAS 100 $\mu$m band [3].

There was an independent attempt to establish a set of secondary calibrators at sub-millimetre (sub-mm) wavelengths to fill the gap between stars and planets [71]. Ultra-Compact H-II regions, protostars, protoplanetary nebulae and AGB-stars were selected, but often these sources are embedded in dust clouds which produce a strong

[1] Near-IR filter leaks are photometrically problematic when near-IR bright objects -like stars- are observed in far-IR bands.

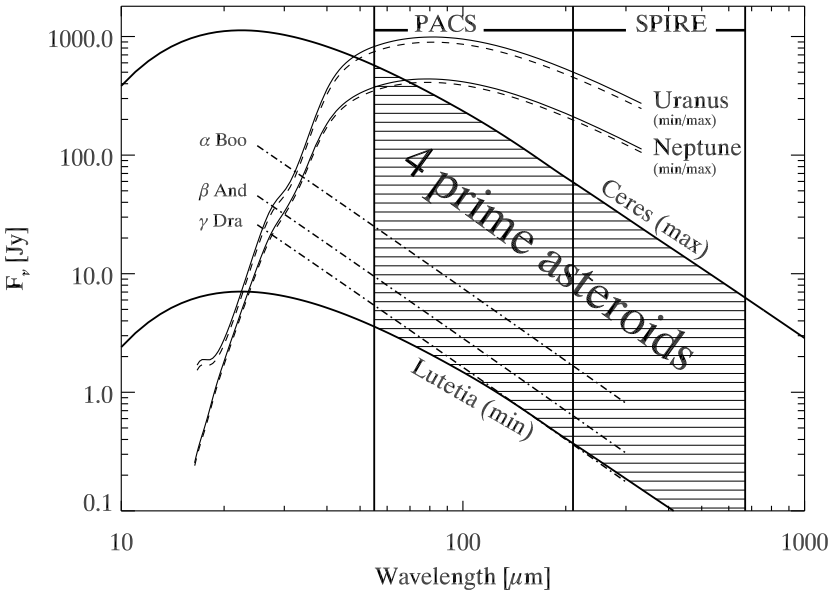


**Fig. 1** Overview with the flux densities of the different far-IR/sub-mm/mm calibrators. The Uranus and Neptune SEDs represent the minimum and maximum fluxes during Herschel visibility phases. Three fiducial stars are also shown, their flux coverage is representative for the brightest stellar calibrators. For Ceres and Lutetia we show the minimum and maximum fluxes during Herschel observations.

and sometimes variable background. The modeling proves to be difficult and accurate far-IR extrapolations are almost impossible.

The Infrared Space Observatory (ISO) [28] was also lacking reliable photometric standards at far-IR wavelength (50 - 250 $\mu$m) in the flux regime between the stars [24, 11, 12] and the planetary calibrators Uranus and Neptune [22, 62, 38, 29, 74]. Müller & Lagerros [46] provided a set of 10 asteroids, based on a previously developed thermophysical model code by Lagerros [32–34]. These sources have been extensively observed by ISO for the far-IR photometric calibration, for testing relative spectral response functions and for many technical instrument and satellite purposes.

AKARI [59] followed the same route to calibrate the Far-Infrared Surveyor (FIS) [26] via stars, asteroids and planets in the wavelengths regime 50 - 200 $\mu$m.

The Spitzer mission [81] considered in the beginning only stars for calibration purposes. But due to a near-IR filter leak of the MIPS [68] 160 $\mu$m band, the calibration scientists were forced to establish and verify calibration aspects by using cooler objects. The asteroids served as reference for the flux calibration of the 160 $\mu$m band as well as for testing the non-linear MIPS detector behaviour [75].

In preparation for Herschel [64] and ALMA[2] a dedicated asteroid programme was established [53]. This led to a sample of about 50 asteroids for various cali-

[2] `http://en.wikipedia.org/wiki/Atacama_Large_Millimeter_Array`

bration purposes. Along the mission only the 12 asteroids with the highest quality characterization were continued to be observed for calibration.

Here we present **the Herschel observations and the data reduction of all photometrically relevant asteroid measurements (Section 2). First, the asteroid instrumental fluxes in engineering units were converted to absolute fluxes using conversion factors derived from stellar calibrators (PACS), Neptune (SPIRE) and Mars (HIFI). Next, the absolute fluxes were corrected for differences in spectral energy distribution between the prime calibrator(s) and the asteroids to obtain mono-chromatic flux densities at predefined reference wavelengths. In Section 3 we document** recently updated asteroid models for Ceres, Pallas, Vesta, and Lutetia. The models are entirely based on physical and thermal properties taken from literature and derived from independent measurements, like occultation measurements, HST[3], adaptive optics, or **flyby missions**. We compare (Section 4) the absolute model predictions with all available photometric Herschel (PACS [65], SPIRE [23], HIFI [13]) measurements and discuss the validity and limitations. **The dispersion in the ratio of model to measured fluxes for the four asteroids determines the error in the calibration factor.** The conclusions are given in Section 5. It is important to note here that the derived Herschel flux densities of the asteroids were independently calibrated against 5 fiducial stars (PACS), the planet Neptune (SPIRE) and the planet Mars (HIFI). The asteroids are therefore also serving as unique cross-calibration objects between the different calibration concepts, the different instruments, observing modes, wavelengths- and flux regimes.

## 2 Observations & data reduction

### 2.1 PACS photometer observations

The Photodetector Array Camera and Spectrograph (PACS [65]) on board the Herschel Space Observatory [64] provides imaging and spectroscopy capabilities. Here, we only considered photometric measurements of the four asteroids, taken with the imaging bolometer arrays either at 70/160 $\mu$m (blue/red) or at 100/160 $\mu$m (green/red). Most of the observations were taken as part of calibration programmes, with the majority of the measurements taken in high gain and only a few in low gain. The observations have either been taken in scan-map mode or in chop-nod mode. The data were reduced in a standard way, following the steps defined in the officially recommended chop-nod and scan-map reduction scripts, described in more detail in [2,60], with flagging of bad and saturated pixels. The calibration was based on the latest versions of the bolometer response file (responsivity: FM,7) and the flat-fielding (flatField: FM,3). The non-linearity correction was needed, with correction of up to 6% for the highest asteroid fluxes. The bolometer signals were also corrected for the evaporator temperature effect (see [43]), with correction factors of -0.3% to 3.2%. Since the asteroids have apparent Herschel-centric motions of up to 80″/h, the frames were projected in an asteroid-centered (co-moving) reference frame for the final maps. We

[3] Hubble Space Telescope

used map pixel sizes of 1.1″, 1.4″, and 2.1″ at 70, 100, and 160 $\mu$m, respectively, to sample the point spread function in an optimal way.

*PACS bolometer scan-map observations.* The scan-map observations of the four prime asteroids are listed in Tables 2, 6, 9, 12 (observing mode 'PACS-SM'). They were obtained using the mini scan-map mode [1,57] with the telescope scanning at a speed of 20″/s along parallel legs of about 3′-4′ length. Typically 10 scan-legs, separated by a few arcseconds, have been taken. The scans were performed in such a way that the source was moving along the array diagonals (70° and 110° scan-angles in array coordinates) for optimized coverage and sensitivity. The data were reduced in a standard way (see above), with details about the masking, high-pass filtering, speed selection and deglitching of the data given in [2]. We constructed final images in the asteroid co-moving reference frame for each individual OBSID[4] and band. The combination of the scan and cross-scan observations was not necessary for our bright point-sources.

*PACS bolometer chop-nod observations.* The chop-nod observations of the four prime asteroids are listed in Tables 3, 7, 10, 13 (observing mode 'PACS-CN'). They were obtained using the point-source photometry Astronomical Observing Template (AOT) that is carried out by chopping and nodding in perpendicular directions and with amplitudes of 52″ (see [1,57,60] for further details). The data reduction included -in addition to what has been done for scan-maps- an adjustment for the apparent response drift and offset in this mode (see [60]) resulting in corrections of 4.3% to 7.6% for the four asteroids, depending on the time of the observation (before/after OD 300) and the band [60]. We produced final point-source maps in the asteroid co-moving reference frame.

*Aperture photometry.* We applied aperture photometry with radii of 12″ in blue/green and 22″ in red, centered on the source image in the final maps. Depending on the band, 78-82% of the source flux is inside these apertures (see [40]). The sky noise in scan-maps was determined in a sky annulus with inner and outer radii of 35″ and 45″, respectively (see [2]). The sky noise in the chop-nod images was taken from a sky annulus with inner/outer radii of 20″/25″ in the blue and green maps and 24″/28″ in red maps (see [60]). We performed colour corrections [56] of 1.00, 1.02[5], and 1.07 for the blue, green, and red band data to obtain monochromatic flux densities at the PACS key wavelength of 70.0, 100.0, and 160.0 $\mu$m, respectively[6]. These corrections were calculated on basis of model SEDs for the four asteroids and correspond roughly to the corrections for a 200-300 K black body. The absolute flux uncertainties were calculated by adding quadratically the measured sky noise (corrected for correlated noise, see [2]), 1% for the uncertainties in colour correction, and 5% for errors related to the fiducial star models which are the baseline for the absolute flux calibration of

[4] Herschel unique observation identifier

[5] The Vesta SED requires a colour correction value of 1.03 in the green band

[6] The PACS photometric calibration is based on the assumption of a constant energy spectrum of the observed source $\nu \times F_\nu = \lambda \times F_\lambda$. Asteroid SEDs deviate from this assumption and colour-corrections are required

the PACS photometer. The derived flux densities and errors (typically around 5-6%) are given in Tables 16, 17, 18, 19 together with the observing log and conditions (observation mid-time, object distance from Sun and Herschel, phase angle).

### 2.2 SPIRE photometer observations

The SPIRE [23,76] photometer observations of the four prime asteroids are listed in Tables 4, 8, 11, 14. The data were taken in four different observing modes "Sm Map" (small map), "Lg Map" (large map), "Scan" (scan map), "PS" (point-source), mainly as part of calibration programmes, but here we only use data taken in the standard small and large map modes. The measurements were reduced through HIPE[7] version 11 -using the SPIRE Calibration Tree version 11- by SPIRE instrument experts and calibrated against a reference Neptune model (ESA4) [45,5,63]. The processing of different observing modes is essentially identical, with the exception of the so-called cooler burp correction which was only done for large maps in a dedicated interactive analysis step. Point source photometry was extracted from Level 1 data using the timeline fitter task [5], fitting an elliptical Gaussian to the asteroid in the co-moving reference frame. The object fluxes have been colour-corrected assuming a spectral index of 2 [79] to obtain mono-chromatic flux densities at 250, 350, and 500 $\mu$m (corrections are in the order of 5-6% here). More details about the reduction and calibration are given in Section 6.1 in [21]. The absolute flux uncertainties were calculated by adding quadratically the individual errors from the Gaussian timeline fitting (typically well below 1%), 2% for the uncertainties in colour correction, and 5% for errors related to the Neptune model which is the baseline for the absolute flux calibration of the SPIRE photometer. The derived flux densities and errors (typically around 5-6%) are given in Tables 16, 17, 18, 19 together with the observing log and conditions (observation mid-time, object distance from Sun and Herschel, phase angle).

### 2.3 HIFI continuum observations

The HIFI [13] point-source observations of Ceres are listed in Table 5. The data were taken [41] in band 1a (OD 1392) and band 1b (ODs 923, 1247, 1260) as part of two science programmes. Here we only consider the continuum fluxes of Ceres, which are a by-product of the data reduction, but not of interest for the original science case. The HIFI continuum fluxes were derived from the observations taken during the four ODs. For each of the four data sets (i.e. for the 10 h of integration on OD 1392) all data from both polarizations -H and V- have been averaged. The conversion of double-sideband antenna temperatures to flux densities uses values for the aperture efficiencies derived from observations of Mars and are therefore tied to a model of this planet[8]. The aperture efficiencies have recently been reviewed and we use the new values kindly

[7] HIPE is a joint development by the Herschel Science Ground Segment Consortium, consisting of ESA, the NASA Herschel Science Center, and the HIFI, PACS and SPIRE consortia.

[8] `http://www.lesia.obspm.fr/perso/emmanuel-lellouch/mars/`

provided to us by Willem Jellema (priv. comm.), which, at the frequencies considered here, are smaller by 3.8% and 5.9% in the H and V polarization, respectively, than values quoted in [69]. The given flux densities are averages of both polarizations (i.e. H and V) observed by HIFI and are derived from the median values of the observed continuum baselines. The error calculation takes into account the noise r.m.s. after smoothing to a resolution of 100 MHz, quadratically added to the estimated 5% error in the Mars model which we tie our calibration to. For continuum measurements there is no side-band ratio error, and standing wave effects are also averaged out. The two polarizations of HIFI in band 1 are misaligned by $6.6''$, leading to a coupling loss of order 2% (for a perfect Gaussian beam and no satellite pointing error). Allowing for additional pointing errors, we estimate that the derived flux densities could be too low by $\approx 5\%$. The derived flux densities and errors are given in Table 16 together with the observing log and conditions (observation mid-time, object distance from Sun and Herschel, phase angle).

## 3 Thermalphysical model and asteroid-specific model parameters

The applied thermophysical model (TPM) is based on the work by Lagerros [32–34]. This model is frequently and successfully applied to near-Earth asteroids (e.g., [52, 54, 55, 58]), to main-belt asteroids (e.g., [46, 51, 61]), and also to more distant objects (e.g., [25, 39]). The TPM takes into account the true observing and illumination geometry for each observational data point, a crucial aspect for the interpretation of the main-belt asteroid observations which cover a wide range of phase angles and helio-/observer-centric distances, as well as different spin-axis obliquities.

**High quality size and geometric albedo values are fundamental for reliable TPM predictions. For all four asteroids we used literature values, but only after a critical inspection of the published sizes and albedos and their error estimates.** The TPM **also** allows **one** to specify simple or complex shape models and spin-vector properties. The **one-dimensional vertical** heat conduction into the surface is controlled by the thermal inertia $\Gamma$[9]. The observed mid-/far-IR/sub-mm fluxes are connected to the hottest regions on the asteroid surface and dominated by the diurnal heat wave. The seasonal heat wave is less important and therefore not considered here. The infrared beaming effects (similar to opposition effects at optical wavelengths) are calculated via a surface roughness model, described by segments of hemispherical craters. Here, mutual heating is included and the true crater illumination and the visibility of shadows is considered.

**For the calculation of the Bond albedo (which is assumed to be close to the bolometric albedo) also the object specific slope parameters for the phase curve G and the absolute magnitudes H are needed (IAU two-parameter magnitude system for asteroids [36, 6]). The Bond albedo is given by $p_V \cdot q$, with the geometric V-band albedo $p_V$, and the phase integral $q = 0.290 + 0.684 \cdot G$. In cases where $p_V$ was measured in-situ, only G is required, in cases where $p_V$ was not directly measured, we derived $p_V$ from $H_V$ and the object's effective size $D_{eff}$ via: $p_V$**

[9] **The thermal inertia $\Gamma$ is defined as $\sqrt{\kappa \rho c}$, where $\kappa$ is the thermal conductivity, $\rho$ the density, and $c$ the heat capacity.**

**$= 10^{(2 \cdot log_{10}(S_0) - 2 \cdot log_{10}(D_{eff}) - 0.4 \cdot H_V)}$, with the Solar constant, $S_0$ = 1361 W/m$^2$. We used literature values for H-G based on large samples of measurements covering many aspect and phase angles from several apparitions. Typical uncertainties in G values have a negligible influence on the TPM flux predictions over the entire Herschel wavelength-range and for the accessible phase angles (approximatly 15-30°) for main-belt asteroids. Errors in H are directly influencing the geometric albedo: 0.05 mag in H translate into a 5% error in albedo, with a corresponding flux change well below 1%.**

The level of roughness is driven by the r.m.s. of the surface slopes which correspond to a given crater depth-to-radius value combined with the fraction $f$ of the surface covered by craters, see also Lagerros ([32]) for further details. For all four targets we used the "default" roughness settings ($\rho$=0.7, f=0.6) [47].

We used wavelength-dependent emissivity models with emissivities of 0.9 up to 150 $\mu$m and slowly decreasing values beyond $\sim$150 $\mu$m. The "default" model -used for Ceres, Pallas, and Lutetia- has lowest emissivities of around 0.8 in the sub-mm-range, the Vesta-specific emissivity model is more extreme and has values going down to 0.6 at 600 $\mu$m. Both models are used as specified and applied in [46–48].

For the thermal inertia $\Gamma$ we used a "default" value for large, regolith-covered main-belt asteroids, namely $\Gamma$ = 15 Jm$^{-2}$s$^{-0.5}$K$^{-1}$ [47]. This value is not very well constrained and in the literature one can find smaller values down to 5 Jm$^{-2}$s$^{-0.5}$K$^{-1}$ (e.g., [61]) or larger values of 25 Jm$^{-2}$s$^{-0.5}$K$^{-1}$ (e.g., [46]). The precise value has very little influence on far-IR and sub-mm-fluxes [49] -at least for large regolith-covered main-belt asteroids- and it agrees very well with the lunar value of $\Gamma$ = 39 J m$^{-2}$ s$^{-0.5}$ K$^{-1}$ [27] considering the lower temperature environment at 2-3 AU from the Sun which lowers the thermal conductivity within the top surface dust layer considerably.

### 3.1 (1) Ceres

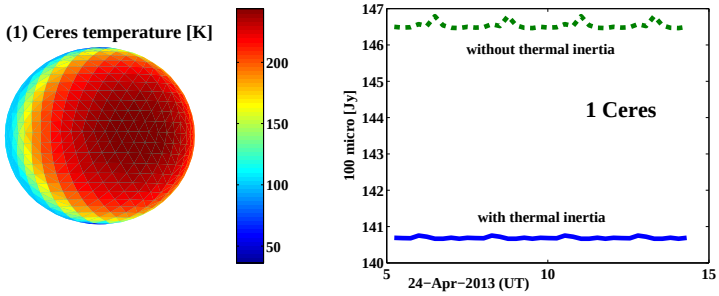


**Fig. 2** Left: Shape model of Ceres with the TPM temperature coding on the surface, calculated for the Herschel point-of-view on OD 1441, OBSID 1342270856, rotation axis is along the vertical direction. Right: the corresponding thermal light-curve at 100 $\mu$m with and without thermal effects included.

Ceres is the largest and most massive asteroid in the main-belt. It is presumed to be homogeneous, gravitationally relaxed and it has a low density, low albedo and relatively featureless visible reflectance spectrum [78]. The shape that best reproduces the available data (occultations, HST measurements, adaptive optics studies, light-curve, ...) is an oblate spheroid [42, 78, 7, 17] with an equatorial diameter of 974.6 km and a polar diameter of 909.4 km, resulting in an equivalent diameter of an equal volume sphere of 952.4 $\pm$ 3.4 km [78]. The semi-major axes ratios are therefore a/b = 1.0 and b/c = 1.072. The spin-axis is within 3° of ($\lambda_{sv}^{ecl}$, $\beta_{sv}^{ecl}$) = (346°, +82°) [17] in ecliptic reference frame, with a siderial rotation period of 9.074170 $\pm$ 0.000001 h [10]. The spin-vector is therefore oriented close to perpendicular to the line-of-sight and the optical light-curve amplitude is generally small (up to 0.04 mag [46]). The geometric V-band albedo is $p_V$ = 0.090 $\pm$ 0.0055 [37, 17]. **For the calculation of the Bond albedo we used an absolute magnitude $H_V$ = 3.28 mag and a slope parameter G = 0.05 [30, 46].**

## 3.2 (2) Pallas

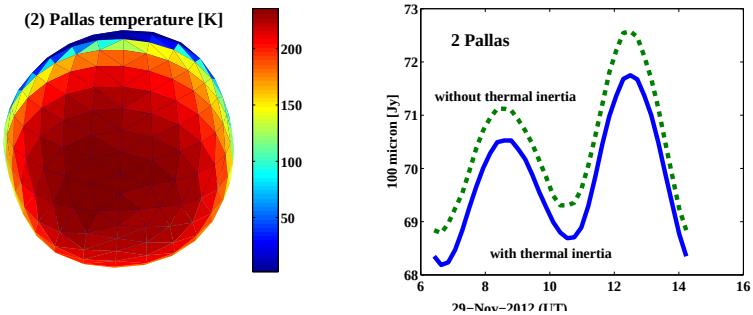


**Fig. 3** Left: Shape model of Pallas with the TPM temperature coding on the surface, calculated for the Herschel point-of-view on OD 1295, OBSID 1342256236, rotation axis is along the vertical direction. Right: the corresponding thermal light-curve at 100 $\mu$m with and without thermal effects included.

Pallas has about half the size of Ceres and is considered as an intact protoplanet which has undergone impact excavation [73]. Its published size, shape, and spin-properties have substantially changed over the last years [80, 18, 73, 16, 8]. We used the latest nonconvex shape model from DAMIT[10] with a siderial rotation period of 7.81322 h. This solution includes all available information from occultations, HST, light-curves over several decades, and adaptive optics measurements. The shape can roughly be described as a triaxial-ellipsoid body with a/b = 1.06, b/c=1.09. Its spin-axis is oriented towards celestial directions ($\lambda_{ecl}$, $\beta_{ecl}$) = (31° ± 5°, -16° ± 5°), which means it has a high obliquity of 84°, leading to high seasonal contrasts. Shape-introduced light-curve amplitudes can reach up to 0.16 mag [31]. The effective size $2\times(\mathrm{abc})^{1/3}$, a critical parameter for our calculations, was given as 533 ± 6 km [18], 545 ± 18 km [73], 513 ± 7 km [8]. We adopted the first value which has the smallest errorbar and which is based on multiple occultations, including one of the best observed occultation of a star ever. We use $H_V$ = 4.13 mag and G = 0.16 [30, 46, 31]. Our geometric albedo $p_V$ = 0.139 was calculated from $H_V$ and the effective size of 533 km.

[10] Database of Asteroid Models from Inversion Techniques, `http://astro.troja.mff.cuni.cz/projects/asteroids3D/`

### 3.3 (4) Vesta

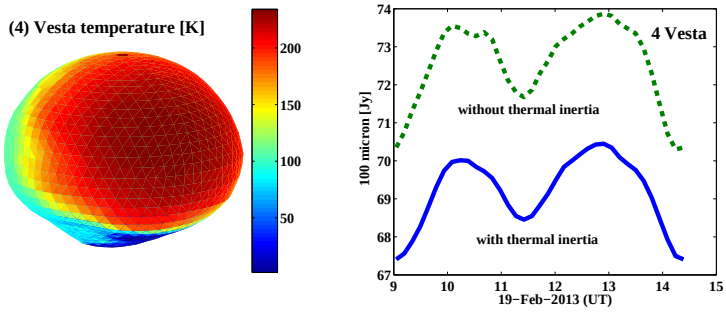


**Fig. 4** Left: Shape model of Vesta with the TPM temperature coding on the surface, calculated for the Herschel point-of-view on OD 1377, OBSID 1342263924, rotation axis is along the vertical direction. Right: the corresponding thermal light-curve at 100 $\mu$m with and without thermal effects included.

Vesta is one of the largest and the second most massive asteroid in the main-belt. It has recently been visited by the DAWN[11] mission. Most of the key elements for our thermophysical model purposes are very well known, but the final shape models are not yet publically released. Our calculations are based on the HST shape model [77] with a spin-vector ($\lambda_{ecl}$, $\beta_{ecl}$) = (319° ± 5°, 59° ± 5°), very close to values derived recently from DAWN [70]. The siderial rotation period is $P_{sid}$ = 5.3421289 h [77, 15]. The obliquity of about 27° combined with a more extreme triaxial body leads to shape-introduced light-curve amplitudes of up to 0.18 mag [31]. We assigned a mean size of 525.4 ± 0.2 km [70], roughly corresponding to a triaxial-ellipsoid body with a/b = 1.03, b/c=1.25. We took $H_V$ = 3.20 mag and G = 0.34 [46], the corresponding geometric albedo $p_V$ = 0.336 was calculated from the effective size of 525.4 km.

[11] http://dawn.jpl.nasa.gov/

### 3.4 (21) Lutetia

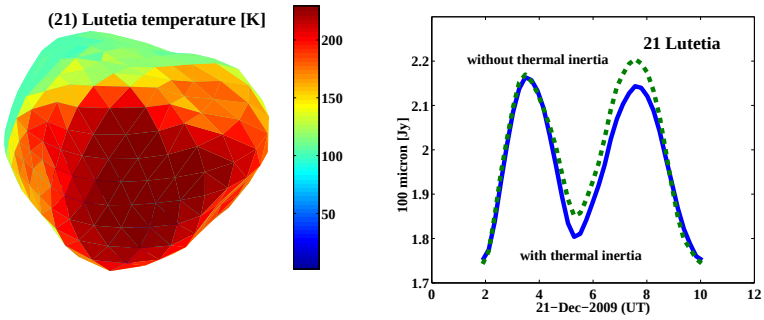


**Fig. 5** Left: Shape model of Lutetia with the TPM temperature coding on the surface, calculated for the Herschel point-of-view on OD 221, OBSID 1342188334, rotation axis is along the vertical direction. Right: the corresponding thermal light-curve at 100 $\mu$m with and without thermal effects included.

Lutetia is significantly smaller and more irregularly shaped than the other three objects. Due to its unusual spectral type with indications of a high metal content, it was originally not considered in our list of potential flux calibrators. But Lutetia was very well characterized by a ROSETTA[12] flyby in 2011 and we took advantage of the derived, high-quality properties. Our shape model is the latest nonconvex shape model from DAMIT[13], which is based on a combination of flyby information, occultations, radiometry, light-curve datasets, radar echoes, interferometry, and disk-resolved imaging [9]. It has a spin-vector of ($\lambda_{ecl}$, $\beta_{ecl}$) = (52° ± 2°, -6° ± 2°), and a siderial rotation period of $P_{sid}$ = 8.168271 h [35,9]. The absolute effective size of the final shape model is $D_{eff}$ = 99.3 km and the measured geometric albedo is $p_V$ = 0.19 ± 0.01 [9]. Typical shape-introduced light-curve amplitudes can reach up to 0.25 mag [31]. The absolute magnitude and the slope paramemeter, both normalised to the mean light-curve value, are given as $H_V$ = 7.25 and G = 0.12 [4].

[12] http://www.esa.int/Our_Activities/Space_Science/Rosetta

[13] Database of Asteroid Models from Inversion Techniques, http://astro.troja.mff.cuni.cz/projects/asteroids3D/

## 4 Results, Validity and Limitations

Based on the thermophysical model and object setup in Section 3, we calculated TPM flux densities at the PACS, SPIRE, and HIFI reference wavelengths for the mid-time of each observation (Start-time + 0.5×duration of each OBSID, Herschel-centric reference system). The calculations have been done for the true Herschel-centric observing geometry with the asteroid placed at the correct helio-centric and Herschel-centric distance, under the true phase angle and spin-vector orientation. The observed and calibrated mono-chromatic flux densities have then been divided by the TPM predictions. The ratios are shown in the following figures 6, 7, 8, 9, and are listed in Tables 16, 17, 18, 19, and discussed below.

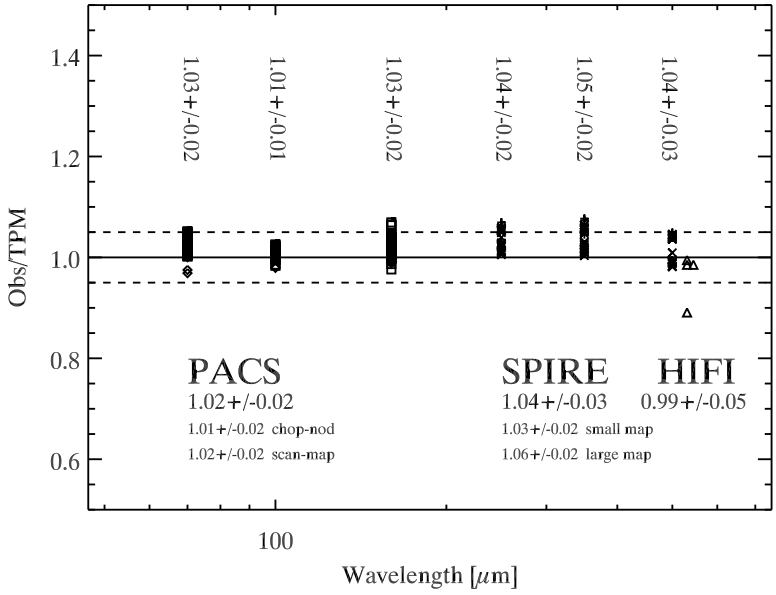


**Fig. 6** Observed and calibrated Herschel flux densities of Ceres divided by the corresponding TPM predictions **(one point per OBSID)**. The median ratios for each instrument and each band are given together with the standard deviations of the ratios. For PACS and SPIRE we also give the ratios per observing mode. **PACS data are shown as diamonds (chop-nod data) and squares (scan-map data), SPIRE data are shown as plus-symbols (large map mode) and crosses (small map mode), HIFI data are shown as triangles.**

**Absolute flux level.** The median ratios for all four asteroids and in all PACS & SPIRE bands are well within 1.00 ± 0.05. There are no systematic outliers visible. A few individual measurements are slightly outside the 5% boundary, but here it is not clear if the problem is related to instrumental/technical issues or sky background related effects. Our sources have apparent sky motions of up to about 80″/h

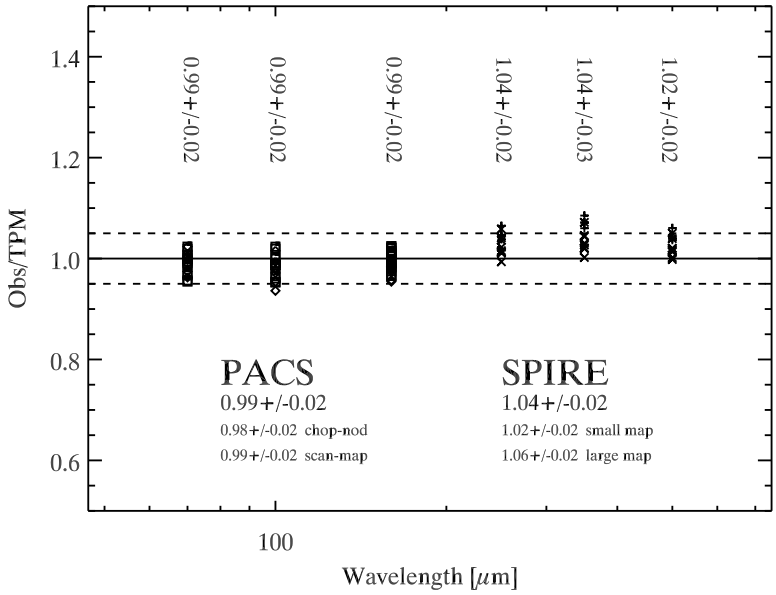


**Fig. 7** Observed and calibrated Herschel flux densities of Pallas divided by the corresponding TPM predictions, like in Fig. 6.

(as seen from Herschel) and they cross background sources and dense star fields. And indeed, Ceres, Vesta and Lutetia reached galactic latitudes below 5° during Herschel observing periods and bright sources (not easily recognized in automatic processing) could have influenced the photometry in rare cases. The influence of lower S/N levels can be seen in the increased ratio scatter in the PACS 160 $\mu$m and SPIRE 500 $\mu$m measurements of Lutetia.

The maximum-to-minimum observed flux ratios in a given band are 2.3, 2.7, 3.5, 4.3 for Ceres, Pallas, Vesta, and Lutetia, respectively (see Tables 16, 17, 18, 19). This flux change is mainly dominated by changing distances between the asteroid and Herschel, with smaller influences from changing heliocentric asteroid distances and phase angles. The TPM setup handles these seasonal effects with high accuracy. We found no significant remaining trends in the obs/TPM-ratios with helio-centric and Herschel-centric distance.

**Short-term variations.** The four asteroids are not spherical and optical lightcurves show amplitudes of up to 0.25 mag. These variations are caused mainly by rotationally changing cross-sections and therefore expected to be **seen** in disk-integrated thermal emission as well. In our model setup this is handled by complex shape models combined with spin-vector information (derived from occultation results, light-curve inversion techniques, high resultion imaging techniques and/or flyby information), and object-specific zero-points in time and rotational phase. Our setup explains the

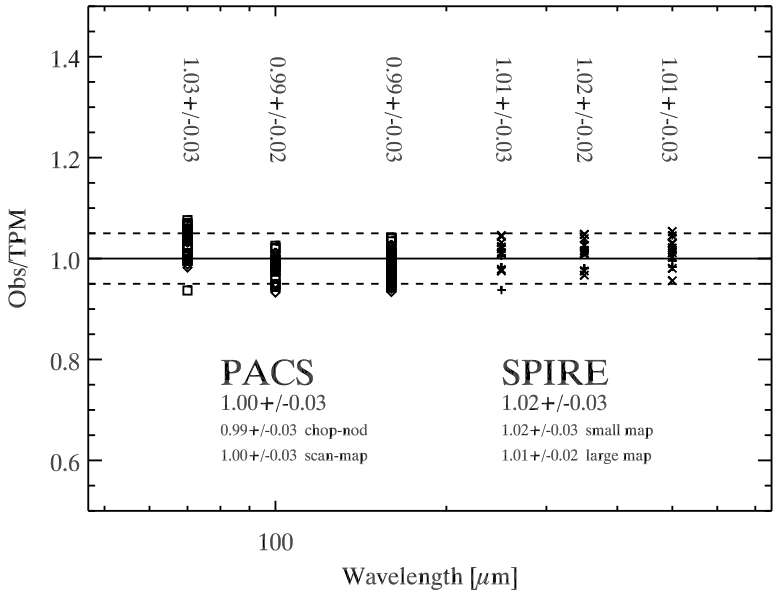


**Fig. 8** Observed and calibrated Herschel flux densities of Vesta divided by the corresponding TPM predictions, like in Fig. 6.

available optical light-curves and other cross-section related data very well, but it is not entirely clear if such models would also explain the rotational changes in thermal emission. Figures 6, 7, 8, 9 show -at least in the most reliable shortest wavelength bands at 70 and 250 $\mu$m- very small standard deviations in the obs/TPM ratios. For Ceres and Pallas we find standard deviations of 2%, while for the more complex shaped objects Vesta and Lutetia we find 3%. This very low scatter agrees with findings on non-variable reference stars (see [2]) and tells us that the shape and rotational properties of the four asteroids are modeled with sufficient accuracy.

**Spectral shape aspects.** The obs/TPM ratios for a given object are almost identical for all bands of the same instrument. This is an indication that our TPM reproduces the observed slopes in spectral energy distribution (SED) correctly. The modeled object SEDs are summing up all different surface temperatures over the entire disk. Here, at long wavelength and close to the Rayleigh-Jeans SED approximation, the SEDs are closely correlated with the disk-averaged temperatures, while at shorter wavelengths (e.g., in the mid-IR) the hottest sub-solar regions dominate the SED shapes. The constant ratios over all three bands of an instrument also confirm the validity of the strongly band-dependent colour-correction (see Sections 2.1 and 2.2). These corrections are calculated from the lab-measured relative spectral response functions of the individual bands [21,56]. Our results show no problems with the

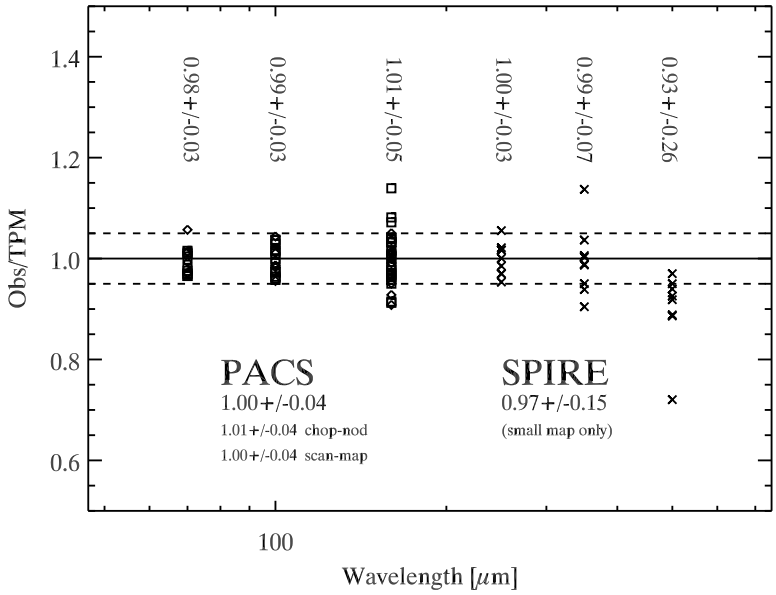


**Fig. 9** Observed and calibrated Herschel flux densities of Lutetia divided by the corresponding TPM predictions, like in Fig. 6.

tabulated colour-correction values, a nice confirmation that the bands are well characterized and that there are no indications for filter leaks.

**PACS/SPIRE cross-calibration and emissivity aspects.** For the 3 bright sources Ceres, Pallas, and Vesta the SPIRE ratios are 2-5% higher than the PACS ratios. The cause is not clear, but there are different possibilities: (i) A systematic difference in the absolute flux calibrators (5 fiducial stars for PACS [2] and a specific Neptune model for SPIRE [5]). Both calibration systems are given with an absolute accuracy of $\pm$5% and the offset we see in the asteroids is within this range. Both calibration systems underwent recent adjustments and re-adjustments with typical changes of a few percent. Discussions are still ongoing and the related publications -possibly with slight adjustments- are in preparation. (ii) A flux-dependency in the reduction/calibration steps which is not correctly accounted for: the PACS asteroid data are corrected for detector non-linearities (up to 6% for the highest asteroid fluxes), but an absolute validation at these flux levels is difficult. The SPIRE asteroid data are well below the flux level of Neptune which is used as reference object and the asteroids also move much faster than Neptune on the sky. Both aspects might cause an offset of a few percent on the final fluxes. (iii) The asteroid models use a wavelength-dependent emissivity model [46–48] and the largest emissivity changes happen between 200 and 500 $\mu$m. But if there are problems in the emissivity model solution we would expect to see obs/TPM ratios changing gradually with wavelengths and not in

a step-function as we see it here. We also tested a constant emissivity model ($\varepsilon$ = 0.9 = const.) which clearly confirms that lower and wavelength-dependent emissivities are needed to explain the SPIRE measurements. However, the effective emissivity changes are not precisely known for the region beyond $\approx$150 $\mu$m where subsurface layers (probably with different thermal properties [27]) start to become visible. A future scientific analysis of all combined PACS and SPIRE observations might reveal a new and slightly different wavelength-dependent emissivity model for the large main-belt asteroids.

One additional element in this context is the outcome of a dedicated PACS/SPIRE cross-calibration study for the fiducial calibration stars and -at a much higher flux level- for the planets Uranus and Neptune. In this way, one could investigate further the reason for the small jump between PACS and SPIRE fluxes.

There are a few additional points which deserve mentioning:

- For Lutetia we find significantly larger standard deviations in the obs/TPM ratios at 350 and 500 $\mu$m, but Lutetia is already faint at these wavelength (below 600 mJy at 350 $\mu$m and some measurement are even below 100 mJy at 500 $\mu$m) and background contamination and instrument noise levels start to contribute.

- The 70 $\mu$m obs/TPM ratio for Vesta is about 4% higher than the ratios at 100 and 160 $\mu$m. We don't know the reason for this effect, but we speculate that this might be the result of a broadband mineralogic surface feature covered by the 70 $\mu$m-band ($\sim$55 - 95 $\mu$m). We plan to follow this up via PACS spectrometer measurements of Vesta.

- For the 3 brightest targets we also see a very small difference between PACS data taken in chop-nod mode and scan-map mode. The chop-nod ratios are about 1% lower than the corresponding scan-map ratios. We expected to see slightly underestimated fluxes in the chop-nod mode for very bright targets (see [60]), but it was not clear how big the effect would be. Based on the asteroid results, we expect to see a 2-3% flux differences for even brighter targets, like Neptune and Uranus, between measurements taken in these two different PACS observing modes.

- The HIFI ratios are very close to the PACS ratios and about 5% lower than the SPIRE ratios. But the derived fluxes are very sensitive to pointing errors. Additional pointing errors could increase the derived flux densities by up to $\approx$ 5% which would then bring the HIFI ratios very close to the SPIRE ones.

- There was one SPIRE observation (OD 411, OBSID 1342199329, Large Map mode) which produced fluxes which are about 35% higher than the corresponding model predictions in all 3 bands, probably due to a contaminating background source. We eliminated this measurement from our analysis.

- We see a 3-4% offset between SPIRE large and small scan map observations of Ceres and Pallas, but not for Vesta. This offset is not present in observa-

**Table 1 Statistical comparison between observed and TPM fluxes. The numbers indicate how many observations are matched by the corresponding TPM prediction within the given 1-$\sigma$ error bars and how many are not matched. The last two lines give the agreement per band in percent, based on the 1-$\sigma$ and 2-$\sigma$ errors in the observed fluxes.**

| Object | | 70 $\mu$m | 100 $\mu$m | 160 $\mu$m | 250 $\mu$m | 350 $\mu$m | 500 $\mu$m |
|---|---|---|---|---|---|---|---|
| 1 | Ceres | 51/0 | 39/0 | 84/4 | 20/4 | 18/6 | 24/0 |
| 2 | Pallas | 20/0 | 19/1 | 40/0 | 11/2 | 8/5 | 12/1 |
| 4 | Vesta | 32/8 | 25/7 | 64/8 | 14/1 | 15/0 | 15/0 |
| 21 | Lutetia | 14/1 | 19/0 | 29/5 | 9/0 | 6/3 | 5/4 |
| 1-$\sigma$ agreement | | 92% | 92% | 92% | 87% | 70% | 91% |
| 2-$\sigma$ agreement | | 100% | 100% | 100% | 100% | 100% | 97% |

tions taken in both modes close in time. The cause is therefore either related to satellite/instrument effects changing with time (like the changing telescope flux) or by a time-dependent thermal effect which is not covered by our current model-setup. A first investigation seems to point towards a small effect related to subsurface emission which seems to play a role at the longest SPIRE wavelengths and which is at present only approximated by our wavelength-dependent emissivity models.

- Ceres, Pallas, and Vesta also have SPIRE observations taken in non-standard scanning mode. A first comparison with our model predictions confirms the validity of the data. They will be included in future analysis projects.

**Quality of model parameters.** The fact that our TPM predictions agree -on absolute scale- very well with the Herschel measurements does not automatically mean that all our object properties (mainly effective size, albedo, thermal properties) are correct. The object-related quantities have uncertainties and could be even slightly off. But we aimed for finding the most accurate object sizes, and derived preferentially from direct measurements and published in literature. The thermal properties influence the predictions in an absolute sense and also in a wavelength-dependent manner. We took default values from literature to avoid any dependency of our object properties from Herschel-related information. Overall, our model settings allow us to reproduce the observed absolute fluxes and SED shapes with high accuracy and we have therefore great confidence in our model solutions.

**Accuracy. We made a statistical analysis of the observation-to-model ratios for all four asteroids (Table 1, Figure 10) to see how many observational data points are matched by the corresponding TPM prediction.**

**For this comparison we considered the absolute flux errors for each individual measurement as it was produced by the general data reduction and calibration procedure mentioned above. The absolute flux errors include the processing errors, the photometry errors (corrected for correlated noise) and the absolute flux calibration error as provided by the three instrument teams. In all three**

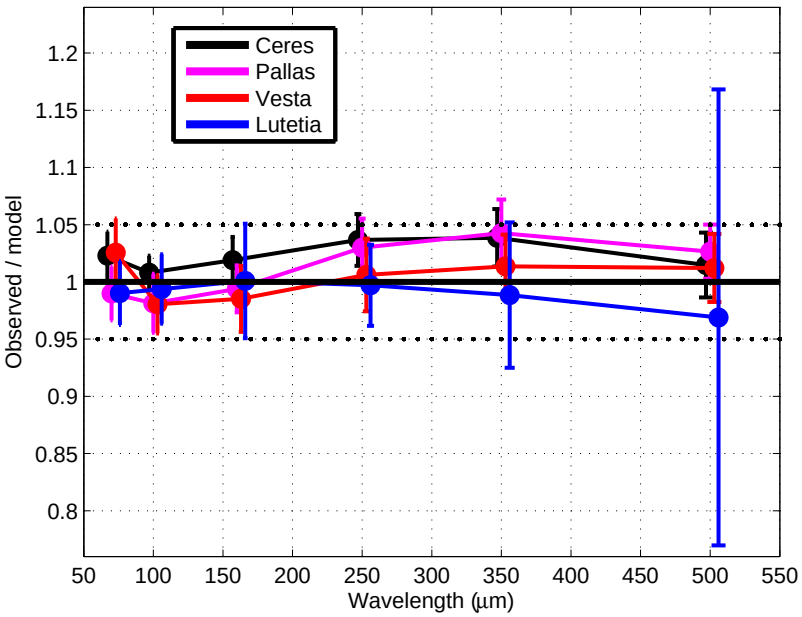


**Fig. 10** Dispersion in the ratios of measured-to-model fluxes for the four asteroids as a function of wavelength. The weighted mean ratios are shown with errorbars reflecting the absolute flux calibration of individual measurements as well as the variance of the sample.

**PACS bands more than 90% of all measurements agree within their 1-$\sigma$ errorbars with the corresponding TPM prediction. In the SPIRE bands the agreement is still between about 70% and 90%. If we allow for 2-$\sigma$ errorbars we find 100% agreement for Ceres, Pallas and Vesta in all six bands. For Lutetia there are only two measurements in the 500 $\mu$m band which are outside the 2-$\sigma$ threshold. Figure 10 shows the agreement between observations and TPM predictions in a graphical way. For each object we calculated the weighted mean ratio and errorbars adding up quadratically the variance of the weighted mean and the weighted sample variance. These errorbars are dominated by the 5% absolute flux calibration errors of our measurements, the variance of the weighted mean (as can be seen in Figures 6, 7, 8, 9) is typically 2-3% only, with exception of the long-wavelength channels for Lutetia. This excellent agreement between observed and TPM fluxes confirms the validity of the four asteroids as prime calibrators on a similar quality level as given for the fiducial star models in the PACS range (5%), the Neptune model in the SPIRE range (5%), and the Mars model in the HIFI band 1a/1b (5%).**

**Limitations. Our comparison between TPM predictions and measurements is limited to a wavelength range between about 50 $\mu$m (short wavelength end of the PACS 70 $\mu$m filter) and about 700 $\mu$m (long wavelength end of the SPIRE**

**500 $\mu$m filter). The Herschel visibility contrained the tested phase angles to values between about 15° and 30° before and after opposition. Outside these wavelengths and phase angle ranges the TPM might have slightly higher uncertainties. Some of the asteroids have complex shapes and the shape models used might not characterize the true shape very accurately. This could also cause small deviations between TPM predictions and the true measured fluxes for specific viewing geometries. The rotation periods are known with high accuracy for all four asteroids and the applied spin vectors are of sufficient quality for the next decades.**

**Overall, the TPM deviations outside the specified wavelengths and phase-angle ranges are expected to be small and absolute model accuracies of better than 10% seem to be reasonable for all four asteroids. Further testing against additional thermal data is foreseen in the near future to cover the full ALMA and SPICA[14] regime.**

## 5 Conclusions

We find the following general results related to the 4 asteroids:

- The new asteroid models predict the observed fluxes on absolute scales with better than 5% accuracy in the in the 50 to 700 $\mu$m range. This means that the effective size and albedo values in our model setup are of high quality.
- Shape and spin properties dominate the short-term brightness variations: our shape, rotation-period and spin-axis approximations are sufficient for our purposes.
- In general, the rotational and seasonal flux changes are modeled with high quality to account for short-term (rotational effects on time scales of hours) and long-term (effects with phase angle and changing distance to the Sun on time scales of months or years) object variability.
- Our "default" description of the thermal properties is sufficient to explain the observed far-IR/sub-mm fluxes. Please note that the Vesta emissivity is very different from the emissivity model used for the other objects.
- The asteroid surfaces of all 4 asteroids are very well described by a low-conductivity, hence low thermal inertia surface regolith with very little heat transport to the nightside of the object (they are observed at phase angles up to about 30°).
- There are indications that Vesta has a broad shallow mineralogic emission feature which contributes up to 4% to the total flux measured in the PACS 70 $\mu$m band.

We find the following Herschel-related results:

[14] `http://www.ir.isas.jaxa.jp/SPICA/SPICA_HP/index_English.html`

- The PACS chop-nod and scan-map derived fluxes agree very well (within 1%), although there seems to be a small tendency that the chop-nod fluxes are slightly underestimated for very bright targets.
- The SPIRE observation/model ratios for Ceres, Pallas, and Vesta are 2-5% higher than the PACS related ones. This could be related to the very different calibration schemes of both instruments, but there is also the possibility of a model-introduced effect (e.g., related to the object emissivity models).
- The reduced and calibrated HIFI continuum fluxes for Ceres agree very well with the PACS measurements and confirm the high photometric quality of the HIFI continuum measurements.

**Ceres, Pallas, Vesta, and Lutetia as prime calibrators:**

- **The new TPM setup for the four asteroids predict the observed fluxes on absolute scales with better than 5% accuracy in the wavelength range 50 to 700 $\mu$m and for phase angles between $\sim$15$^\circ$ and $\sim$30$^\circ$.**
- **Outside the Herschel PACS/SPIRE wavelength range and for extreme phase angles we still expect that the absolute accuracy of the TPM predictions are better than 10%.**

Overall, our thermophysical model predictions for the four asteroids agree within 5% with the available (and independently calibrated) Herschel measurements. The achieved absolute accuracy is similar to the ones quoted for the official Herschel prime calibrators, the stellar photosphere models, the Neptune and Mars planet models, which justifies to upgrade the four asteroid models to the rank of prime calibrators. The four objects cover the flux regime from just below 1,000 Jy (Ceres at mid-IR) down to fluxes below 0.1 Jy (Lutetia at the longest wavelengths). Based on the comparison with PACS, SPIRE and HIFI measurements and pre-Herschel experience, the validity of prime calibrators ranges from mid-infrared to about 600 $\mu$m, connecting nicely the absolute stellar reference system in the mid-IR with the planet-based calibration at sub-mm/mm wavelengths.

**Acknowledgements** We would like to thank the PIs of the various scientific projects for permission to use their Herschel science data in the context of our calibration work.

## References

1. Altieri, B. (2011), PACS Observer's Manual, HERSCHEL-HSC-DOC-0832, v. 2.4, Dec. 22, 2011, `http://herschel.esac.esa.int/Docs/PACS/html/pacs_om.html`
2. Balog, Z., Müller, T. G., Nielbock, M. et al.: The Herschel-PACS photometer calibration: Point-source flux calibration, Exp. Astronomy (2013), this issue
3. Beichman, C. A., Neugebauer, G., Habing, H. J., Clegg, P. E., Chester, T. J. (1988), Infrared astronomical satellite (IRAS) catalogs and atlases. Volume 1: Explanatory supplement
4. Belskaya, I. N., Fornasier, S., Krugly, Yu. N. et al.: Puzzling asteroid 21 Lutetia: our knowledge prior to the Rosetta fly-by, A&A 515, 29 (2010)
5. Bendo, G. J., Griffin, M. J., Bock, J. J. et al.: Flux calibration of the Herschel-SPIRE photometer, MNRAS (2013), accepted for publication (http://arxiv.org/abs/1306.1217)

6. **Bowell, E., Hapke, B., Domingue, D. et al.: Application of photometric models to asteroids, in Asteroids II, Eds. Binzel et al., Univ. of Arizona Press, 524-556 (1989)**
7. Carry, B., Dumas, C., Fulchignoni, M. et al.: Near-infrared mapping and physical properties of the dwarf-planet Ceres, A&A 478, 235 (2008)
8. Carry, B., Dumas, C., Kaasalainen, M. et al.: Physical properties of (2) Pallas, Icarus 205, 460 (2010)
9. Carry, B., Kaasalainen, M., Merline, W. J. et al.: Shape modeling technique KOALA validated by ESA Rosetta at (21) Lutetia, P&SS 66, 200 (2012)
10. Chamberlain, M. A., Boynton, W. V.: Ceres lightcurve analysisPeriod determination, Icarus 188, 451 (2007)
11. Cohen M.: Stellar calibration in the infrared: extending the legacy of the KAO, ISO, and MSX to SIRTF and beyond, Proceedings of the Conference "The Calibration Legacy of the ISO Mission", Metcalfe, Salama, Peschke, Kessler (eds.), ESA SP-481, 135 (2003)
12. Decin, L.: Stellar Models in IR Calibration, Proceedings of the Conference "The Calibration Legacy of the ISO Mission", Metcalfe, Salama, Peschke, Kessler (eds.), ESA SP-481, 141 (2003)
13. de Graauw, Th., Helmich, F. P., Phillips, T. G. et al.: The Herschel-Heterodyne Instrument for the Far-Infrared (HIFI) A&A, 518, 6D (2010)
14. Dehaes, S., Bauwens, E., Decin, L. et al.: Structure of the outer layers of cool standard stars, A&A 533, A107 (2011)
15. Drummond, J. D., Weidenschilling, S. J., Chapman, C. R., Davis, D. R.: Photometric geodesy of main-belt asteroids. II - Analysis of lightcurves for poles, periods, and shapes, Icarus 76, 19 (1988)
16. Drummond, J. D., Christou, J., Nelson, J.: Triaxial ellipsoid dimensions and poles of asteroids from AO observations at the Keck-II telescope, Icarus 202, 147 (2009)
17. Drummond, J. D. et al. 2013, in preparation
18. Dunham, D. W., Dunham, J. B., Binzel, R. P. et al.: The size and shape of (2) Pallas from the 1983 occultation of 1 Vulpeculae, AJ 99, 1636 (1990)
19. Engelbracht, C. W., Blaylock, M., Su, K. Y. L. et al.: Absolute Calibration and Characterization of the Multiband Imaging Photometer for Spitzer. I. The Stellar Calibrator Sample and the 24 micron Calibration PASP 119, 994-1018 (2007)
20. Gordon, K. D., Engelbracht, C. W., Fadda, D. et al.: Absolute Calibration and Characterization of the Multiband Imaging Photometer for Spitzer. II. 70 micron Imaging PASP 119, 1019-1037 (2007)
21. Griffin, M. J., North, C. E., Schulz, B. et al.: Flux Calibration of Broadband Far Infrared and Submillimetre Photometric Instruments: Theory and Application to Herschel-SPIRE MNRAS (2013), accepted for publication (http://arxiv.org/abs/1306.1778)
22. Griffin, M. J. & Orton, G. S.: The near-millimeter brightness temperature spectra of Uranus and Neptune, Icarus 105, 537 (1993)
23. Griffin, M. J., Abergel, A., Abreu, A. et al.: The Herschel-SPIRE instrument and its in-flight performance A&A, 518, 3G (2010)
24. Hammersley, P. L. & Jourdain de Muizon, M.: The Development of Stellar Photometric Standards for ISO, Proceedings of the Conference "The Calibration Legacy of the ISO Mission", Metcalfe, Salama, Peschke, Kessler (eds.), ESA SP-481, 129 (2003)
25. Horner, J., Müller, T. G., Lykawka, P. S.: (1173) Anchises - thermophysical and dynamical studies of a dynamically unstable Jovian Trojan MNRAS 423, 2587-2596 (2012)
26. Kawada, M., Baba, H., Barthel, P. D. et al.: The Far-Infrared Surveyor (FIS) for AKARI PASJ 59, 389 (2007)
27. Keihm, S. J.: Interpretation of the lunar microwave brightness temperature spectrum - Feasibility of orbital heat flow mapping, Icarus 60, 568 (2013)
28. Kessler, M. F., Steinz, J. A., Anderegg, M. E. et al.: The Infrared Space Observatory (ISO) mission, A&A 315, 27 (1996)
29. Klaas, U., Abraham, P., Acosta-Pulido, J. A. et al.: ISOPHOT In-flight Calibration Strategies, Proceedings of the Conference "The Calibration Legacy of the ISO Mission", Metcalfe, Salama, Peschke, Kessler (eds.), ESA SP-481, 19 (2003)
30. Lagerkvist, C.-I., Magnusson, P., Williams, I. P. et al.: Physical studies of asteroids. XXIV - Phase relations for 48 asteroids obtained with the Carlsberg Meridian Circle, A&AS 94, 43 (1992)
31. Lagerkvist, C.-I., Piironen, J., and Erikson, A. eds. (2001) Asteroid Photometric Catalogue, 5th edition, Astronomical Observatory, Uppsala University, Sweden 201 pp.
32. Lagerros, J. S. V.: Thermal physics of asteroids. I. Effects of shape, heat conduction and beaming, A&A 310, 1011 (1996)
33. Lagerros, J. S. V.: Thermal physics of asteroids. III. Irregular shapes and albedo variegations, A&A 325, 1226 (1997)

34. Lagerros, J. S. V.: Thermal physics of asteroids. IV. Thermal Infrared Beaming, A&A 332, 1123 (1998)
35. Lamy, P. L., Faury, G., Jorda, L. et al.: Multi-color, rotationally resolved photometry of asteroid 21 Lutetia from OSIRIS/Rosetta observations, A&A 521, 19 (2010)
36. **Lebofsky, L. A., Sykes, M. V., Tedesco, E. T. et al.: A Refined "Standard" Thermal Model for Asteroids Based on Observations of 1 Ceres and 2 Pallas, Icarus 68, 239-251 (1986)**
37. Li, J.-Y., McFadden, L. A., Parker, J. Wm. et al.: Photometric analysis of 1 Ceres and surface mapping from HST observations, Icarus 182, 143 (2006)
38. Lim, T. L., Swinyard, B. M., Burgdorf, M. J. et al.: The LWS Calibration Strategy, Proceedings of the Conference "The Calibration Legacy of the ISO Mission", Metcalfe, Salama, Peschke, Kessler (eds.), ESA SP-481, 13 (2003)
39. Lim, T. L., Stansberry, J., Müller, T. G. et al.: "TNOs are Cool": A survey of the trans-Neptunian region . III. Thermophysical properties of 90482 Orcus and 136472 Makemake A&A 518, 148-152 (2010)
40. Lutz, D. (2012), PACS photometer point spread function, PICC-ME-TN-033, v. 2.0, April 4, 2012, `http://herschel.esac.esa.int/twiki/pub/Public/PacsCalibrationWeb/bolopsf_20.pdf`
41. Marston, A. P. & Teyssier, D. (2011), HIFI Observer's Manual, HERSCHEL-HSC-DOC-0784, v. 2.4, June 1, 2011, `http://herschel.esac.esa.int/Docs/HIFI/html/hifi_om.html`
42. Millis, R. L., Wassermann, L. H., Franz, O. G. et al.: The Size, Shape, Density, and Abledo of Ceres from Its Occultation of BD+8deg471, Icarus 72, 507-518 (1987)
43. Moór, A., Müller, T. G., Kiss, C. et al.: PACS photometer calibration block analysis, Exp. Astronomy (2013), this issue
44. Moreno, R. (1998), PhD thesis, Université de Paris
45. Moreno, R. (2012), Neptune and Uranus planetary brightness temperature tabulation. Tech. rep., ESA Herschel Science Centre, available from ftp://ftp.sciops.esa.int/pub/hsc-calibration/PlanetaryModels/ESA4/
46. Müller, T. G. & Lagerros, J. S. V.: Asteroids as IR Standards for ISOPHOT, A&A, 338, 340-352 (1998)
47. Müller, T. G., Lagerros, J. S. V., Burgdorf, M. et al.: Fundamental thermal emission parameters of main-belt asteroids derived from ISO, in ESA SP-427, in The Universe as Seen by ISO, P. Cox & M. F. Kessler (Eds.), 141 (1999)
48. Müller, T. G. & Lagerros, J. S. V.: Asteroids as calibration standards in the thermal infrared for space observatories, A&A 381, 324-339 (2002)
49. Müller, T. G.: Thermophysical analysis of infrared observations of asteroids, M&PS, 37, 1919 (2002)
50. Müller, T. G. & Lagerros, J. S. V.: Asteroids as Calibration Standards in the Thermal Infrared - Applications and Results from ISO, Proceedings of the Conference "The Calibration Legacy of the ISO Mission", Metcalfe, Salama, Peschke, Kessler (eds.), ESA SP-481, 157 (2003)
51. Müller, T. G. & Blommaert, J. A. D. L.: 65 Cybele in the thermal infrared: Multiple observations and thermophysical analysis, A&A, 418, 347-356 (2004)
52. Müller, T. G., Sterzik, M. F., Schütz, O. et al.: Thermal infrared observations of near-Earth asteroid 2002 NY40, A&A, 424, 1075-1080 (2004)
53. Müller, T. G.: The Asteroid Preparatory Programme for HERSCHEL, ASTRO-F & ALMA, Proceedings of the dusty and molecular universe: a prelude to Herschel and ALMA, Ed. by A. Wilson, ESA SP-577, 471 (2005)
54. Müller, T. G., Sekiguchi, T., Kaasalainen, M. et al.: Thermal infrared observations of the Hayabusa spacecraft target asteroid 25143 Itokawa, A&A, 443, 347-355 (2005)
55. Müller, T. G., Ďurech, J., Hasegawa, S. et al.: Thermo-physical properties of 162173 (1999 JU3), a potential flyby and rendezvous target for interplanetary missions - Based on the experience from the Hayabusa flyby target 25143 Itokawa A&A, 525, 145 (2011)
56. Müller, T. G., Okumura, K., Klaas, U. (2011), PACS Photometer Passbands and Colour Correction Factors for Various Source SEDs, PICC-ME-TN-038, v. 1.0, April 12, 2011, `http://herschel.esac.esa.int/twiki/pub/Public/PacsCalibrationWeb/cc_report_v1.pdf`
57. Müller, T. G., Nielbock, M., Balog, Z. et al. (2011), PACS Photometer - Point-Source Flux Calibration, PICC-ME-TN-037, v. 1.0, April 12, 2011
58. Müller, T. G., O'Rourke, L., Barucci, A. M. et al.: Physical properties of OSIRIS-REx target asteroid (101955) 1999 RQ36. Derived from Herschel, VLT/ VISIR, and Spitzer observations A&A, 548, 36-45 (2012)
59. Murakami, H., Baba, H., Barthel, P. et al.: The Infrared Astronomical Mission AKARI, PASJ 59, 369 (2007)

60. Nielbock, M., Müller, T. G., Balog, Z. et al.: The Herschel-PACS photometer calibration: A time dependent flux calibration for the PACS chopped photometry AOT mode, Exp. Astronomy (2013), this issue
61. O'Rourke, L., Müller, T. G., Valtchanov, I. et al.: Thermal & Shape properties of Asteroid (21) Lutetia from Herschel Observations around the Rosetta Flyby, P&SS 55, 192 (2012)
62. Orton, G. S. & Burgdorf, M. J.: Planetary Spectral Models as References for Calibration, Proceedings of the Conference "The Calibration Legacy of the ISO Mission", Metcalfe, Salama, Peschke, Kessler (eds.), ESA SP-481, 147 (2003)
63. Pearson, C., Lim, T., North, C. E. et al.: SPIRE Point Source Photometry within the Herschel Interactive Processing Environment (HIPE), Exp. Astronomy (2013), this issue
64. Pilbratt, G. L., Riedinger, J. R., Passvogel, T. et al.: Herschel Space Observatory. An ESA facility for far-infrared and submillimetre astronomy, A&A, 518, L1 (2010)
65. Poglitsch, A., Waelkens, C., Geis, N. et al.: The Photodetector Array Camera and Spectrometer (PACS) on the Herschel Space Observatory, A&A, 518, L2 (2010)
66. Reach, W. T., Megeath, S. T., Cohen, M. et al.: Absolute Calibration of the Infrared Array Camera on the Spitzer Space Telescope, PASP 117, 978-990 (2005)
67. Rieke G. H., Lebofsky, M. J., Low, F. J.: An absolute photometric system at 10 and 20 microns, AJ, 90, 900 (1985)
68. Rieke G. H., Young, E. T., Engelbracht, C. W. et al.: The Multiband Imaging Photometer for Spitzer (MIPS), ApJS, 154, 25 (2004)
69. Roelfsema, R. R., Helmich, F. P., Teyssier, D. et al.: In-orbit performance of Herschel-HIFI, A&A 537, A17 (2012)
70. Russell, C. T., Raymond, C. A., Coradini, A. et al.: Dawn at Vesta: Testing the Protoplanetary Paradigm, Science 336, 684 (2012)
71. Sandell, G.: Secondary calibrators at submillimetre wavelengths, MNRAS 271, 75 (1994)
72. Sandell, G.: Submillimetre Calibration - Experience from Ground-based Observations, Proceedings of the Conference "The Calibration Legacy of the ISO Mission", Metcalfe, Salama, Peschke, Kessler (eds.), ESA SP-481, 439 (2003)
73. Schmidt, B. E., Thomas, P. C., Bauer, J. M. et al.: The Shape and Surface Variation of 2 Pallas from the Hubble Space Telescope, Science 326, 275 (2009)
74. Schulz, B.: ISOPHOT Point Source Calibration - Wrapping It Up, Proceedings of the Conference "The Calibration Legacy of the ISO Mission", Metcalfe, Salama, Peschke, Kessler (eds.), ESA SP-481, 83 (2003)
75. Stansberry, J. A., Gordon, K. D., Bhattacharya, B. et al.: Absolute Calibration and Characterization of the Multiband Imaging Photometer for Spitzer. III. An Asteroid-based Calibration of MIPS at 160 micron, PASP 119, 1038 (2007)
76. Swinyard, B. M., Ade, P., Baluteau, J.-P. et al.: In-flight calibration of the Herschel-SPIRE instrument A&A, 518, 4S (2010)
77. Thomas, P. C., Binzel, R. P., Gaffey, M. J. et al.: Vesta: Spin Pole, Size, and Shape from HST Images, Icarus 128, 88, (1997)
78. Thomas, P. C., Parker, J. W., McFadden, L. A. et al.: Differentiation of the asteroid Ceres as revealed by its shape, Nature 437, 224-226 (2005)
79. Valtchanov, I. (2011), SPIRE Observer's Manual, HERSCHEL-DOC-0798, v. 2.4, June 7, 2011, `http://herschel.esac.esa.int/Docs/SPIRE/html/spire_om.html`
80. Wasserman, L. H., Millis, R. L., Franz, O. G. et al.: The diameter of Pallas from its occultation of SAO 85009, AJ 84, 259 (1979)
81. Werner, M. W., Roellig, T. L., Low, F. J. et al.: The Spitzer Space Telescope Mission, ApJS, 154, 1 (2004)
82. Wright, E. L., Eisenhardt, P. R. M., Mainzer, A. K. et al.: The wide-field infrared survey explorer (WISE): Mission description and initial on-orbit performance AJ 140, 1868-1881 (2010)

## Overview of available Herschel photometric measurements

In the following tables we list the available photometric observations (calibration and science observations) with one of the four asteroids in the field of view. Some of the early measurements were used with very different instrument settings and non-standard observing modes. The corresponding fluxes are not well calibrated and we excluded them from our analysis.

**Table 2** Overview of all relevant Herschel-PACS photometer scan-map observations of (1) Ceres.

| OD | OBSID | Proposal | Dur. | Start time | AOR Label |
|---|---|---|---|---|---|
| 1441 | 1342270856 | DDT_dbockele_3 | 286 | 2013-04-24T05:11:49Z | PPhoto-Ceres_Visit12 |
| 1441 | 1342270851 | DDT_dbockele_3 | 286 | 2013-04-24T04:04:45Z | PPhoto-Ceres_Visit11 |
| 1441 | 1342270846 | DDT_dbockele_3 | 286 | 2013-04-24T02:57:05Z | PPhoto-Ceres_Visit10 |
| 1441 | 1342270841 | DDT_dbockele_3 | 286 | 2013-04-24T01:51:57Z | PPhoto-Ceres_Visit09 |
| 1441 | 1342270828 | DDT_dbockele_3 | 286 | 2013-04-24T01:00:51Z | PPhoto-Ceres_Visit08 |
| 1441 | 1342270823 | DDT_dbockele_3 | 286 | 2013-04-23T23:54:43Z | PPhoto-Ceres_Visit07 |
| 1441 | 1342270818 | DDT_dbockele_3 | 286 | 2013-04-23T22:48:42Z | PPhoto-Ceres_Visit06 |
| 1441 | 1342270813 | DDT_dbockele_3 | 286 | 2013-04-23T21:41:50Z | PPhoto-Ceres_Visit05 |
| 1441 | 1342270808 | DDT_dbockele_3 | 286 | 2013-04-23T20:37:24Z | PPhoto-Ceres_Visit04 |
| 1441 | 1342270803 | DDT_dbockele_3 | 286 | 2013-04-23T19:43:14Z | PPhoto-Ceres_Visit03 |
| 1441 | 1342270798 | DDT_dbockele_3 | 286 | 2013-04-23T18:36:38Z | PPhoto-Ceres_Visit02 |
| 1441 | 1342270787 | DDT_dbockele_3 | 286 | 2013-04-23T17:41:20Z | PPhoto-Ceres_Visit01 |
| 1420 | 1342269279 | rppacs_189 | 286 | 2013-04-03T00:14:13Z | RPPhotFlux_1-RPPhotFlux_324B_sPS_110_200Jy_grn_Ceres_0007 |
| 1420 | 1342269278 | rppacs_189 | 286 | 2013-04-03T00:08:24Z | RPPhotFlux_1-RPPhotFlux_324B_sPS_070_200Jy_grn_Ceres_0007 |
| 1420 | 1342269276 | rppacs_189 | 286 | 2013-04-02T23:58:50Z | RPPhotFlux_1-RPPhotFlux_324B_sPS_110_200Jy_blu_Ceres_0007 |
| 1420 | 1342269275 | rppacs_189 | 286 | 2013-04-02T23:53:01Z | RPPhotFlux_1-RPPhotFlux_324B_sPS_070_200Jy_blu_Ceres_0007 |
| 1244 | 1342252878 | rppacs_159 | 1055 | 2012-10-09T14:41:09Z | RPPhotSpatial_1-RPPhotSpatial_314D_StdScan135_med_grn_Ceres_0003 |
| 1244 | 1342252877 | rppacs_159 | 1055 | 2012-10-09T14:22:31Z | RPPhotSpatial_1-RPPhotSpatial_314D_StdScan045_med_grn_Ceres_0003 |
| 1244 | 1342252876 | rppacs_159 | 1055 | 2012-10-09T14:03:53Z | RPPhotSpatial_1-RPPhotSpatial_314D_StdScan135_med_blue_Ceres_0003 |
| 1244 | 1342252875 | rppacs_159 | 1055 | 2012-10-09T13:45:15Z | RPPhotSpatial_1-RPPhotSpatial_314D_StdScan045_med_blue_Ceres_0003 |
| 1244 | 1342252874 | rppacs_159 | 286 | 2012-10-09T13:39:26Z | RPPhotFlux_1-RPPhotFlux_323B_sPS_110_210Jy_grn_c76_Ceres_06 |
| 1244 | 1342252873 | rppacs_159 | 286 | 2012-10-09T13:33:37Z | RPPhotFlux_1-RPPhotFlux_323B_sPS_070_210Jy_grn_c76_Ceres_06 |
| 1244 | 1342252871 | rppacs_159 | 286 | 2012-10-09T13:24:03Z | RPPhotFlux_1-RPPhotFlux_323B_sPS_110_370Jy_blu_c76_Ceres_06 |
| 1244 | 1342252870 | rppacs_159 | 286 | 2012-10-09T13:18:14Z | RPPhotFlux_1-RPPhotFlux_323B_sPS_070_370Jy_blu_c76_Ceres_06 |
| 1237 | 1342252062 | rppacs_157 | 286 | 2012-10-02T05:42:14Z | RPPhotFlux_1-RPPhotFlux_323B_sPS_110_156Jy_grn_c75_Ceres_05 |
| 1237 | 1342252061 | rppacs_157 | 286 | 2012-10-02T05:36:25Z | RPPhotFlux_1-RPPhotFlux_323B_sPS_070_156Jy_grn_c75_Ceres_05 |
| 1237 | 1342252059 | rppacs_157 | 286 | 2012-10-02T05:26:51Z | RPPhotFlux_1-RPPhotFlux_323B_sPS_110_274Jy_blu_c75_Ceres_05 |
| 1237 | 1342252058 | rppacs_157 | 286 | 2012-10-02T05:21:02Z | RPPhotFlux_1-RPPhotFlux_323B_sPS_070_274Jy_blu_c75_Ceres_05 |
| 947 | 1342234471 | rppacs_115 | 286 | 2011-12-17T00:53:38Z | RPPhotFlux_1-RPPhotFlux_631A_sPS_110_Planck_grn_Ceres_0003 |
| 947 | 1342234470 | rppacs_115 | 286 | 2011-12-17T00:47:49Z | RPPhotFlux_1-RPPhotFlux_631A_sPS_070_Planck_grn_Ceres_0003 |
| 947 | 1342234468 | rppacs_115 | 286 | 2011-12-17T00:38:15Z | RPPhotFlux_1-RPPhotFlux_631A_sPS_110_Planck_blu_Ceres_0003 |
| 947 | 1342234467 | rppacs_115 | 286 | 2011-12-17T00:32:26Z | RPPhotFlux_1-RPPhotFlux_631A_sPS_070_Planck_blu_Ceres_0003 |
| 782 | 1342223707 | rppacs_88 | 1055 | 2011-07-05T04:06:57Z | RPPhotSpatial_1-RPPhotSpatial_314D_StdScan135_med_grn_Ceres_0002 |
| 782 | 1342223706 | rppacs_88 | 1055 | 2011-07-05T03:48:19Z | RPPhotSpatial_1-RPPhotSpatial_314D_StdScan045_med_grn_Ceres_0002 |
| 782 | 1342223705 | rppacs_88 | 286 | 2011-07-05T03:42:30Z | RPPhotFlux_1-RPPhotFlux_323B_sPS_110_144Jy_grn_c43_Ceres_03 |
| 782 | 1342223704 | rppacs_88 | 286 | 2011-07-05T03:36:41Z | RPPhotFlux_1-RPPhotFlux_323B_sPS_070_144Jy_grn_c43_Ceres_03 |
| 782 | 1342223702 | rppacs_88 | 1055 | 2011-07-05T03:14:18Z | RPPhotSpatial_1-RPPhotSpatial_314D_StdScan135_med_blue_Ceres_0002 |
| 782 | 1342223701 | rppacs_88 | 1055 | 2011-07-05T02:55:40Z | RPPhotSpatial_1-RPPhotSpatial_314D_StdScan045_med_blue_Ceres_0002 |
| 782 | 1342223700 | rppacs_88 | 286 | 2011-07-05T02:49:51Z | RPPhotFlux_1-RPPhotFlux_323B_sPS_110_251Jy_blu_c43_Ceres_03 |
| 782 | 1342223699 | rppacs_88 | 286 | 2011-07-05T02:44:02Z | RPPhotFlux_1-RPPhotFlux_323B_sPS_070_251Jy_blu_c43_Ceres_03 |
| 769 | 1342222942 | rppacs_86 | 286 | 2011-06-22T14:28:59Z | RPPhotFlux_1-RPPhotFlux_323B_sPS_110_127Jy_grn_c42_Ceres_03 |
| 769 | 1342222941 | rppacs_86 | 286 | 2011-06-22T14:23:10Z | RPPhotFlux_1-RPPhotFlux_323B_sPS_070_127Jy_grn_c42_Ceres_03 |
| 769 | 1342222939 | rppacs_86 | 286 | 2011-06-22T14:13:36Z | RPPhotFlux_1-RPPhotFlux_323B_sPS_110_222Jy_blu_c42_Ceres_03 |
| 769 | 1342222938 | rppacs_86 | 286 | 2011-06-22T14:07:47Z | RPPhotFlux_1-RPPhotFlux_323B_sPS_070_222Jy_blu_c42_Ceres_03 |
| 759 | 1342222570 | rppacs_84 | 286 | 2011-06-12T07:36:42Z | RPPhotFlux_1-RPPhotFlux_323B_sPS_110_116Jy_grn_c41_Ceres_03 |
| 759 | 1342222569 | rppacs_84 | 286 | 2011-06-12T07:30:53Z | RPPhotFlux_1-RPPhotFlux_323B_sPS_070_116Jy_grn_c41_Ceres_03 |
| 759 | 1342222567 | rppacs_84 | 286 | 2011-06-12T07:21:19Z | RPPhotFlux_1-RPPhotFlux_323B_sPS_110_202Jy_blu_c41_Ceres_03 |
| 759 | 1342222566 | rppacs_84 | 286 | 2011-06-12T07:15:30Z | RPPhotFlux_1-RPPhotFlux_323B_sPS_070_202Jy_blu_c41_Ceres_03 |
| 743 | 1342221742 | rppacs_82 | 286 | 2011-05-27T06:23:31Z | RPPhotFlux_1-RPPhotFlux_323B_sPS_110_100Jy_grn_c40_Ceres_03 |
| 743 | 1342221741 | rppacs_82 | 286 | 2011-05-27T06:17:42Z | RPPhotFlux_1-RPPhotFlux_323B_sPS_070_100Jy_grn_c40_Ceres_03 |
| 743 | 1342221739 | rppacs_82 | 286 | 2011-05-27T06:08:08Z | RPPhotFlux_1-RPPhotFlux_323B_sPS_110_174Jy_blu_c40_Ceres_03 |
| 743 | 1342221738 | rppacs_82 | 286 | 2011-05-27T06:02:19Z | RPPhotFlux_1-RPPhotFlux_323B_sPS_070_174Jy_blu_c40_Ceres_03 |
| 734 | 1342221353 | rppacs_79 | 1055 | 2011-05-18T12:15:24Z | RPPhotSpatial_1-RPPhotSpatial_314D_StdScan135_med_grn_Ceres_0001 |
| 734 | 1342221352 | rppacs_79 | 1055 | 2011-05-18T11:56:46Z | RPPhotSpatial_1-RPPhotSpatial_314D_StdScan045_med_grn_Ceres_0001 |
| 734 | 1342221351 | rppacs_79 | 1055 | 2011-05-18T11:38:08Z | RPPhotSpatial_1-RPPhotSpatial_314D_StdScan135_med_blue_Ceres_0001 |
| 734 | 1342221350 | rppacs_79 | 1055 | 2011-05-18T11:19:30Z | RPPhotSpatial_1-RPPhotSpatial_314D_StdScan045_med_blue_Ceres_0001 |
| 726 | 1342220297 | rppacs_79 | 286 | 2011-05-10T03:03:46Z | RPPhotFlux_1-RPPhotFlux_323B_sPS_110_95Jy_grn_c39_Ceres_03 |
| 726 | 1342220296 | rppacs_79 | 286 | 2011-05-10T02:57:57Z | RPPhotFlux_1-RPPhotFlux_323B_sPS_070_95Jy_grn_c39_Ceres_03 |
| 726 | 1342220294 | rppacs_79 | 286 | 2011-05-10T02:48:23Z | RPPhotFlux_1-RPPhotFlux_323B_sPS_110_166Jy_blu_c39_Ceres_03 |
| 726 | 1342220293 | rppacs_79 | 286 | 2011-05-10T02:42:34Z | RPPhotFlux_1-RPPhotFlux_323B_sPS_070_166Jy_blu_c39_Ceres_03 |
| 485 | 1342204328 | rppacs_43 | 286 | 2010-09-10T22:30:35Z | RPPhotFlux_1-RPPhotFlux_631A_sPS_110_Planck_grn_Ceres_0001 |
| 485 | 1342204327 | rppacs_43 | 286 | 2010-09-10T22:24:46Z | RPPhotFlux_1-RPPhotFlux_631A_sPS_070_Planck_grn_Ceres_0001 |
| 485 | 1342204325 | rppacs_43 | 286 | 2010-09-10T22:15:12Z | RPPhotFlux_1-RPPhotFlux_631A_sPS_110_Planck_blu_Ceres_0001 |
| 485 | 1342204324 | rppacs_43 | 286 | 2010-09-10T22:09:23Z | RPPhotFlux_1-RPPhotFlux_631A_sPS_070_Planck_blu_Ceres_0001 |
| 286 | 1342191134 | rppacs_7 | 276 | 2010-02-24T04:08:56Z | RPPhotFlux_1-RPPhotFlux_324B_sPS_110_200Jy_grn_Ceres_0001 |
| 286 | 1342191133 | rppacs_7 | 276 | 2010-02-24T04:03:17Z | RPPhotFlux_1-RPPhotFlux_324B_sPS_070_200Jy_grn_Ceres_0001 |
| 286 | 1342191131 | rppacs_7 | 276 | 2010-02-24T03:53:53Z | RPPhotFlux_1-RPPhotFlux_324B_sPS_110_200Jy_blu_Ceres_0001 |
| 286 | 1342191130 | rppacs_7 | 276 | 2010-02-24T03:48:14Z | RPPhotFlux_1-RPPhotFlux_324B_sPS_070_200Jy_blu_Ceres_0001 |

**Table 3** Overview of all relevant Herschel-PACS photometer chop-nod observations of (1) Ceres.

| OD | OBSID | Proposal | Dur. | Start time | AOR Label |
|---|---|---|---|---|---|
| 1420 | 1342269277 | rppacs_189 | 162 | 2013-04-03T00:04:39Z | RPPhotFlux_1-RPPhotFlux_324A_cPS_200Jy_grn_Ceres_0007 |
| 1420 | 1342269274 | rppacs_189 | 162 | 2013-04-02T23:49:16Z | RPPhotFlux_1-RPPhotFlux_324A_cPS_200Jy_blu_Ceres_0007 |
| 1244 | 1342252872 | rppacs_159 | 162 | 2012-10-09T13:29:52Z | RPPhotFlux_1-RPPhotFlux_323A_cPS_210Jy_grn_c76_Ceres_06 |
| 1244 | 1342252869 | rppacs_159 | 162 | 2012-10-09T13:14:29Z | RPPhotFlux_1-RPPhotFlux_323A_cPS_370Jy_blu_c76_Ceres_06 |
| 1237 | 1342252060 | rppacs_157 | 162 | 2012-10-02T05:32:40Z | RPPhotFlux_1-RPPhotFlux_323A_cPS_156Jy_grn_c75_Ceres_05 |
| 1237 | 1342252057 | rppacs_157 | 162 | 2012-10-02T05:17:17Z | RPPhotFlux_1-RPPhotFlux_323A_cPS_274Jy_blu_c75_Ceres_05 |
| 947 | 1342234469 | rppacs_115 | 162 | 2011-12-17T00:44:04Z | RPPhotFlux_1-RPPhotFlux_324A_cPS_200Jy_grn_Ceres_0004 |
| 947 | 1342234466 | rppacs_115 | 162 | 2011-12-17T00:28:41Z | RPPhotFlux_1-RPPhotFlux_324A_cPS_200Jy_blu_Ceres_0004 |
| 782 | 1342223703 | rppacs_88 | 162 | 2011-07-05T03:32:56Z | RPPhotFlux_1-RPPhotFlux_323A_cPS_144Jy_grn_c43_Ceres_03 |
| 782 | 1342223698 | rppacs_88 | 162 | 2011-07-05T02:40:17Z | RPPhotFlux_1-RPPhotFlux_323A_cPS_251Jy_blu_c43_Ceres_03 |
| 769 | 1342222940 | rppacs_86 | 162 | 2011-06-22T14:19:25Z | RPPhotFlux_1-RPPhotFlux_323A_cPS_127Jy_grn_c42_Ceres_03 |
| 769 | 1342222937 | rppacs_86 | 162 | 2011-06-22T14:04:02Z | RPPhotFlux_1-RPPhotFlux_323A_cPS_222Jy_blu_c42_Ceres_03 |
| 759 | 1342222568 | rppacs_84 | 162 | 2011-06-12T07:27:08Z | RPPhotFlux_1-RPPhotFlux_323A_cPS_116Jy_grn_c41_Ceres_03 |
| 759 | 1342222565 | rppacs_84 | 162 | 2011-06-12T07:11:45Z | RPPhotFlux_1-RPPhotFlux_323A_cPS_202Jy_blu_c41_Ceres_03 |
| 743 | 1342221740 | rppacs_82 | 162 | 2011-05-27T06:13:57Z | RPPhotFlux_1-RPPhotFlux_323A_cPS_95Jy_grn_c40_Ceres_03 |
| 743 | 1342221737 | rppacs_82 | 162 | 2011-05-27T05:58:34Z | RPPhotFlux_1-RPPhotFlux_323A_cPS_174Jy_blu_c40_Ceres_03 |
| 726 | 1342220295 | rppacs_79 | 162 | 2011-05-10T02:54:12Z | RPPhotFlux_1-RPPhotFlux_323A_cPS_95Jy_grn_c39_Ceres_03 |
| 726 | 1342220292 | rppacs_79 | 162 | 2011-05-10T02:38:49Z | RPPhotFlux_1-RPPhotFlux_323A_cPS_166Jy_blu_c39_Ceres_03 |
| 485 | 1342204326 | rppacs_43 | 162 | 2010-09-10T22:21:01Z | RPPhotFlux_1-RPPhotFlux_324A_cPS_200Jy_grn_Ceres_0002 |
| 485 | 1342204323 | rppacs_43 | 162 | 2010-09-10T22:05:38Z | RPPhotFlux_1-RPPhotFlux_324A_cPS_200Jy_blu_Ceres_0002 |
| 286 | 1342191132 | rppacs_7 | 162 | 2010-02-24T03:59:32Z | RPPhotFlux_1-RPPhotFlux_324A_cPS_200Jy_grn_Ceres_0001 |
| 286 | 1342191129 | rppacs_7 | 162 | 2010-02-24T03:44:29Z | RPPhotFlux_1-RPPhotFlux_324A_cPS_200Jy_blu_Ceres_0001 |

**Table 4** Overview of all relevant Herschel-SPIRE photometer observations of (1) Ceres. SmMap: small scan map mode; LgMap: large scan map mode; Scan: non-standard scan map; PS: point-source mode.

| OD | OBSID | Proposal | Dur. | Start time | Mode | AOR Label |
|---|---|---|---|---|---|---|
| 1434 | 1342270325 | rpspire_164 | 593 | 2013-04-17T11:24:44Z | SmMap | cycle89_1-SPhoto-SmallM-Rep4-Ceres |
| 1411 | 1342268344 | rpspire_162 | 593 | 2013-03-25T02:48:32Z | SmMap | cycle88_1-SPhoto-SmallM-Rep4-Ceres |
| 1403 | 1342267748 | rpspire_160 | 593 | 2013-03-17T05:06:15Z | SmMap | cycle87_1-SPhoto-SmallM-Rep4-Ceres |
| 1387 | 1342266670 | rpspire_158 | 2057 | 2013-03-01T03:26:27Z | SmMap | cycle86_1-SPhoto-LargeM-Rep4-10x10-Ceres |
| 1249 | 1342253388 | rpspire_138 | 593 | 2012-10-13T22:38:27Z | SmMap | cycle76_1-SPhoto-SmallM-Rep4-Ceres |
| 1235 | 1342251687 | rpspire_136 | 593 | 2012-09-29T22:43:32Z | SmMap | cycle75_3-SPhoto-SmallM-Rep4-Ceres |
| 1215 | 1342250803 | rpspire_132 | 593 | 2012-09-10T12:49:19Z | SmMap | cycle74_1-SPhoto-SmallM-Rep4-Ceres |
| 1201 | 1342250325 | rpspire_130 | 593 | 2012-08-26T16:59:32Z | SmMap | cycle73_1-SPhoto-SmallM-Rep4-Ceres |
| 1197 | 1342250643 | rpspire_128 | 593 | 2012-08-22T16:21:13Z | SmMap | cycle72_1-SPhoto-SmallM-Rep4-Ceres |
| 964 | 1342236236 | rpspire_92 | 593 | 2012-01-02T17:09:51Z | SmMap | cycle56_1-SPhoto-SmallM-Rep4-Ceres |
| 964 | 1342236235 | rpspire_92 | 602 | 2012-01-02T16:59:19Z | SmMap | cycle56_1-SPhoto-SmallM-Rep4-Ceres-Bright |
| 948 | 1342234931 | rpspire_90 | 593 | 2011-12-18T11:43:28Z | SmMap | cycle55_1-SPhoto-SmallM-Rep4-Ceres |
| 775 | 1342223221 | rpspire_64 | 593 | 2011-06-28T14:02:23Z | SmMap | cycle42_1-SPhoto-SmallM-Rep4-Ceres |
| 725 | 1342220642 | rpspire_58 | 593 | 2011-05-08T23:05:52Z | SmMap | cycle39_3-SPhoto-SmallM-Rep4-Ceres |
| 529 | 1342207050 | rpspire_30 | 593 | 2010-10-24T22:55:51Z | SmMap | cycle25_1-SPhoto-SmallM-Rep4-Ceres |
| 521 | 1342206682 | rpspire_28 | 593 | 2010-10-17T14:18:39Z | SmMap | cycle24_1-SPhoto-SmallM-Rep4-Ceres - 0001 |
| 515 | 1342206204 | rpspire_28 | 593 | 2010-10-11T09:35:44Z | SmMap | cycle24_1-SPhoto-SmallM-Rep4-Ceres |
| 499 | 1342205096 | rpspire_27 | 593 | 2010-09-25T15:46:17Z | SmMap | cycle23_2-SPhoto-SmallM-Rep4-Ceres |
| 486 | 1342204371 | rpspire_26 | 2977 | 2010-09-12T14:59:47Z | LgMap | cycle22_1-SPhoto-LargeM-Rep4-15x15-Ceres |
| 479 | 1342204062 | rpspire_25 | 1356 | 2010-09-05T14:15:13Z | PS | cycle21_1-SPhoto-PointS-Rep4-Ceres |
| 479 | 1342204061 | rpspire_25 | 593 | 2010-09-05T14:04:55Z | SmMap | cycle21_1-SPhoto-SmallM-Rep4-Ceres - 0001 |
| 326 | 1342193790 | rpspire_14 | 1334 | 2010-04-05T03:24:54Z | LgMap | cycle11_1-SPhoto-Large-Rep4-8x8-Ceres |
| 326 | 1342193789 | rpspire_14 | 1356 | 2010-04-05T03:01:46Z | PS | cycle11_1-SPhoto-Point-Rep4-Ceres |
| 326 | 1342193788 | rpspire_14 | 593 | 2010-04-05T02:51:28Z | SmMap | cycle11_1-SPhoto-SmallRep4-Ceres |
| 287 | 1342191193 | rpspire_8 | 1351 | 2010-02-25T16:53:39Z | LgMap | cycle8_1-SPhoto-Large-Rep4-8x8-Ceres - copy |
| 287 | 1342191192 | rpspire_8 | 1371 | 2010-02-25T16:30:16Z | PS | cycle8_1-SPhoto-Point-Rep4-Ceres - copy |
| 275 | 1342190670 | rpspire_8 | 610 | 2010-02-13T11:51:24Z | SmMap | cycle8_1-SpirePhotoSmallScanGen-Rep4-Ceres |
| 275 | 1342190669 | rpspire_8 | 1351 | 2010-02-13T11:28:19Z | LgMap | cycle8_1-SPhoto-Large-Rep4-8x8-Ceres |
| 275 | 1342190668 | rpspire_8 | 1371 | 2010-02-13T11:04:56Z | PS | cycle8_1-SPhoto-Point-Rep4-Ceres |
| 50 | 1342179358 | copspire_18 | 2340 | 2009-07-02T23:46:08Z | Scan | H_COP_SJL_OD50_01_1-SPhoto-10x10AB4RepNominal-Ceres |
| 50 | 1342179356 | copspire_18 | 2159 | 2009-07-02T23:05:52Z | Scan | H_COP_SJL_OD50_01_1-SPhoto-10x10AB4RepFast-Ceres |

**Table 5** Overview of all relevant Herschel-HIFI point observations of (1) Ceres.

| OD | OBSID | Proposal | Dur. | Start time | AOR Label |
|---|---|---|---|---|---|
| 1392 | 1342266021 | DDT_mkuepper_1 | 9146 | 2013-03-06T10:37:47Z | HPoint-Ceres-DDT-Feb2013_Part4 |
| 1392 | 1342266020 | DDT_mkuepper_1 | 9146 | 2013-03-06T08:03:55Z | HPoint-Ceres-DDT-Feb2013_Part3 |
| 1392 | 1342266019 | DDT_mkuepper_1 | 9146 | 2013-03-06T05:30:03Z | HPoint-Ceres-DDT-Feb2013_Part2 |
| 1392 | 1342266018 | DDT_mkuepper_1 | 8575 | 2013-03-06T03:05:42Z | HPoint-Ceres-DDT-Feb2013_Part1 |
| 1260 | 1342254428 | DDT_mkuepper_1 | 8575 | 2012-10-24T20:04:28Z | HPoint-Ceres-GT1-lorourke-DDT-Oct2012 |
| 1247 | 1342253122 | GT1_lorourke_9 | 8245 | 2012-10-11T19:53:46Z | HPoint-Ceres-GT1-lorourke-Feb2013 |
| 923 | 1342232694 | GT1_lorourke_9 | 4010 | 2011-11-23T11:31:20Z | HPoint-Ceres-GT1-lorourke- Nov2011 |

**Table 6** Overview of all relevant Herschel-PACS photometer scan-map observations of (2) Pallas.

| OD | OBSID | Proposal | Dur. | Start time | AOR Label |
|---|---|---|---|---|---|
| 1295 | 1342256237 | rppacs_167 | 286 | 2012-11-29T06:28:31Z | RPPhotFlux_1-RPPhotFlux_324B_sPS_110_200Jy_blu_Pallas_0006 |
| 1295 | 1342256236 | rppacs_167 | 286 | 2012-11-29T06:22:42Z | RPPhotFlux_1-RPPhotFlux_324B_sPS_070_200Jy_blu_Pallas_0006 |
| 1295 | 1342256234 | rppacs_167 | 286 | 2012-11-29T06:13:08Z | RPPhotFlux_1-RPPhotFlux_324B_sPS_110_50Jy_red_Pallas_0006 |
| 1295 | 1342256233 | rppacs_167 | 286 | 2012-11-29T06:07:19Z | RPPhotFlux_1-RPPhotFlux_324B_sPS_070_50Jy_red_Pallas_0006 |
| 1139 | 1342247437 | rppacs_143 | 286 | 2012-06-25T21:08:55Z | RPPhotFlux_1-RPPhotFlux_324B_sPS_110_200Jy_blu_Pallas_0005 |
| 1139 | 1342247436 | rppacs_143 | 286 | 2012-06-25T21:03:06Z | RPPhotFlux_1-RPPhotFlux_324B_sPS_070_200Jy_blu_Pallas_0005 |
| 1139 | 1342247434 | rppacs_143 | 286 | 2012-06-25T20:53:32Z | RPPhotFlux_1-RPPhotFlux_324B_sPS_110_50Jy_red_Pallas_0005 |
| 1139 | 1342247433 | rppacs_143 | 286 | 2012-06-25T20:47:43Z | RPPhotFlux_1-RPPhotFlux_324B_sPS_070_50Jy_red_Pallas_0005 |
| 889 | 1342231268 | rppacs_105 | 286 | 2011-10-20T04:39:02Z | RPPhotFlux_1-RPPhotFlux_631A_sPS_110_Planck_grn_Pallas_0003 |
| 889 | 1342231267 | rppacs_105 | 286 | 2011-10-20T04:33:13Z | RPPhotFlux_1-RPPhotFlux_631A_sPS_070_Planck_grn_Pallas_0003 |
| 889 | 1342231265 | rppacs_105 | 286 | 2011-10-20T04:23:39Z | RPPhotFlux_1-RPPhotFlux_631A_sPS_110_Planck_blu_Pallas_0003 |
| 889 | 1342231264 | rppacs_105 | 286 | 2011-10-20T04:17:50Z | RPPhotFlux_1-RPPhotFlux_631A_sPS_070_Planck_blu_Pallas_0003 |
| 720 | 1342220591 | rppacs_77 | 286 | 2011-05-04T11:45:19Z | RPPhotFlux_1-RPPhotFlux_631A_sPS_110_Planck_grn_Pallas_0002 |
| 720 | 1342220590 | rppacs_77 | 286 | 2011-05-04T11:39:30Z | RPPhotFlux_1-RPPhotFlux_631A_sPS_070_Planck_grn_Pallas_0002 |
| 720 | 1342220589 | rppacs_77 | 286 | 2011-05-04T11:33:41Z | RPPhotFlux_1-RPPhotFlux_631A_sPS_110_Planck_blu_Pallas_0002 |
| 720 | 1342220588 | rppacs_77 | 286 | 2011-05-04T11:27:52Z | RPPhotFlux_1-RPPhotFlux_631A_sPS_070_Planck_blu_Pallas_0002 |
| 686 | 1342217785 | rppacs_74 | 286 | 2011-03-31T13:25:38Z | RPPhotFlux_1-RPPhotFlux_324B_sPS_110_50Jy_red_Pallas_0003 |
| 686 | 1342217784 | rppacs_74 | 286 | 2011-03-31T13:19:49Z | RPPhotFlux_1-RPPhotFlux_324B_sPS_070_50Jy_red_Pallas_0003 |
| 686 | 1342217782 | rppacs_74 | 286 | 2011-03-31T13:10:15Z | RPPhotFlux_1-RPPhotFlux_324B_sPS_110_200Jy_blu_Pallas_0003 |
| 686 | 1342217781 | rppacs_74 | 286 | 2011-03-31T13:04:26Z | RPPhotFlux_1-RPPhotFlux_324B_sPS_070_200Jy_blu_Pallas_0003 |
| 446 | 1342202080 | rppacs_33 | 286 | 2010-08-02T18:35:22Z | RPPhotFlux_1-RPPhotFlux_631A_sPS_110_Planck_grn_Pallas_0001 |
| 446 | 1342202079 | rppacs_33 | 286 | 2010-08-02T18:29:33Z | RPPhotFlux_1-RPPhotFlux_631A_sPS_070_Planck_grn_Pallas_0001 |
| 446 | 1342202077 | rppacs_33 | 286 | 2010-08-02T18:19:59Z | RPPhotFlux_1-RPPhotFlux_631A_sPS_110_Planck_blu_Pallas_0001 |
| 446 | 1342202076 | rppacs_33 | 286 | 2010-08-02T18:14:10Z | RPPhotFlux_1-RPPhotFlux_631A_sPS_070_Planck_blu_Pallas_0001 |
| 245 | 1342189267 | rppacs_5 | 254 | 2010-01-14T08:00:09Z | RPPhotFlux_1-RPPhotFlux_324B_sPS_117_50Jy_red_Pallas_0001 |
| 245 | 1342189266 | rppacs_5 | 254 | 2010-01-14T07:54:52Z | RPPhotFlux_1-RPPhotFlux_324B_sPS_063_50Jy_red_Pallas_0001 |
| 245 | 1342189265 | rppacs_5 | 254 | 2010-01-14T07:49:35Z | RPPhotFlux_1-RPPhotFlux_324B_sPS_117_200Jy_blu_Pallas_0001 |
| 245 | 1342189264 | rppacs_5 | 254 | 2010-01-14T07:44:18Z | RPPhotFlux_1-RPPhotFlux_324B_sPS_063_200Jy_blu_Pallas_0001 |

**Table 7** Overview of all relevant Herschel-PACS photometer chop-nod observations of (2) Pallas.

| OD | OBSID | Proposal | Dur. | Start time | AOR Label |
|---|---|---|---|---|---|
| 1295 | 1342256235 | rppacs_167 | 162 | 2012-11-29T06:18:57Z | RPPhotFlux_1-RPPhotFlux_324A_cPS_200Jy_blu_Pallas_0006 |
| 1295 | 1342256232 | rppacs_167 | 162 | 2012-11-29T06:03:34Z | RPPhotFlux_1-RPPhotFlux_324A_cPS_50Jy_red_Pallas_0006 |
| 1139 | 1342247435 | rppacs_143 | 162 | 2012-06-25T20:59:21Z | RPPhotFlux_1-RPPhotFlux_324A_cPS_200Jy_blu_Pallas_0005 |
| 1139 | 1342247432 | rppacs_143 | 162 | 2012-06-25T20:43:58Z | RPPhotFlux_1-RPPhotFlux_324A_cPS_50Jy_red_Pallas_0005 |
| 889 | 1342231266 | rppacs_105 | 162 | 2011-10-20T04:29:28Z | RPPhotFlux_1-RPPhotFlux_324A_cPS_50Jy_red_Pallas_0004 |
| 889 | 1342231263 | rppacs_105 | 162 | 2011-10-20T04:14:05Z | RPPhotFlux_1-RPPhotFlux_324A_cPS_200Jy_blu_Pallas_0004 |
| 686 | 1342217783 | rppacs_74 | 162 | 2011-03-31T13:16:04Z | RPPhotFlux_1-RPPhotFlux_324A_cPS_50Jy_red_Pallas_0003 |
| 686 | 1342217780 | rppacs_74 | 162 | 2011-03-31T13:00:41Z | RPPhotFlux_1-RPPhotFlux_324A_cPS_200Jy_blu_Pallas_0003 |
| 446 | 1342202078 | rppacs_33 | 162 | 2010-08-02T18:25:48Z | RPPhotFlux_1-RPPhotFlux_324A_cPS_50Jy_red_Pallas_0002 |
| 446 | 1342202075 | rppacs_33 | 162 | 2010-08-02T18:10:25Z | RPPhotFlux_1-RPPhotFlux_324A_cPS_200Jy_blu_Pallas_0002 |
| 245 | 1342189263 | rppacs_5 | 162 | 2010-01-14T07:40:33Z | RPPhotFlux_1-RPPhotFlux_324A_cPS_50Jy_red_Pallas_0001 |
| 245 | 1342189262 | rppacs_5 | 162 | 2010-01-14T07:36:48Z | RPPhotFlux_1-RPPhotFlux_324A_cPS_200Jy_blu_Pallas_0001 |

**Table 8** Overview of all relevant Herschel-SPIRE photometer observations of (2) Pallas, like in Table 4.

| OD | OBSID | Proposal | Dur. | Start time | Mode | AOR Label |
|---|---|---|---|---|---|---|
| 1348 | 1342261598 | rpspire_152 | 1356 | 2013-01-20T17:07:59Z | PS | cycle83_1-SPhoto-PointS-Rep4-Pallas |
| 1348 | 1342261597 | rpspire_152 | 593 | 2013-01-20T16:57:41Z | SmMap | cycle83_1-SPhoto-SmallM-Rep4-Pallas |
| 1330 | 1342258378 | rpspire_150 | 593 | 2013-01-03T03:48:49Z | SmMap | cycle82_1-SPhoto-SmallM-Rep4-Pallas |
| 1314 | 1342257361 | rpspire_148 | 593 | 2012-12-17T18:49:33Z | SmMap | cycle81_1-SPhoto-SmallM-Rep4-Pallas |
| 1156 | 1342247987 | rpspire_123 | 593 | 2012-07-12T21:20:45Z | SmMap | cycle70_1-SPhoto-SmallM-Rep4-Pallas |
| 1156 | 1342247986 | rpspire_123 | 1356 | 2012-07-12T20:57:41Z | PS | cycle70_1-SPhoto-PointS-Rep4-Pallas |
| 1116 | 1342246576 | rpspire_117 | 593 | 2012-06-02T20:31:54Z | SmMap | cycle67_1-SPhoto-SmallM-Rep4-Pallas |
| 915 | 1342232342 | rpspire_84 | 593 | 2011-11-15T14:26:03Z | SmMap | cycle52_1-SPhoto-SmallM-Rep4-Pallas |
| 880 | 1342230881 | rpspire_80 | 593 | 2011-10-11T13:23:13Z | SmMap | cycle50_1-SPhoto-SmallM-Rep4-Pallas |
| 718 | 1342219819 | rpspire_56 | 2977 | 2011-05-02T22:08:38Z | LgMap | cycle38_2-SPhoto-LargeM-Rep4-15x15-Pallas |
| 683 | 1342216957 | rpspire_52 | 593 | 2011-03-28T23:08:45Z | SmMap | cycle36_1-SPhoto-SmallM-Rep4-Pallas |
| 467 | 1342203584 | rpspire_24 | 593 | 2010-08-23T20:01:40Z | SmMap | cycle20_1-SPhoto-SmallM-Rep4-Pallas - 0001 |
| 458 | 1342203076 | rpspire_24 | 593 | 2010-08-15T13:13:44Z | SmMap | cycle20_1-SPhoto-SmallM-Rep4-Pallas |
| 447 | 1342202207 | rpspire_22 | 2977 | 2010-08-04T11:56:14Z | LgMap | cycle19_1-SPhoto-LargeM-Rep4-15x15-Pallas |
| 423 | 1342200202 | rpspire_20 | 1334 | 2010-07-11T07:15:37Z | LgMap | cycle17_1-SPhoto-LargeM-Rep4-8x8-Pallas - 0001 |
| 423 | 1342200201 | rpspire_20 | 593 | 2010-07-11T07:05:11Z | SmMap | cycle17_1-SPhoto-SmallM-Rep4-Pallas - 0001 |
| 423 | 1342200200 | rpspire_20 | 1356 | 2010-07-11T06:42:07Z | PS | cycle17_1-SPhoto-PointS-Rep4-Pallas - 0001 |
| 417 | 1342199784 | rpspire_20 | 1334 | 2010-07-05T11:32:44Z | LgMap | cycle17_1-SPhoto-LargeM-Rep4-8x8-Pallas |
| 417 | 1342199783 | rpspire_20 | 593 | 2010-07-05T11:22:18Z | SmMap | cycle17_1-SPhoto-SmallM-Rep4-Pallas |
| 417 | 1342199782 | rpspire_20 | 1356 | 2010-07-05T10:59:14Z | PS | cycle17_1-SPhoto-PointS-Rep4-Pallas |

**Table 9** Overview of all relevant Herschel-PACS photometer scan-map observations of (4) Vesta.

| OD | OBSID | Proposal | Dur. | Start time | AOR Label |
|---|---|---|---|---|---|
| 1377 | 1342263925 | rppacs_179 | 286 | 2013-02-19T09:06:16Z | RPPhotFlux_1-RPPhotFlux_324B_sPS_110_200Jy_blu_Vesta_0006 |
| 1377 | 1342263924 | rppacs_179 | 286 | 2013-02-19T09:00:27Z | RPPhotFlux_1-RPPhotFlux_324B_sPS_070_200Jy_blu_Vesta_0006 |
| 1377 | 1342263922 | rppacs_179 | 286 | 2013-02-19T08:50:53Z | RPPhotFlux_1-RPPhotFlux_324B_sPS_110_100Jy_grn_Vesta_0006 |
| 1377 | 1342263921 | rppacs_179 | 286 | 2013-02-19T08:45:04Z | RPPhotFlux_1-RPPhotFlux_324B_sPS_070_100Jy_grn_Vesta_0006 |
| 1202 | 1342250299 | rppacs_153 | 286 | 2012-08-28T04:03:03Z | RPPhotFlux_1-RPPhotFlux_323B_sPS_110_88Jy_blu_c73_Vesta_05 |
| 1202 | 1342250298 | rppacs_153 | 286 | 2012-08-28T03:57:14Z | RPPhotFlux_1-RPPhotFlux_323B_sPS_070_88Jy_blu_c73_Vesta_05 |
| 900 | 1342231693 | rppacs_105 | 286 | 2011-10-31T03:31:07Z | RPPhotFlux_1-RPPhotFlux_631A_sPS_110_Planck_grn_Vesta_0003 |
| 900 | 1342231692 | rppacs_105 | 286 | 2011-10-31T03:25:18Z | RPPhotFlux_1-RPPhotFlux_631A_sPS_070_Planck_grn_Vesta_0003 |
| 900 | 1342231690 | rppacs_105 | 286 | 2011-10-31T03:15:44Z | RPPhotFlux_1-RPPhotFlux_631A_sPS_110_Planck_blu_Vesta_0003 |
| 900 | 1342231689 | rppacs_105 | 286 | 2011-10-31T03:09:55Z | RPPhotFlux_1-RPPhotFlux_631A_sPS_070_Planck_blu_Vesta_0003 |
| 743 | 1342221728 | rppacs_82 | 286 | 2011-05-27T02:27:26Z | RPPhotFlux_1-RPPhotFlux_323B_sPS_110_120Jy_grn_c40_Vesta_03 |
| 743 | 1342221727 | rppacs_82 | 286 | 2011-05-27T02:21:37Z | RPPhotFlux_1-RPPhotFlux_323B_sPS_070_120Jy_grn_c40_Vesta_03 |
| 743 | 1342221725 | rppacs_82 | 286 | 2011-05-27T02:12:03Z | RPPhotFlux_1-RPPhotFlux_323B_sPS_110_211Jy_blu_c40_Vesta_03 |
| 743 | 1342221724 | rppacs_82 | 286 | 2011-05-27T02:06:14Z | RPPhotFlux_1-RPPhotFlux_323B_sPS_070_211Jy_blu_c40_Vesta_03 |
| 726 | 1342220291 | rppacs_79 | 286 | 2011-05-10T02:27:48Z | RPPhotFlux_1-RPPhotFlux_323B_sPS_110_100Jy_grn_c39_Vesta_03 |
| 726 | 1342220290 | rppacs_79 | 286 | 2011-05-10T02:21:59Z | RPPhotFlux_1-RPPhotFlux_323B_sPS_070_100Jy_grn_c39_Vesta_03 |
| 726 | 1342220288 | rppacs_79 | 286 | 2011-05-10T02:12:25Z | RPPhotFlux_1-RPPhotFlux_323B_sPS_110_176Jy_blu_c39_Vesta_03 |
| 726 | 1342220287 | rppacs_79 | 286 | 2011-05-10T02:06:36Z | RPPhotFlux_1-RPPhotFlux_323B_sPS_070_176Jy_blu_c39_Vesta_03 |
| 720 | 1342220587 | rppacs_77 | 286 | 2011-05-04T11:17:05Z | RPPhotFlux_1-RPPhotFlux_323B_sPS_110_90Jy_grn_c38_Vesta_03 |
| 720 | 1342220586 | rppacs_77 | 286 | 2011-05-04T11:11:16Z | RPPhotFlux_1-RPPhotFlux_323B_sPS_070_90Jy_grn_c38_Vesta_03 |
| 720 | 1342220584 | rppacs_77 | 286 | 2011-05-04T11:01:42Z | RPPhotFlux_1-RPPhotFlux_323B_sPS_110_159Jy_blu_c38_Vesta_03 |
| 720 | 1342220583 | rppacs_77 | 286 | 2011-05-04T10:55:53Z | RPPhotFlux_1-RPPhotFlux_323B_sPS_070_159Jy_blu_c38_Vesta_03 |
| 703 | 1342218748 | rppacs_75 | 286 | 2011-04-17T14:18:51Z | RPPhotFlux_1-RPPhotFlux_323B_sPS_110_75Jy_grn_c37_Vesta_03 |
| 703 | 1342218747 | rppacs_75 | 286 | 2011-04-17T14:13:02Z | RPPhotFlux_1-RPPhotFlux_323B_sPS_070_75Jy_grn_c37_Vesta_03 |
| 703 | 1342218745 | rppacs_75 | 286 | 2011-04-17T14:03:28Z | RPPhotFlux_1-RPPhotFlux_323B_sPS_110_132Jy_blu_c37_Vesta_03 |
| 703 | 1342218744 | rppacs_75 | 286 | 2011-04-17T13:57:39Z | RPPhotFlux_1-RPPhotFlux_323B_sPS_070_132Jy_blu_c37_Vesta_03 |
| 686 | 1342217779 | rppacs_74 | 286 | 2011-03-31T12:50:07Z | RPPhotFlux_1-RPPhotFlux_323B_sPS_110_120Jy_blu_c36_Vesta_03 |
| 686 | 1342217778 | rppacs_74 | 286 | 2011-03-31T12:44:18Z | RPPhotFlux_1-RPPhotFlux_323B_sPS_070_120Jy_blu_c36_Vesta_03 |
| 677 | 1342216613 | rppacs_72 | 1055 | 2011-03-22T11:04:25Z | RPPhotSpatial_1-RPPhotSpatial_314C_StdScan135_med_grn_Vesta_0001 |
| 677 | 1342216612 | rppacs_72 | 1055 | 2011-03-22T10:45:47Z | RPPhotSpatial_1-RPPhotSpatial_314C_StdScan045_med_grn_Vesta_0001 |
| 677 | 1342216611 | rppacs_72 | 1055 | 2011-03-22T10:27:09Z | RPPhotSpatial_1-RPPhotSpatial_314C_StdScan135_med_blu_Vesta_0001 |
| 677 | 1342216610 | rppacs_72 | 1055 | 2011-03-22T10:08:31Z | RPPhotSpatial_1-RPPhotSpatial_314C_StdScan045_med_blu_Vesta_0001 |
| 677 | 1342216609 | rppacs_72 | 286 | 2011-03-22T10:02:42Z | RPPhotFlux_1-RPPhotFlux_323B_sPS_110_106Jy_blu_c35_Vesta_03 |
| 677 | 1342216608 | rppacs_72 | 286 | 2011-03-22T09:56:53Z | RPPhotFlux_1-RPPhotFlux_323B_sPS_070_106Jy_blu_c35_Vesta_03 |
| 348 | 1342195628 | rppacs_18 | 276 | 2010-04-27T03:29:56Z | RPPhotFlux_1-RPPhotFlux_631A_sPS_110_Planck_grn_Vesta_0001 |
| 348 | 1342195627 | rppacs_18 | 276 | 2010-04-27T03:24:17Z | RPPhotFlux_1-RPPhotFlux_631A_sPS_070_Planck_grn_Vesta_0001 |
| 348 | 1342195625 | rppacs_18 | 276 | 2010-04-27T03:14:53Z | RPPhotFlux_1-RPPhotFlux_631A_sPS_110_Planck_blu_Vesta_0001 |
| 348 | 1342195624 | rppacs_18 | 276 | 2010-04-27T03:09:14Z | RPPhotFlux_1-RPPhotFlux_631A_sPS_070_Planck_blu_Vesta_0001 |
| 348 | 1342195622 | rppacs_18 | 3926 | 2010-04-27T01:59:00Z | RPPhotSpatial_1-RPPhotSpatial_314B_StdScan+20_med_grn_Vesta_0001 |
| 345 | 1342195477 | rppacs_18 | 741 | 2010-04-24T01:43:57Z | RPPhotSpatial_1-RPPhotSpatial_314A_StdScan-42_med_grn_Vesta_0001 |
| 345 | 1342195476 | rppacs_18 | 741 | 2010-04-24T01:30:33Z | RPPhotSpatial_1-RPPhotSpatial_314A_StdScan+42_med_grn_Vesta_0001 |
| 345 | 1342195475 | rppacs_18 | 703 | 2010-04-24T01:17:47Z | RPPhotSpatial_1-RPPhotSpatial_314A_StdScan-42_hi_grn_Vesta_0001 |
| 345 | 1342195474 | rppacs_18 | 703 | 2010-04-24T01:05:01Z | RPPhotSpatial_1-RPPhotSpatial_314A_StdScan+42_hi_grn_Vesta_0001 |
| 345 | 1342195473 | rppacs_18 | 741 | 2010-04-24T00:51:37Z | RPPhotSpatial_1-RPPhotSpatial_314A_StdScan-42_med_blu_Vesta_0001 |
| 345 | 1342195472 | rppacs_18 | 741 | 2010-04-24T00:38:13Z | RPPhotSpatial_1-RPPhotSpatial_314A_StdScan+42_med_blu_Vesta_0001 |
| 345 | 1342195471 | rppacs_18 | 703 | 2010-04-24T00:25:27Z | RPPhotSpatial_1-RPPhotSpatial_314A_StdScan-42_hi_blu_Vesta_0001 |
| 345 | 1342195470 | rppacs_18 | 703 | 2010-04-24T00:12:41Z | RPPhotSpatial_1-RPPhotSpatial_314A_StdScan+42_hi_blu_Vesta_0001 |
| 160 | 1342186137 | pvpacs_60 | 831 | 2009-10-21T02:33:52Z | PVPhotSpatial_1-PVPhotSpatial_314D_StdScan_bluhigh_Vesta_0001 |
| 160 | 1342186136 | pvpacs_60 | 865 | 2009-10-21T02:18:24Z | PVPhotSpatial_1-PVPhotSpatial_314D_StdScan_blumed_Vesta_0001 |
| 160 | 1342186135 | pvpacs_60 | 1227 | 2009-10-21T01:56:54Z | PVPhotSpatial_1-PVPhotSpatial_314D_StdScan_blulow_Vesta_0001 |
| 160 | 1342186134 | pvpacs_60 | 831 | 2009-10-21T01:42:00Z | PVPhotSpatial_1-PVPhotSpatial_314D_StdScan_grnhigh_Vesta_0001 |
| 160 | 1342186133 | pvpacs_60 | 865 | 2009-10-21T01:26:32Z | PVPhotSpatial_1-PVPhotSpatial_314D_StdScan_grnmed_Vesta_0001 |
| 160 | 1342186132 | pvpacs_60 | 1227 | 2009-10-21T01:05:02Z | PVPhotSpatial_1-PVPhotSpatial_314D_StdScan_grnlow_Vesta_0001 |

**Table 10** Overview of all relevant Herschel-PACS photometer chop-nod observations of (4) Vesta.

| OD | OBSID | Proposal | Dur. | Start time | AOR Label |
|---|---|---|---|---|---|
| 1377 | 1342263923 | rppacs_179 | 162 | 2013-02-19T08:56:42Z | RPPhotFlux_1-RPPhotFlux_324A_cPS_200Jy_blu_Vesta_0006 |
| 1377 | 1342263920 | rppacs_179 | 162 | 2013-02-19T08:41:19Z | RPPhotFlux_1-RPPhotFlux_324A_cPS_100Jy_grn_Vesta_0006 |
| 1202 | 1342250297 | rppacs_153 | 162 | 2012-08-28T03:53:29Z | RPPhotFlux_1-RPPhotFlux_323A_cPS_88Jy_blu_c73_Vesta_05 |
| 1181 | 1342249193 | rppacs_149 | 162 | 2012-08-07T02:54:22Z | RPPhotFlux_1-RPPhotFlux_323A_cPS_200Jy_blu_c71_Vesta_05 |
| 1181 | 1342249192 | rppacs_149 | 162 | 2012-08-07T02:50:37Z | RPPhotFlux_1-RPPhotFlux_324A_cPS_100Jy_grn_Vesta_0005 |
| 900 | 1342231691 | rppacs_105 | 162 | 2011-10-31T03:21:33Z | RPPhotFlux_1-RPPhotFlux_324A_cPS_100Jy_grn_Vesta_0004 |
| 900 | 1342231688 | rppacs_105 | 162 | 2011-10-31T03:06:10Z | RPPhotFlux_1-RPPhotFlux_324A_cPS_200Jy_blu_Vesta_0004 |
| 743 | 1342221726 | rppacs_82 | 162 | 2011-05-27T02:17:52Z | RPPhotFlux_1-RPPhotFlux_323A_cPS_120Jy_grn_c40_Vesta_03 |
| 743 | 1342221723 | rppacs_82 | 162 | 2011-05-27T02:02:29Z | RPPhotFlux_1-RPPhotFlux_323A_cPS_211Jy_blu_c40_Vesta_03 |
| 726 | 1342220289 | rppacs_79 | 162 | 2011-05-10T02:18:14Z | RPPhotFlux_1-RPPhotFlux_323A_cPS_100Jy_grn_c39_Vesta_03 |
| 726 | 1342220286 | rppacs_79 | 162 | 2011-05-10T02:02:51Z | RPPhotFlux_1-RPPhotFlux_323A_cPS_176Jy_blu_c39_Vesta_03 |
| 720 | 1342220585 | rppacs_77 | 162 | 2011-05-04T11:07:31Z | RPPhotFlux_1-RPPhotFlux_323A_cPS_90Jy_grn_c38_Vesta_03 |
| 720 | 1342220582 | rppacs_77 | 162 | 2011-05-04T10:52:08Z | RPPhotFlux_1-RPPhotFlux_323A_cPS_159Jy_blu_c38_Vesta_03 |
| 703 | 1342218746 | rppacs_75 | 162 | 2011-04-17T14:09:17Z | RPPhotFlux_1-RPPhotFlux_323A_cPS_75Jy_grn_c37_Vesta_03 |
| 703 | 1342218743 | rppacs_75 | 162 | 2011-04-17T13:53:54Z | RPPhotFlux_1-RPPhotFlux_323A_cPS_132Jy_blu_c37_Vesta_03 |
| 686 | 1342217777 | rppacs_74 | 162 | 2011-03-31T12:40:33Z | RPPhotFlux_1-RPPhotFlux_323A_cPS_120Jy_blu_c36_Vesta_03 |
| 677 | 1342216607 | rppacs_72 | 162 | 2011-03-22T09:53:08Z | RPPhotFlux_1-RPPhotFlux_323A_cPS_106Jy_blu_c35_Vesta_03 |
| 348 | 1342195626 | rppacs_18 | 162 | 2010-04-27T03:20:32Z | RPPhotFlux_1-RPPhotFlux_324A_cPS_100Jy_grn_Vesta_0001 |
| 348 | 1342195623 | rppacs_18 | 162 | 2010-04-27T03:05:29Z | RPPhotFlux_1-RPPhotFlux_324A_cPS_200Jy_blu_Vesta_0001 |

**Table 11** Overview of all relevant Herschel-Spire photometer observations of (4) Vesta like in Table 4.

| OD | OBSID | Proposal | Dur. | Start time | Mode | AOR Label |
|---|---|---|---|---|---|---|
| 1403 | 1342267747 | rpspire_160 | 593 | 2013-03-17T04:53:35Z | SmMap | cycle87_1-SPhoto-SmallM-Rep4-Vesta |
| 1388 | 1342265385 | rpspire_158 | 593 | 2013-03-02T06:55:50Z | SmMap | cycle86_1-SPhoto-SmallM-Rep4-Vesta |
| 1375 | 1342263811 | rpspire_156 | 593 | 2013-02-17T00:23:02Z | SmMap | cycle85_1-SPhoto-SmallM-Rep4-Vesta |
| 1201 | 1342250324 | rpspire_130 | 593 | 2012-08-26T16:47:24Z | SmMap | cycle73_1-SPhoto-SmallM-Rep4-Vesta |
| 1179 | 1342249090 | rpspire_126 | 593 | 2012-08-05T12:26:59Z | SmMap | cycle71_1-SPhoto-SmallM-Rep4-Vesta |
| 916 | 1342232369 | rpspire_86 | 593 | 2011-11-16T12:04:22Z | SmMap | cycle53_1-SPhoto-SmallM-Rep4-Vesta |
| 892 | 1342231347 | rpspire_82 | 593 | 2011-10-23T13:43:33Z | SmMap | cycle51_1-SPhoto-SmallM-Rep4-Vesta |
| 702 | 1342218688 | rpspire_54 | 593 | 2011-04-16T01:26:07Z | SmMap | cycle37_1-SPhoto-SmallM-Rep4-Vesta |
| 669 | 1342215994 | rpspire_51 | 593 | 2011-03-13T21:11:57Z | SmMap | cycle35_1-SPhoto-SmallM-Rep4-Vesta |
| 411 | 1342199329 | rpspire_19 | 1334 | 2010-06-28T20:36:13Z | LgMap | cycle16_1-SPhoto-LargeM-Rep4-8x8-Vesta - 0001 |
| 411 | 1342199328 | rpspire_19 | 593 | 2010-06-28T20:25:47Z | SmMap | cycle16_1-SPhoto-SmallM-Rep4-Vesta - 0001 |
| 411 | 1342199327 | rpspire_19 | 1356 | 2010-06-28T20:02:43Z | PS | cycle16_1-SPhoto-PointS-Rep4-Vesta - 0001 |
| 402 | 1342198575 | rpspire_19 | 1334 | 2010-06-19T16:02:47Z | LgMap | cycle16_1-SPhoto-LargeM-Rep4-8x8-Vesta |
| 402 | 1342198574 | rpspire_19 | 593 | 2010-06-19T15:52:21Z | SmMap | cycle16_1-SPhoto-SmallM-Rep4-Vesta |
| 402 | 1342198573 | rpspire_19 | 1356 | 2010-06-19T15:29:17Z | PS | cycle16_1-SPhoto-PointS-Rep4-Vesta |
| 393 | 1342198144 | rpspire_18 | 593 | 2010-06-10T16:49:59Z | SmMap | cycle15_1-SPhoto-SmallRep4-Vesta |
| 393 | 1342198143 | rpspire_18 | 1356 | 2010-06-10T16:26:55Z | PS | cycle15_1-SPhoto-Point-Rep4-Vesta |
| 393 | 1342198142 | rpspire_18 | 1334 | 2010-06-10T16:04:11Z | LgMap | cycle15_1-SPhoto-Large-Rep4-8x8-Vesta |
| 381 | 1342197317 | rpspire_17 | 1261 | 2010-05-30T15:44:54Z | LgMap | cycle14_1-SPhoto-Large-Rep4-8x8-Vesta-Fast |
| 381 | 1342197316 | rpspire_17 | 1334 | 2010-05-30T15:21:59Z | LgMap | cycle14_1-SPhoto-Large-Rep4-8x8-Vesta |
| 381 | 1342197315 | rpspire_17 | 593 | 2010-05-30T15:11:33Z | SmMap | cycle14_1-SPhoto-SmallRep4-Vesta |
| 381 | 1342197314 | rpspire_17 | 1356 | 2010-05-30T14:48:29Z | PS | cycle14_1-SPhoto-Point-Rep4-Vesta |
| 369 | 1342196667 | rpspire_16 | 1334 | 2010-05-18T14:34:08Z | LgMap | cycle13_1-SPhoto-Large-Rep4-8x8-Vesta |
| 369 | 1342196666 | rpspire_16 | 593 | 2010-05-18T14:23:42Z | SmMap | cycle13_1-SPhoto-SmallRep4-Vesta |
| 369 | 1342196665 | pvspire_67 | 1356 | 2010-05-18T14:00:38Z | PS | cycle13_2-SPhoto-Point-Rep4-Vesta |
| 354 | 1342195750 | rpspire_15 | 1334 | 2010-05-03T10:39:14Z | LgMap | cycle12_1-SPhoto-Large-Rep4-8x8-Vesta |
| 354 | 1342195749 | rpspire_15 | 593 | 2010-05-03T10:28:48Z | SmMap | cycle12_1-SPhoto-SmallRep4-Vesta |
| 354 | 1342195748 | pvspire_65 | 1356 | 2010-05-03T10:05:44Z | PS | cycle12_2-SPhoto-Point-Rep4-Vesta |
| 181 | 1342186948 | pvspire_49 | 1468 | 2009-11-11T19:28:15Z | PS | phot_1-SPhoto-PointRep4-bright |
| 181 | 1342186947 | pvspire_49 | 1468 | 2009-11-11T19:03:31Z | PS | phot_1-SpirePhotoPointJiggleGen-otherWay-bright |
| 181 | 1342186946 | pvspire_49 | 1459 | 2009-11-11T18:38:56Z | PS | phot_1-SPhoto-PointRep4 |
| 181 | 1342186944 | pvspire_49 | 1459 | 2009-11-11T17:55:21Z | PS | phot_1-SpirePhotoPointJiggleGen-otherWay |
| 168 | 1342186507 | pvspire_46 | 1449 | 2009-10-29T01:15:33Z | Scan | phot-flux-cal_2-SpirePhotoLargeScanGen-Array-Scan-Y-Rep2-4Vesta |
| 167 | 1342186490 | pvspire_45 | 1458 | 2009-10-28T20:28:58Z | Scan | phot-flux-cal_2-SpirePhotoLargeScanGen-Array-Scan+Y-Rep2-4Vesta-br |
| 167 | 1342186489 | pvspire_45 | 1468 | 2009-10-28T20:03:45Z | PS | phot-flux-cal_2-SPhoto-PointRep4-bright |
| 153 | 1342186002 | pvspire_42 | 427 | 2009-10-14T21:27:42Z | PS | phot-other_1-SPhoto-7pt-Rep1-Vesta - copy - 0003 |
| 153 | 1342186001 | pvspire_42 | 243 | 2009-10-14T21:23:13Z | PS | phot-other_1-SpirePhotoPeakupGen-PSW-E6 - 4 Vesta |
| 153 | 1342186000 | pvspire_42 | 427 | 2009-10-14T21:15:40Z | PS | phot-other_1-SPhoto-7pt-Rep1-Vesta - copy - 0004 |
| 153 | 1342185999 | pvspire_42 | 243 | 2009-10-14T21:11:11Z | PS | phot-other_1-SpirePhotoPeakupGen-PSW-E10 - 4 Vesta |
| 153 | 1342185989 | pvspire_42 | 427 | 2009-10-14T20:07:39Z | PS | phot-other_1-SPhoto-7pt-Rep1-Vesta - copy - 0002 |
| 153 | 1342185988 | pvspire_42 | 243 | 2009-10-14T20:03:24Z | PS | phot-other_1-SpirePhotoPeakupGen-0000 - 4 Vesta |
| 153 | 1342185987 | pvspire_42 | 427 | 2009-10-14T19:56:05Z | PS | phot-other_1-SPhoto-7pt-Rep1-Vesta - copy - 0001 |
| 153 | 1342185938 | pvspire_42 | 1458 | 2009-10-14T16:12:24Z | Scan | phot-flux-cal_1-SpirePhotoLargeScanGen-Array-Scan+Y-Rep2-4Vesta-br |
| 153 | 1342185926 | pvspire_42 | 1468 | 2009-10-14T15:22:00Z | PS | phot-flux-cal_1-SpirePhotoPointJiggleGen-otherWay-bright |
| 153 | 1342185924 | pvspire_42 | 1468 | 2009-10-14T14:38:27Z | PS | phot-flux-cal_1-SPhoto-PointRep4-bright |
| 153 | 1342185922 | pvspire_42 | 1459 | 2009-10-14T13:55:03Z | PS | phot-flux-cal_1-SPhoto-PointRep4 - copy |
| 153 | 1342185921 | pvspire_42 | 1459 | 2009-10-14T13:30:32Z | PS | phot-flux-cal_1-SpirePhotoPointJiggleGen-otherWay |
| 153 | 1342185909 | pvspire_42 | 1449 | 2009-10-14T12:40:22Z | Scan | phot-flux-cal_1-SpirePhotoLargeScanGen-Array-Scan+Y-Rep2-4Vesta |
| 153 | 1342185908 | pvspire_42 | 1449 | 2009-10-14T12:15:51Z | Scan | phot-flux-cal_1-SpirePhotoLargeScanGen-Array-Scan-Y-Rep2-4Vesta |
| 153 | 1342185810 | pvspire_42 | 1459 | 2009-10-14T00:22:32Z | PS | phot-flux-cal_1-SPhoto-PointRep4 |
| 153 | 1342185807 | pvspire_42 | 427 | 2009-10-14T00:10:39Z | PS | phot-other_1-SPhoto-7pt-Rep1-Vesta |
| 153 | 1342185794 | pvspire_42 | 1161 | 2009-10-13T23:24:15Z | Scan | phot-flux-cal_1-SpirePhotoLargeScan-Array-Scan-Y-PMW-Rep2-4Vesta |
| 153 | 1342185793 | pvspire_42 | 1161 | 2009-10-13T23:04:32Z | Scan | phot-flux-cal_1-SpirePhotoLargeScan-Array-Scan+Y-PMW-Rep2-4Vesta |
| 153 | 1342185792 | pvspire_42 | 1170 | 2009-10-13T22:44:40Z | Scan | phot-flux-cal_1-SpirePhotoLargeScan-Array-Scan-Y-PMW-Rep2-4Vesta-b |
| 153 | 1342185791 | pvspire_42 | 1170 | 2009-10-13T22:24:48Z | Scan | phot-flux-cal_1-SpirePhotoLargeScan-Array-Scan+Y-PMW-Rep2-4Vesta-b |

**Table 12** Overview of all relevant Herschel-PACS photometer scan-map observations of (21) Lutetia.

| OD | OBSID | Proposal | Dur. | Start time | AOR Label |
|---|---|---|---|---|---|
| 1399 | 1342267265 | rppacs_183 | 286 | 2013-03-13T02:22:43Z | RPPhotFlux_1-RPPhotFlux_324B_sPS_110_5Jy_blu_Lutetia_0006 |
| 1399 | 1342267264 | rppacs_183 | 286 | 2013-03-13T02:16:54Z | RPPhotFlux_1-RPPhotFlux_324B_sPS_070_5Jy_blu_Lutetia_0006 |
| 1399 | 1342267262 | rppacs_183 | 286 | 2013-03-13T02:07:20Z | RPPhotFlux_1-RPPhotFlux_324B_sPS_110_2Jy_grn_Lutetia_0006 |
| 1399 | 1342267261 | rppacs_183 | 286 | 2013-03-13T02:01:31Z | RPPhotFlux_1-RPPhotFlux_324B_sPS_070_2Jy_grn_Lutetia_0006 |
| 1198 | 1342250108 | rppacs_153 | 286 | 2012-08-23T22:51:36Z | RPPhotFlux_1-RPPhotFlux_324B_sPS_110_5Jy_blu_Lutetia_0005 |
| 1198 | 1342250107 | rppacs_153 | 286 | 2012-08-23T22:45:47Z | RPPhotFlux_1-RPPhotFlux_324B_sPS_070_5Jy_blu_Lutetia_0005 |
| 1198 | 1342250105 | rppacs_153 | 286 | 2012-08-23T22:36:13Z | RPPhotFlux_1-RPPhotFlux_324B_sPS_110_2Jy_grn_Lutetia_0005 |
| 1198 | 1342250104 | rppacs_153 | 286 | 2012-08-23T22:30:24Z | RPPhotFlux_1-RPPhotFlux_324B_sPS_070_2Jy_grn_Lutetia_0005 |
| 859 | 1342228951 | rppacs_98 | 286 | 2011-09-19T21:23:31Z | RPPhotFlux_1-RPPhotFlux_631A_sPS_110_Planck_grn_Lutetia_0001 |
| 859 | 1342228950 | rppacs_98 | 286 | 2011-09-19T21:17:42Z | RPPhotFlux_1-RPPhotFlux_631A_sPS_070_Planck_grn_Lutetia_0001 |
| 859 | 1342228948 | rppacs_98 | 286 | 2011-09-19T21:08:08Z | RPPhotFlux_1-RPPhotFlux_631A_sPS_110_Planck_blu_Lutetia_0001 |
| 859 | 1342228947 | rppacs_98 | 286 | 2011-09-19T21:02:19Z | RPPhotFlux_1-RPPhotFlux_631A_sPS_070_Planck_blu_Lutetia_0001 |
| 684 | 1342217415 | rppacs_74 | 286 | 2011-03-29T21:08:58Z | RPPhotFlux_1-RPPhotFlux_324B_sPS_110_2Jy_grn_Lutetia_0003 |
| 684 | 1342217414 | rppacs_74 | 286 | 2011-03-29T21:03:09Z | RPPhotFlux_1-RPPhotFlux_324B_sPS_070_2Jy_grn_Lutetia_0003 |
| 684 | 1342217412 | rppacs_74 | 286 | 2011-03-29T20:53:35Z | RPPhotFlux_1-RPPhotFlux_324B_sPS_110_5Jy_blu_Lutetia_0003 |
| 684 | 1342217411 | rppacs_74 | 286 | 2011-03-29T20:47:46Z | RPPhotFlux_1-RPPhotFlux_324B_sPS_070_5Jy_blu_Lutetia_0003 |
| 400 | 1342198495 | rppacs_27 | 286 | 2010-06-17T17:22:53Z | RPPhotFlux_1-RPPhotFlux_324B_sPS_110_500mJy_red_Lutetia_0002 |
| 400 | 1342198494 | rppacs_27 | 286 | 2010-06-17T17:17:04Z | RPPhotFlux_1-RPPhotFlux_324B_sPS_070_500mJy_red_Lutetia_0002 |
| 400 | 1342198493 | rppacs_27 | 286 | 2010-06-17T17:11:15Z | RPPhotFlux_1-RPPhotFlux_324B_sPS_110_2Jy_grn_Lutetia_0002 |
| 400 | 1342198492 | rppacs_27 | 286 | 2010-06-17T17:05:26Z | RPPhotFlux_1-RPPhotFlux_324B_sPS_070_2Jy_grn_Lutetia_0002 |
| 221 | 1342188337 | rppacs_3 | 254 | 2009-12-21T02:07:02Z | RPPhotFlux_1-RPPhotFlux_324B_sPS_117_500mJy_red_Lutetia_0001 |
| 221 | 1342188336 | rppacs_3 | 254 | 2009-12-21T02:01:45Z | RPPhotFlux_1-RPPhotFlux_324B_sPS_063_500mJy_red_Lutetia_0001 |
| 221 | 1342188335 | rppacs_3 | 254 | 2009-12-21T01:56:28Z | RPPhotFlux_1-RPPhotFlux_324B_sPS_117_2Jy_grn_Lutetia_0001 |
| 221 | 1342188334 | rppacs_3 | 254 | 2009-12-21T01:51:11Z | RPPhotFlux_1-RPPhotFlux_324B_sPS_063_2Jy_grn_Lutetia_0001 |

**Table 13** Overview of all relevant Herschel-PACS photometer chop-nod observations of (21) Lutetia.

| OD | OBSID | Proposal | Dur. | Start time | AOR Label |
|---|---|---|---|---|---|
| 1399 | 1342267263 | rppacs_183 | 162 | 2013-03-13T02:13:09Z | RPPhotFlux_1-RPPhotFlux_324A_cPS_5Jy_blu_Lutetia_0006 |
| 1399 | 1342267260 | rppacs_183 | 162 | 2013-03-13T01:57:46Z | RPPhotFlux_1-RPPhotFlux_324A_cPS_2Jy_grn_Lutetia_0006 |
| 1198 | 1342250106 | rppacs_153 | 162 | 2012-08-23T22:42:02Z | RPPhotFlux_1-RPPhotFlux_324A_cPS_5Jy_blu_Lutetia_0005 |
| 1198 | 1342250103 | rppacs_153 | 162 | 2012-08-23T22:26:39Z | RPPhotFlux_1-RPPhotFlux_324A_cPS_2Jy_grn_Lutetia_0005 |
| 859 | 1342228949 | rppacs_98 | 162 | 2011-09-19T21:13:57Z | RPPhotFlux_1-RPPhotFlux_324A_cPS_2Jy_grn_Lutetia_0004 |
| 859 | 1342228946 | rppacs_98 | 162 | 2011-09-19T20:58:34Z | RPPhotFlux_1-RPPhotFlux_324A_cPS_5Jy_blu_Lutetia_0004 |
| 684 | 1342217413 | rppacs_74 | 162 | 2011-03-29T20:59:24Z | RPPhotFlux_1-RPPhotFlux_324A_cPS_2Jy_grn_Lutetia_0003 |
| 684 | 1342217410 | rppacs_74 | 162 | 2011-03-29T20:44:01Z | RPPhotFlux_1-RPPhotFlux_324A_cPS_5Jy_blu_Lutetia_0003 |
| 221 | 1342188333 | rppacs_3 | 162 | 2009-12-21T01:47:26Z | RPPhotFlux_1-RPPhotFlux_324A_cPS_500mJy_red_Lutetia_0001 |
| 221 | 1342188332 | rppacs_3 | 162 | 2009-12-21T01:43:41Z | RPPhotFlux_1-RPPhotFlux_324A_cPS_2Jy_grn_Lutetia_0001 |

**Table 14** Overview of all relevant Herschel-SPIRE photometer observations of (21) Lutetia like in Table 4.

| OD | OBSID | Proposal | Dur. | Start time | Mode | AOR Label |
|---|---|---|---|---|---|---|
| 1434 | 1342270326 | rpspire_164 | 593 | 2013-04-17T11:36:39Z | SmMap | cycle89_1-SPhoto-SmallM-Rep4-Lutetia |
| 1411 | 1342268345 | rpspire_162 | 593 | 2013-03-25T03:00:27Z | SmMap | cycle88_1-SPhoto-SmallM-Rep4-Lutetia |
| 1402 | 1342267716 | rpspire_160 | 593 | 2013-03-16T04:13:22Z | SmMap | cycle87_1-SPhoto-SmallM-Rep4-Lutetia |
| 1388 | 1342265386 | rpspire_158 | 593 | 2013-03-02T07:08:54Z | SmMap | cycle86_1-SPhoto-SmallM-Rep4-Lutetia |
| 1215 | 1342250802 | rpspire_132 | 593 | 2012-09-10T12:37:25Z | SmMap | cycle74_1-SPhoto-SmallM-Rep4-Lutetia |
| 1196 | 1342250637 | rpspire_128 | 593 | 2012-08-22T12:58:26Z | SmMap | cycle72_1-SPhoto-SmallM-Rep4-Lutetia |
| 892 | 1342231344 | rpspire_82 | 593 | 2011-10-23T13:07:52Z | SmMap | cycle51_1-SPhoto-SmallM-Rep4-Lutetia |
| 861 | 1342229193 | rpspire_78 | 593 | 2011-09-22T08:32:17Z | SmMap | cycle49_1-SPhoto-SmallM-Rep4-Lutetia |
| 423 | 1342200204 | OT1_lorourke_9 | 179 | 2010-07-11T07:55:55Z | SmMap | SPhoto-Lutetia-Smallmap |

**Table 15** Additional Herschel fixed position photometer observations (no tracking).

| OD | OBSID | Target | RA | Dec | Proposal | Dur. | Start time | AOT | Mode |
|---|---|---|---|---|---|---|---|---|---|
| 50 | 1342179352 | Ceres02072009 | 11h28m31.080s | +13d24m21.90s | copspire_18 | 158 | 2009-07-02T22:23:12Z | SpirePhoto | Scan |
| 50 | 1342179351 | Ceres02072009 | 11h28m31.080s | +13d24m21.90s | copspire_18 | 42 | 2009-07-02T22:22:10Z | SpirePhoto | Scan |
| 50 | 1342179350 | Ceres02072009 | 11h28m31.080s | +13d24m21.90s | copspire_18 | 3891 | 2009-07-02T21:17:03Z | SpirePhoto | Scan |
| 50 | 1342179349 | Ceres02072009 | 11h28m31.080s | +13d24m21.90s | copspire_18 | 42 | 2009-07-02T21:16:05Z | SpirePhoto | Scan |
| 50 | 1342179348 | Ceres02072009 | 11h28m31.080s | +13d24m21.90s | copspire_18 | 158 | 2009-07-02T21:13:15Z | SpirePhoto | Scan |
| 42 | 1342179028 | Ceres20090624 | 11h19m05.500s | +14d50m01.50s | copspire_15 | 42 | 2009-06-25T01:52:45Z | SpirePhoto | Scan |
| 42 | 1342179027 | Ceres20090624 | 11h19m05.500s | +14d50m01.50s | copspire_15 | 6303 | 2009-06-25T00:07:24Z | SpirePhoto | Scan |
| 42 | 1342179026 | Ceres20090624 | 11h19m05.500s | +14d50m01.50s | copspire_15 | 42 | 2009-06-25T00:06:24Z | SpirePhoto | Scan |
| 1179 | 1342249091 | Vesta_alpTau-1 | 4h35m49.350s | +16d37m02.60s | rpspire_126 | 1854 | 2012-08-05T12:38:02Z | SpirePacsParallel | |
| 1179 | 1342249093 | midPos_aTau_Vesta | 4h35m51.430s | +16d37m06.40s | rppacs_149 | 1576 | 2012-08-05T13:37:18Z | PacsPhoto | scan-ma |
| 1179 | 1342249092 | midPos_aTau_Vesta | 4h35m50.510s | +16d37m04.70s | rppacs_149 | 1576 | 2012-08-05T13:09:59Z | PacsPhoto | scan-ma |

## Observational results of the Herschel photometric measurements

Table 16: Photometric Herschel data of (1) Ceres together with the observing geometry and the TPM predictions. The instrument observing modes are: PACS-SM/-CN are PACS photometer scan-map and chop-nod observations, SPIRE-LM/-SM are SPIRE photometer large and small map modes. The last entry for HIFI is an average of four individual observations. The HIFI measurement on OD 1247 (OBSID 1342253122) had some problems: the H- and V-band results were systematically different by about 16%.

| OD | OBSID | mid-time [JD] | $\lambda$ [$\mu$m] | FD [Jy] | $\sigma$ [Jy] | r [AU] | $\Delta$ [AU] | $\alpha$ [°] | TPM [Jy] | FD/TPM | Instr./Mode |
|---|---|---|---|---|---|---|---|---|---|---|---|
| 1244 | 1342252875 | 2456210.07473 | 70.00 | 409.887 | 20.901 | 2.7180 | 2.2836 | 21.0 | 394.159 | 1.04 | PACS-SM |
| 1244 | 1342252876 | 2456210.08767 | 70.00 | 411.248 | 20.970 | 2.7180 | 2.2834 | 21.0 | 394.279 | 1.04 | PACS-SM |
| 1441 | 1342270856 | 2456406.71818 | 70.00 | 246.876 | 12.588 | 2.5827 | 2.8983 | -20.4 | 245.037 | 1.01 | PACS-SM |
| 1441 | 1342270851 | 2456406.67161 | 70.00 | 246.037 | 12.546 | 2.5827 | 2.8978 | -20.4 | 245.142 | 1.00 | PACS-SM |
| 1441 | 1342270846 | 2456406.62462 | 70.00 | 248.024 | 12.647 | 2.5827 | 2.8973 | -20.4 | 245.189 | 1.01 | PACS-SM |
| 1441 | 1342270841 | 2456406.57939 | 70.00 | 246.495 | 12.569 | 2.5828 | 2.8968 | -20.4 | 245.318 | 1.00 | PACS-SM |
| 1441 | 1342270828 | 2456406.54390 | 70.00 | 247.050 | 12.597 | 2.5828 | 2.8964 | -20.4 | 245.318 | 1.01 | PACS-SM |
| 1441 | 1342270823 | 2456406.49797 | 70.00 | 247.781 | 12.634 | 2.5828 | 2.8959 | -20.4 | 245.356 | 1.01 | PACS-SM |
| 1441 | 1342270818 | 2456406.45213 | 70.00 | 247.739 | 12.632 | 2.5828 | 2.8954 | -20.4 | 245.474 | 1.01 | PACS-SM |
| 1441 | 1342270813 | 2456406.40569 | 70.00 | 247.050 | 12.597 | 2.5829 | 2.8949 | -20.4 | 245.558 | 1.01 | PACS-SM |
| 1441 | 1342270808 | 2456406.36095 | 70.00 | 246.601 | 12.574 | 2.5829 | 2.8944 | -20.4 | 245.602 | 1.00 | PACS-SM |
| 1441 | 1342270803 | 2456406.32333 | 70.00 | 247.116 | 12.601 | 2.5829 | 2.8940 | -20.4 | 245.683 | 1.01 | PACS-SM |
| 1441 | 1342270798 | 2456406.27708 | 70.00 | 247.304 | 12.610 | 2.5829 | 2.8935 | -20.4 | 245.876 | 1.01 | PACS-SM |
| 1441 | 1342270787 | 2456406.23868 | 70.00 | 247.654 | 12.628 | 2.5829 | 2.8931 | -20.4 | 245.787 | 1.01 | PACS-SM |
| 1420 | 1342269275 | 2456385.49679 | 70.00 | 289.112 | 14.742 | 2.5936 | 2.6519 | -22.2 | 288.117 | 1.00 | PACS-SM |
| 1420 | 1342269276 | 2456385.50083 | 70.00 | 288.769 | 14.724 | 2.5936 | 2.6519 | -22.2 | 288.300 | 1.00 | PACS-SM |
| 1244 | 1342252870 | 2456210.05597 | 70.00 | 407.485 | 20.778 | 2.7180 | 2.2838 | 21.0 | 394.135 | 1.03 | PACS-SM |
| 1244 | 1342252871 | 2456210.06001 | 70.00 | 405.165 | 20.660 | 2.7180 | 2.2838 | 21.0 | 394.149 | 1.03 | PACS-SM |
| 1237 | 1342252058 | 2456202.72458 | 70.00 | 370.605 | 18.897 | 2.7240 | 2.3861 | 21.5 | 359.514 | 1.03 | PACS-SM |
| 1237 | 1342252059 | 2456202.72862 | 70.00 | 370.578 | 18.896 | 2.7240 | 2.3861 | 21.5 | 359.555 | 1.03 | PACS-SM |
| 947 | 1342234467 | 2455912.52418 | 70.00 | 238.085 | 12.140 | 2.9324 | 2.8235 | -19.8 | 233.768 | 1.02 | PACS-SM |
| 947 | 1342234468 | 2455912.52822 | 70.00 | 237.864 | 12.129 | 2.9324 | 2.8235 | -19.8 | 233.731 | 1.02 | PACS-SM |
| 782 | 1342223699 | 2455747.61557 | 70.00 | 301.806 | 15.389 | 2.9825 | 2.5852 | 19.6 | 288.389 | 1.05 | PACS-SM |
| 782 | 1342223700 | 2455747.61961 | 70.00 | 302.572 | 15.428 | 2.9825 | 2.5852 | 19.6 | 288.505 | 1.05 | PACS-SM |
| 782 | 1342223701 | 2455747.62365 | 70.00 | 301.645 | 15.381 | 2.9824 | 2.5851 | 19.6 | 288.418 | 1.05 | PACS-SM |
| 782 | 1342223702 | 2455747.63659 | 70.00 | 302.951 | 15.448 | 2.9824 | 2.5849 | 19.6 | 288.438 | 1.05 | PACS-SM |
| 769 | 1342222938 | 2455735.09039 | 70.00 | 266.516 | 13.590 | 2.9834 | 2.7522 | 20.1 | 253.850 | 1.05 | PACS-SM |
| 769 | 1342222939 | 2455735.09443 | 70.00 | 267.016 | 13.615 | 2.9834 | 2.7521 | 20.1 | 253.873 | 1.05 | PACS-SM |
| 759 | 1342222566 | 2455724.80409 | 70.00 | 239.730 | 12.224 | 2.9839 | 2.8904 | 20.0 | 230.180 | 1.04 | PACS-SM |
| 759 | 1342222567 | 2455724.80813 | 70.00 | 240.300 | 12.253 | 2.9839 | 2.8904 | 20.0 | 230.180 | 1.04 | PACS-SM |
| 743 | 1342221738 | 2455708.75326 | 70.00 | 209.840 | 10.700 | 2.9842 | 3.1019 | 19.3 | 200.452 | 1.05 | PACS-SM |
| 743 | 1342221739 | 2455708.75730 | 70.00 | 209.750 | 10.695 | 2.9842 | 3.1019 | 19.3 | 200.580 | 1.05 | PACS-SM |
| 734 | 1342221350 | 2455699.97353 | 70.00 | 194.832 | 9.935 | 2.9840 | 3.2130 | 18.5 | 187.525 | 1.04 | PACS-SM |
| 734 | 1342221351 | 2455699.98647 | 70.00 | 194.617 | 9.924 | 2.9840 | 3.2128 | 18.5 | 187.523 | 1.04 | PACS-SM |
| 726 | 1342220293 | 2455691.61455 | 70.00 | 183.897 | 9.377 | 2.9837 | 3.3144 | 17.7 | 176.794 | 1.04 | PACS-SM |
| 726 | 1342220294 | 2455691.61859 | 70.00 | 184.016 | 9.383 | 2.9837 | 3.3144 | 17.7 | 176.786 | 1.04 | PACS-SM |
| 485 | 1342204324 | 2455450.42484 | 70.00 | 279.586 | 14.256 | 2.8992 | 2.6237 | -20.4 | 272.223 | 1.03 | PACS-SM |
| 485 | 1342204325 | 2455450.42888 | 70.00 | 279.873 | 14.271 | 2.8992 | 2.6238 | -20.4 | 272.244 | 1.03 | PACS-SM |
| 286 | 1342191130 | 2455251.66015 | 70.00 | 253.020 | 12.902 | 2.7502 | 2.9026 | 20.1 | 242.630 | 1.04 | PACS-SM |
| 286 | 1342191131 | 2455251.66407 | 70.00 | 253.040 | 12.903 | 2.7502 | 2.9025 | 20.1 | 242.709 | 1.04 | PACS-SM |
| 1420 | 1342269278 | 2456385.50748 | 100.00 | 163.302 | 8.327 | 2.5936 | 2.6520 | -22.2 | 165.672 | 0.99 | PACS-SM |
| 1420 | 1342269279 | 2456385.51152 | 100.00 | 162.930 | 8.308 | 2.5936 | 2.6521 | -22.2 | 165.685 | 0.98 | PACS-SM |
| 1244 | 1342252877 | 2456210.10061 | 100.00 | 228.886 | 11.688 | 2.7180 | 2.2832 | 21.0 | 226.699 | 1.01 | PACS-SM |
| 1244 | 1342252878 | 2456210.11355 | 100.00 | 230.883 | 11.776 | 2.7180 | 2.2830 | 21.0 | 226.724 | 1.02 | PACS-SM |
| 1244 | 1342252873 | 2456210.06666 | 100.00 | 227.991 | 11.639 | 2.7180 | 2.2837 | 21.0 | 226.584 | 1.01 | PACS-SM |

*continued on next page*

Table 16: *continued*

| OD | OBSID | mid-time [JD] | $\lambda$ [$\mu$m] | FD [Jy] | $\sigma$ [Jy] | r [AU] | $\Delta$ [AU] | $\alpha$ [°] | TPM [Jy] | FD/TPM | Instr./Mode |
|---|---|---|---|---|---|---|---|---|---|---|---|
| 1244 | 1342252874 | 2456210.07069 | 100.00 | 229.576 | 11.709 | 2.7180 | 2.2836 | 21.0 | 226.609 | 1.01 | PACS-SM |
| 1237 | 1342252061 | 2456202.73527 | 100.00 | 209.280 | 10.671 | 2.7240 | 2.3860 | 21.5 | 206.929 | 1.01 | PACS-SM |
| 1237 | 1342252062 | 2456202.73931 | 100.00 | 209.326 | 10.674 | 2.7240 | 2.3859 | 21.5 | 206.857 | 1.01 | PACS-SM |
| 947 | 1342234470 | 2455912.53486 | 100.00 | 135.173 | 6.893 | 2.9324 | 2.8236 | -19.8 | 135.767 | 1.00 | PACS-SM |
| 947 | 1342234471 | 2455912.53890 | 100.00 | 134.979 | 6.883 | 2.9324 | 2.8237 | -19.8 | 135.767 | 0.99 | PACS-SM |
| 782 | 1342223704 | 2455747.65213 | 100.00 | 171.144 | 8.727 | 2.9824 | 2.5847 | 19.6 | 167.184 | 1.02 | PACS-SM |
| 782 | 1342223705 | 2455747.65617 | 100.00 | 170.654 | 8.702 | 2.9824 | 2.5847 | 19.6 | 167.167 | 1.02 | PACS-SM |
| 782 | 1342223706 | 2455747.66021 | 100.00 | 170.418 | 8.690 | 2.9824 | 2.5846 | 19.6 | 167.174 | 1.02 | PACS-SM |
| 782 | 1342223707 | 2455747.67315 | 100.00 | 170.381 | 8.688 | 2.9824 | 2.5845 | 19.6 | 167.193 | 1.02 | PACS-SM |
| 769 | 1342222941 | 2455735.10108 | 100.00 | 150.905 | 7.695 | 2.9834 | 2.7520 | 20.1 | 147.118 | 1.03 | PACS-SM |
| 769 | 1342222942 | 2455735.10512 | 100.00 | 149.935 | 7.645 | 2.9834 | 2.7520 | 20.1 | 147.113 | 1.02 | PACS-SM |
| 759 | 1342222569 | 2455724.81477 | 100.00 | 135.885 | 6.929 | 2.9839 | 2.8903 | 20.0 | 133.379 | 1.02 | PACS-SM |
| 759 | 1342222570 | 2455724.81881 | 100.00 | 135.333 | 6.901 | 2.9839 | 2.8902 | 20.0 | 133.411 | 1.01 | PACS-SM |
| 743 | 1342221741 | 2455708.76395 | 100.00 | 118.903 | 6.063 | 2.9842 | 3.1018 | 19.3 | 116.182 | 1.02 | PACS-SM |
| 743 | 1342221742 | 2455708.76799 | 100.00 | 118.688 | 6.052 | 2.9842 | 3.1017 | 19.3 | 116.163 | 1.02 | PACS-SM |
| 734 | 1342221352 | 2455699.99941 | 100.00 | 110.401 | 5.629 | 2.9840 | 3.2127 | 18.5 | 108.593 | 1.02 | PACS-SM |
| 734 | 1342221353 | 2455700.01235 | 100.00 | 110.108 | 5.614 | 2.9840 | 3.2125 | 18.5 | 108.598 | 1.01 | PACS-SM |
| 726 | 1342220296 | 2455691.62523 | 100.00 | 103.990 | 5.303 | 2.9837 | 3.3143 | 17.7 | 102.351 | 1.02 | PACS-SM |
| 726 | 1342220297 | 2455691.62927 | 100.00 | 103.229 | 5.264 | 2.9837 | 3.3142 | 17.7 | 102.359 | 1.01 | PACS-SM |
| 485 | 1342204327 | 2455450.43552 | 100.00 | 157.841 | 8.048 | 2.8992 | 2.6239 | -20.4 | 158.020 | 1.00 | PACS-SM |
| 485 | 1342204328 | 2455450.43956 | 100.00 | 157.735 | 8.043 | 2.8992 | 2.6239 | -20.4 | 157.998 | 1.00 | PACS-SM |
| 286 | 1342191133 | 2455251.67060 | 100.00 | 142.345 | 7.258 | 2.7502 | 2.9025 | 20.1 | 139.605 | 1.02 | PACS-SM |
| 286 | 1342191134 | 2455251.67453 | 100.00 | 141.924 | 7.237 | 2.7502 | 2.9024 | 20.1 | 139.544 | 1.02 | PACS-SM |
| 1420 | 1342269275 | 2456385.49679 | 160.00 | 70.713 | 3.607 | 2.5936 | 2.6519 | -22.2 | 70.796 | 1.00 | PACS-SM |
| 1420 | 1342269276 | 2456385.50083 | 160.00 | 70.844 | 3.613 | 2.5936 | 2.6519 | -22.2 | 70.845 | 1.00 | PACS-SM |
| 1420 | 1342269278 | 2456385.50748 | 160.00 | 70.884 | 3.615 | 2.5936 | 2.6520 | -22.2 | 70.800 | 1.00 | PACS-SM |
| 1420 | 1342269279 | 2456385.51152 | 160.00 | 70.885 | 3.615 | 2.5936 | 2.6521 | -22.2 | 70.805 | 1.00 | PACS-SM |
| 1244 | 1342252875 | 2456210.07473 | 160.00 | 103.468 | 5.329 | 2.7180 | 2.2836 | 21.0 | 96.762 | 1.07 | PACS-SM |
| 1244 | 1342252876 | 2456210.08767 | 160.00 | 103.103 | 5.358 | 2.7180 | 2.2834 | 21.0 | 96.792 | 1.07 | PACS-SM |
| 1244 | 1342252877 | 2456210.10061 | 160.00 | 102.964 | 5.401 | 2.7180 | 2.2832 | 21.0 | 96.801 | 1.06 | PACS-SM |
| 1244 | 1342252878 | 2456210.11355 | 160.00 | 103.009 | 5.478 | 2.7180 | 2.2830 | 21.0 | 96.810 | 1.06 | PACS-SM |
| 1441 | 1342270856 | 2456406.71818 | 160.00 | 60.172 | 3.069 | 2.5827 | 2.8983 | -20.4 | 60.042 | 1.00 | PACS-SM |
| 1441 | 1342270851 | 2456406.67161 | 160.00 | 59.980 | 3.061 | 2.5827 | 2.8978 | -20.4 | 60.069 | 1.00 | PACS-SM |
| 1441 | 1342270846 | 2456406.62462 | 160.00 | 60.404 | 3.081 | 2.5827 | 2.8973 | -20.4 | 60.079 | 1.01 | PACS-SM |
| 1441 | 1342270841 | 2456406.57939 | 160.00 | 60.019 | 3.061 | 2.5828 | 2.8968 | -20.4 | 60.111 | 1.00 | PACS-SM |
| 1441 | 1342270828 | 2456406.54390 | 160.00 | 60.117 | 3.067 | 2.5828 | 2.8964 | -20.4 | 60.113 | 1.00 | PACS-SM |
| 1441 | 1342270823 | 2456406.49797 | 160.00 | 60.270 | 3.073 | 2.5828 | 2.8959 | -20.4 | 60.123 | 1.00 | PACS-SM |
| 1441 | 1342270818 | 2456406.45213 | 160.00 | 60.227 | 3.072 | 2.5828 | 2.8954 | -20.4 | 60.152 | 1.00 | PACS-SM |
| 1441 | 1342270813 | 2456406.40569 | 160.00 | 60.159 | 3.068 | 2.5829 | 2.8949 | -20.4 | 60.173 | 1.00 | PACS-SM |
| 1441 | 1342270808 | 2456406.36095 | 160.00 | 59.914 | 3.056 | 2.5829 | 2.8944 | -20.4 | 60.184 | 1.00 | PACS-SM |
| 1441 | 1342270803 | 2456406.32333 | 160.00 | 60.269 | 3.074 | 2.5829 | 2.8940 | -20.4 | 60.204 | 1.00 | PACS-SM |
| 1441 | 1342270798 | 2456406.27708 | 160.00 | 60.305 | 3.078 | 2.5829 | 2.8935 | -20.4 | 60.252 | 1.00 | PACS-SM |
| 1441 | 1342270787 | 2456406.23868 | 160.00 | 60.149 | 3.070 | 2.5829 | 2.8931 | -20.4 | 60.231 | 1.00 | PACS-SM |
| 1244 | 1342252870 | 2456210.05597 | 160.00 | 95.488 | 5.043 | 2.7180 | 2.2838 | 21.0 | 96.758 | 0.99 | PACS-SM |
| 1244 | 1342252871 | 2456210.06001 | 160.00 | 98.945 | 5.403 | 2.7180 | 2.2838 | 21.0 | 96.760 | 1.02 | PACS-SM |
| 1244 | 1342252873 | 2456210.06666 | 160.00 | 94.444 | 5.228 | 2.7180 | 2.2837 | 21.0 | 96.753 | 0.98 | PACS-SM |
| 1244 | 1342252874 | 2456210.07069 | 160.00 | 100.210 | 5.355 | 2.7180 | 2.2836 | 21.0 | 96.763 | 1.04 | PACS-SM |
| 1237 | 1342252058 | 2456202.72458 | 160.00 | 90.929 | 4.638 | 2.7240 | 2.3861 | 21.5 | 88.330 | 1.03 | PACS-SM |
| 1237 | 1342252059 | 2456202.72862 | 160.00 | 91.166 | 4.649 | 2.7240 | 2.3861 | 21.5 | 88.340 | 1.03 | PACS-SM |
| 1237 | 1342252061 | 2456202.73527 | 160.00 | 90.923 | 4.637 | 2.7240 | 2.3860 | 21.5 | 88.392 | 1.03 | PACS-SM |
| 1237 | 1342252062 | 2456202.73931 | 160.00 | 91.179 | 4.650 | 2.7240 | 2.3859 | 21.5 | 88.359 | 1.03 | PACS-SM |
| 947 | 1342234467 | 2455912.52418 | 160.00 | 58.727 | 2.996 | 2.9324 | 2.8235 | -19.8 | 58.508 | 1.00 | PACS-SM |
| 947 | 1342234468 | 2455912.52822 | 160.00 | 58.633 | 2.991 | 2.9324 | 2.8235 | -19.8 | 58.499 | 1.00 | PACS-SM |

*continued on next page*

Table 16: *continued*

| OD | OBSID | mid-time [JD] | $\lambda$ [$\mu$m] | FD [Jy] | $\sigma$ [Jy] | r [AU] | $\Delta$ [AU] | $\alpha$ [°] | TPM [Jy] | FD/TPM | Instr./Mode |
|---|---|---|---|---|---|---|---|---|---|---|---|
| 947 | 1342234470 | 2455912.53486 | 160.00 | 58.690 | 2.994 | 2.9324 | 2.8236 | -19.8 | 58.496 | 1.00 | PACS-SM |
| 947 | 1342234471 | 2455912.53890 | 160.00 | 58.550 | 2.988 | 2.9324 | 2.8237 | -19.8 | 58.496 | 1.00 | PACS-SM |
| 782 | 1342223699 | 2455747.61557 | 160.00 | 74.612 | 3.805 | 2.9825 | 2.5852 | 19.6 | 71.781 | 1.04 | PACS-SM |
| 782 | 1342223700 | 2455747.61961 | 160.00 | 74.685 | 3.812 | 2.9825 | 2.5852 | 19.6 | 71.816 | 1.04 | PACS-SM |
| 782 | 1342223704 | 2455747.65213 | 160.00 | 74.645 | 3.807 | 2.9824 | 2.5847 | 19.6 | 71.832 | 1.04 | PACS-SM |
| 782 | 1342223705 | 2455747.65617 | 160.00 | 74.359 | 3.795 | 2.9824 | 2.5847 | 19.6 | 71.824 | 1.04 | PACS-SM |
| 782 | 1342223701 | 2455747.62365 | 160.00 | 73.985 | 3.775 | 2.9824 | 2.5851 | 19.6 | 71.792 | 1.03 | PACS-SM |
| 782 | 1342223702 | 2455747.63659 | 160.00 | 74.931 | 3.823 | 2.9824 | 2.5849 | 19.6 | 71.790 | 1.04 | PACS-SM |
| 782 | 1342223706 | 2455747.66021 | 160.00 | 74.537 | 3.801 | 2.9824 | 2.5846 | 19.6 | 71.827 | 1.04 | PACS-SM |
| 782 | 1342223707 | 2455747.67315 | 160.00 | 74.503 | 3.800 | 2.9824 | 2.5845 | 19.6 | 71.836 | 1.04 | PACS-SM |
| 769 | 1342222938 | 2455735.09039 | 160.00 | 66.109 | 3.372 | 2.9834 | 2.7522 | 20.1 | 63.215 | 1.05 | PACS-SM |
| 769 | 1342222939 | 2455735.09443 | 160.00 | 66.156 | 3.375 | 2.9834 | 2.7521 | 20.1 | 63.223 | 1.05 | PACS-SM |
| 769 | 1342222941 | 2455735.10108 | 160.00 | 65.983 | 3.366 | 2.9834 | 2.7520 | 20.1 | 63.224 | 1.04 | PACS-SM |
| 769 | 1342222942 | 2455735.10512 | 160.00 | 65.667 | 3.352 | 2.9834 | 2.7520 | 20.1 | 63.222 | 1.04 | PACS-SM |
| 759 | 1342222566 | 2455724.80409 | 160.00 | 59.187 | 3.020 | 2.9839 | 2.8904 | 20.0 | 57.321 | 1.03 | PACS-SM |
| 759 | 1342222567 | 2455724.80813 | 160.00 | 59.078 | 3.015 | 2.9839 | 2.8904 | 20.0 | 57.321 | 1.03 | PACS-SM |
| 759 | 1342222569 | 2455724.81477 | 160.00 | 59.147 | 3.018 | 2.9839 | 2.8903 | 20.0 | 57.319 | 1.03 | PACS-SM |
| 759 | 1342222570 | 2455724.81881 | 160.00 | 58.846 | 3.004 | 2.9839 | 2.8902 | 20.0 | 57.332 | 1.03 | PACS-SM |
| 743 | 1342221738 | 2455708.75326 | 160.00 | 51.879 | 2.646 | 2.9842 | 3.1019 | 19.3 | 49.886 | 1.04 | PACS-SM |
| 743 | 1342221739 | 2455708.75730 | 160.00 | 51.816 | 2.644 | 2.9842 | 3.1019 | 19.3 | 49.918 | 1.04 | PACS-SM |
| 743 | 1342221741 | 2455708.76395 | 160.00 | 51.923 | 2.649 | 2.9842 | 3.1018 | 19.3 | 49.912 | 1.04 | PACS-SM |
| 743 | 1342221742 | 2455708.76799 | 160.00 | 51.824 | 2.645 | 2.9842 | 3.1017 | 19.3 | 49.905 | 1.04 | PACS-SM |
| 734 | 1342221352 | 2455699.99941 | 160.00 | 47.524 | 2.425 | 2.9840 | 3.2127 | 18.5 | 46.639 | 1.02 | PACS-SM |
| 734 | 1342221353 | 2455700.01235 | 160.00 | 48.043 | 2.451 | 2.9840 | 3.2125 | 18.5 | 46.641 | 1.03 | PACS-SM |
| 726 | 1342220293 | 2455691.61455 | 160.00 | 45.439 | 2.318 | 2.9837 | 3.3144 | 17.7 | 43.941 | 1.03 | PACS-SM |
| 726 | 1342220294 | 2455691.61859 | 160.00 | 45.325 | 2.312 | 2.9837 | 3.3144 | 17.7 | 43.940 | 1.03 | PACS-SM |
| 726 | 1342220296 | 2455691.62523 | 160.00 | 45.257 | 2.309 | 2.9837 | 3.3143 | 17.7 | 43.944 | 1.03 | PACS-SM |
| 726 | 1342220297 | 2455691.62927 | 160.00 | 45.084 | 2.302 | 2.9837 | 3.3142 | 17.7 | 43.947 | 1.03 | PACS-SM |
| 485 | 1342204324 | 2455450.42484 | 160.00 | 68.744 | 3.506 | 2.8992 | 2.6237 | -20.4 | 68.043 | 1.01 | PACS-SM |
| 485 | 1342204325 | 2455450.42888 | 160.00 | 68.675 | 3.505 | 2.8992 | 2.6238 | -20.4 | 68.045 | 1.01 | PACS-SM |
| 485 | 1342204327 | 2455450.43552 | 160.00 | 68.639 | 3.501 | 2.8992 | 2.6239 | -20.4 | 68.045 | 1.01 | PACS-SM |
| 485 | 1342204328 | 2455450.43956 | 160.00 | 68.535 | 3.496 | 2.8992 | 2.6239 | -20.4 | 68.036 | 1.01 | PACS-SM |
| 286 | 1342191130 | 2455251.66015 | 160.00 | 61.271 | 3.126 | 2.7502 | 2.9026 | 20.1 | 59.641 | 1.03 | PACS-SM |
| 286 | 1342191131 | 2455251.66407 | 160.00 | 61.397 | 3.132 | 2.7502 | 2.9025 | 20.1 | 59.659 | 1.03 | PACS-SM |
| 286 | 1342191133 | 2455251.67060 | 160.00 | 61.323 | 3.129 | 2.7502 | 2.9025 | 20.1 | 59.644 | 1.03 | PACS-SM |
| 286 | 1342191134 | 2455251.67453 | 160.00 | 61.338 | 3.131 | 2.7502 | 2.9024 | 20.1 | 59.617 | 1.03 | PACS-SM |
| 286 | 1342191132 | 2455251.66822 | 100.00 | 139.223 | 7.104 | 2.7502 | 2.9025 | 20.1 | 139.530 | 1.00 | PACS-CN |
| 286 | 1342191132 | 2455251.66822 | 160.00 | 60.209 | 3.173 | 2.7502 | 2.9025 | 20.1 | 59.612 | 1.01 | PACS-CN |
| 286 | 1342191129 | 2455251.65777 | 70.00 | 236.587 | 12.070 | 2.7502 | 2.9026 | 20.1 | 242.625 | 0.98 | PACS-CN |
| 286 | 1342191129 | 2455251.65777 | 160.00 | 59.689 | 3.182 | 2.7502 | 2.9026 | 20.1 | 59.639 | 1.00 | PACS-CN |
| 485 | 1342204326 | 2455450.43314 | 100.00 | 154.924 | 7.905 | 2.8992 | 2.6238 | -20.4 | 158.016 | 0.98 | PACS-CN |
| 485 | 1342204326 | 2455450.43314 | 160.00 | 67.533 | 3.518 | 2.8992 | 2.6238 | -20.4 | 68.043 | 0.99 | PACS-CN |
| 485 | 1342204323 | 2455450.42245 | 70.00 | 275.817 | 14.072 | 2.8992 | 2.6237 | -20.4 | 272.223 | 1.01 | PACS-CN |
| 485 | 1342204323 | 2455450.42245 | 160.00 | 67.238 | 3.511 | 2.8992 | 2.6237 | -20.4 | 68.040 | 0.99 | PACS-CN |
| 743 | 1342221740 | 2455708.76156 | 100.00 | 116.394 | 5.940 | 2.9842 | 3.1018 | 19.3 | 116.125 | 1.00 | PACS-CN |
| 743 | 1342221740 | 2455708.76156 | 160.00 | 50.873 | 2.667 | 2.9842 | 3.1018 | 19.3 | 49.888 | 1.02 | PACS-CN |
| 743 | 1342221737 | 2455708.75088 | 70.00 | 194.240 | 9.910 | 2.9842 | 3.1019 | 19.3 | 200.491 | 0.97 | PACS-CN |
| 743 | 1342221737 | 2455708.75088 | 160.00 | 50.245 | 2.635 | 2.9842 | 3.1019 | 19.3 | 49.894 | 1.01 | PACS-CN |
| 726 | 1342220295 | 2455691.62285 | 100.00 | 102.948 | 5.253 | 2.9837 | 3.3143 | 17.7 | 102.341 | 1.01 | PACS-CN |
| 726 | 1342220295 | 2455691.62285 | 160.00 | 44.657 | 2.359 | 2.9837 | 3.3143 | 17.7 | 43.939 | 1.02 | PACS-CN |
| 726 | 1342220292 | 2455691.61216 | 70.00 | 182.225 | 9.296 | 2.9837 | 3.3145 | 17.7 | 176.785 | 1.03 | PACS-CN |
| 726 | 1342220292 | 2455691.61216 | 160.00 | 44.698 | 2.353 | 2.9837 | 3.3145 | 17.7 | 43.938 | 1.02 | PACS-CN |
| 759 | 1342222565 | 2455724.80170 | 70.00 | 231.074 | 11.789 | 2.9839 | 2.8904 | 20.0 | 230.127 | 1.00 | PACS-CN |

*continued on next page*

Table 16: *continued*

| OD | OBSID | mid-time [JD] | $\lambda$ [$\mu$m] | FD [Jy] | $\sigma$ [Jy] | r [AU] | $\Delta$ [AU] | $\alpha$ [°] | TPM [Jy] | FD/TPM | Instr./Mode |
|---|---|---|---|---|---|---|---|---|---|---|---|
| 759 | 1342222565 | 2455724.80170 | 160.00 | 58.747 | 3.083 | 2.9839 | 2.8904 | 20.0 | 57.306 | 1.03 | PACS-CN |
| 759 | 1342222568 | 2455724.81238 | 100.00 | 133.036 | 6.788 | 2.9839 | 2.8903 | 20.0 | 133.395 | 1.00 | PACS-CN |
| 759 | 1342222568 | 2455724.81238 | 160.00 | 58.804 | 3.099 | 2.9839 | 2.8903 | 20.0 | 57.325 | 1.03 | PACS-CN |
| 769 | 1342222940 | 2455735.09869 | 100.00 | 147.943 | 7.550 | 2.9834 | 2.7520 | 20.1 | 147.111 | 1.01 | PACS-CN |
| 769 | 1342222940 | 2455735.09869 | 160.00 | 64.721 | 3.390 | 2.9834 | 2.7520 | 20.1 | 63.221 | 1.02 | PACS-CN |
| 769 | 1342222937 | 2455735.08801 | 70.00 | 261.354 | 13.333 | 2.9834 | 2.7522 | 20.1 | 253.868 | 1.03 | PACS-CN |
| 769 | 1342222937 | 2455735.08801 | 160.00 | 64.849 | 3.397 | 2.9834 | 2.7522 | 20.1 | 63.220 | 1.03 | PACS-CN |
| 782 | 1342223703 | 2455747.64975 | 100.00 | 170.310 | 8.693 | 2.9824 | 2.5848 | 19.6 | 167.160 | 1.02 | PACS-CN |
| 782 | 1342223703 | 2455747.64975 | 160.00 | 73.841 | 3.922 | 2.9824 | 2.5848 | 19.6 | 71.822 | 1.03 | PACS-CN |
| 782 | 1342223698 | 2455747.61318 | 70.00 | 293.901 | 14.993 | 2.9825 | 2.5853 | 19.6 | 288.456 | 1.02 | PACS-CN |
| 782 | 1342223698 | 2455747.61318 | 160.00 | 73.813 | 3.894 | 2.9825 | 2.5853 | 19.6 | 71.799 | 1.03 | PACS-CN |
| 947 | 1342234469 | 2455912.53248 | 100.00 | 135.807 | 6.930 | 2.9324 | 2.8236 | -19.8 | 135.778 | 1.00 | PACS-CN |
| 947 | 1342234469 | 2455912.53248 | 160.00 | 58.072 | 3.062 | 2.9324 | 2.8236 | -19.8 | 58.501 | 0.99 | PACS-CN |
| 947 | 1342234466 | 2455912.52179 | 70.00 | 239.268 | 12.205 | 2.9324 | 2.8235 | -19.8 | 233.797 | 1.02 | PACS-CN |
| 947 | 1342234466 | 2455912.52179 | 160.00 | 58.096 | 3.061 | 2.9324 | 2.8235 | -19.8 | 58.515 | 0.99 | PACS-CN |
| 1237 | 1342252060 | 2456202.73288 | 100.00 | 207.612 | 10.593 | 2.7240 | 2.3860 | 21.5 | 206.784 | 1.00 | PACS-CN |
| 1237 | 1342252060 | 2456202.73288 | 160.00 | 90.059 | 4.694 | 2.7240 | 2.3860 | 21.5 | 88.333 | 1.02 | PACS-CN |
| 1237 | 1342252057 | 2456202.72220 | 70.00 | 365.887 | 18.666 | 2.7240 | 2.3861 | 21.5 | 359.522 | 1.02 | PACS-CN |
| 1237 | 1342252057 | 2456202.72220 | 160.00 | 90.584 | 4.740 | 2.7240 | 2.3861 | 21.5 | 88.331 | 1.03 | PACS-CN |
| 1244 | 1342252872 | 2456210.06427 | 100.00 | 228.250 | 11.659 | 2.7180 | 2.2837 | 21.0 | 226.608 | 1.01 | PACS-CN |
| 1244 | 1342252872 | 2456210.06427 | 160.00 | 96.103 | 5.912 | 2.7180 | 2.2837 | 21.0 | 96.763 | 0.99 | PACS-CN |
| 1244 | 1342252869 | 2456210.05359 | 70.00 | 405.177 | 20.673 | 2.7180 | 2.2838 | 21.0 | 394.058 | 1.03 | PACS-CN |
| 1244 | 1342252869 | 2456210.05359 | 160.00 | 95.938 | 5.415 | 2.7180 | 2.2838 | 21.0 | 96.740 | 0.99 | PACS-CN |
| 1420 | 1342269277 | 2456385.50509 | 100.00 | 162.244 | 8.279 | 2.5936 | 2.6520 | -22.2 | 165.682 | 0.98 | PACS-CN |
| 1420 | 1342269277 | 2456385.50509 | 160.00 | 70.697 | 3.755 | 2.5936 | 2.6520 | -22.2 | 70.804 | 1.00 | PACS-CN |
| 1420 | 1342269274 | 2456385.49441 | 70.00 | 288.315 | 14.708 | 2.5936 | 2.6519 | -22.2 | 288.185 | 1.00 | PACS-CN |
| 1420 | 1342269274 | 2456385.49441 | 160.00 | 70.291 | 3.751 | 2.5936 | 2.6519 | -22.2 | 70.815 | 0.99 | PACS-CN |
| 1434 | 1342270325 | 2456399.97551 | 250.00 | 26.650 | 1.435 | 2.5860 | 2.8231 | -21.0 | 26.508 | 1.01 | SPIRE-SM |
| 1434 | 1342270325 | 2456399.97551 | 350.00 | 13.841 | 0.745 | 2.5860 | 2.8231 | -21.0 | 13.793 | 1.00 | SPIRE-SM |
| 1434 | 1342270325 | 2456399.97551 | 500.00 | 6.810 | 0.367 | 2.5860 | 2.8231 | -21.0 | 6.940 | 0.98 | SPIRE-SM |
| 1411 | 1342268344 | 2456376.61704 | 250.00 | 32.830 | 1.768 | 2.5985 | 2.5420 | -22.5 | 32.344 | 1.02 | SPIRE-SM |
| 1411 | 1342268344 | 2456376.61704 | 350.00 | 17.033 | 0.917 | 2.5985 | 2.5420 | -22.5 | 16.836 | 1.01 | SPIRE-SM |
| 1411 | 1342268344 | 2456376.61704 | 500.00 | 8.326 | 0.448 | 2.5985 | 2.5420 | -22.5 | 8.474 | 0.98 | SPIRE-SM |
| 1403 | 1342267748 | 2456368.71267 | 250.00 | 35.380 | 1.905 | 2.6030 | 2.4420 | -22.7 | 34.988 | 1.01 | SPIRE-SM |
| 1403 | 1342267748 | 2456368.71267 | 350.00 | 18.383 | 0.990 | 2.6030 | 2.4420 | -22.7 | 18.213 | 1.01 | SPIRE-SM |
| 1403 | 1342267748 | 2456368.71267 | 500.00 | 9.008 | 0.485 | 2.6030 | 2.4420 | -22.7 | 9.167 | 0.98 | SPIRE-SM |
| 1249 | 1342253388 | 2456214.44337 | 250.00 | 45.300 | 2.440 | 2.7144 | 2.2239 | 20.6 | 43.025 | 1.05 | SPIRE-SM |
| 1249 | 1342253388 | 2456214.44337 | 350.00 | 23.523 | 1.267 | 2.7144 | 2.2239 | 20.6 | 22.383 | 1.05 | SPIRE-SM |
| 1249 | 1342253388 | 2456214.44337 | 500.00 | 11.662 | 0.628 | 2.7144 | 2.2239 | 20.6 | 11.261 | 1.04 | SPIRE-SM |
| 1235 | 1342251687 | 2456200.44690 | 250.00 | 38.035 | 2.048 | 2.7258 | 2.4182 | 21.6 | 36.162 | 1.05 | SPIRE-SM |
| 1235 | 1342251687 | 2456200.44690 | 350.00 | 19.920 | 1.073 | 2.7258 | 2.4182 | 21.6 | 18.816 | 1.06 | SPIRE-SM |
| 1235 | 1342251687 | 2456200.44690 | 500.00 | 9.884 | 0.532 | 2.7258 | 2.4182 | 21.6 | 9.468 | 1.04 | SPIRE-SM |
| 1215 | 1342250803 | 2456181.03425 | 250.00 | 30.615 | 1.649 | 2.7417 | 2.6948 | 21.5 | 29.033 | 1.05 | SPIRE-SM |
| 1215 | 1342250803 | 2456181.03425 | 350.00 | 15.947 | 0.859 | 2.7417 | 2.6948 | 21.5 | 15.109 | 1.06 | SPIRE-SM |
| 1215 | 1342250803 | 2456181.03425 | 500.00 | 7.905 | 0.426 | 2.7417 | 2.6948 | 21.5 | 7.603 | 1.04 | SPIRE-SM |
| 1201 | 1342250325 | 2456166.20801 | 250.00 | 26.450 | 1.424 | 2.7539 | 2.9020 | 20.5 | 25.052 | 1.06 | SPIRE-SM |
| 1201 | 1342250325 | 2456166.20801 | 350.00 | 13.747 | 0.740 | 2.7539 | 2.9020 | 20.5 | 13.037 | 1.05 | SPIRE-SM |
| 1201 | 1342250325 | 2456166.20801 | 500.00 | 6.816 | 0.367 | 2.7539 | 2.9020 | 20.5 | 6.560 | 1.04 | SPIRE-SM |
| 1197 | 1342250643 | 2456162.18140 | 250.00 | 25.110 | 1.352 | 2.7572 | 2.9566 | 20.2 | 24.155 | 1.04 | SPIRE-SM |
| 1197 | 1342250643 | 2456162.18140 | 350.00 | 13.162 | 0.709 | 2.7572 | 2.9566 | 20.2 | 12.570 | 1.05 | SPIRE-SM |
| 1197 | 1342250643 | 2456162.18140 | 500.00 | 6.616 | 0.356 | 2.7572 | 2.9566 | 20.2 | 6.325 | 1.05 | SPIRE-SM |
| 964 | 1342236236 | 2455929.21517 | 250.00 | 21.667 | 1.167 | 2.9238 | 3.0448 | -19.0 | 21.393 | 1.01 | SPIRE-SM |
| 964 | 1342236236 | 2455929.21517 | 350.00 | 11.319 | 0.610 | 2.9238 | 3.0448 | -19.0 | 11.158 | 1.01 | SPIRE-SM |

*continued on next page*

Table 16: *continued*

| OD | OBSID | mid-time [JD] | $\lambda$ [$\mu$m] | FD [Jy] | $\sigma$ [Jy] | r [AU] | $\Delta$ [AU] | $\alpha$ [°] | TPM [Jy] | FD/TPM | Instr./Mode |
|---|---|---|---|---|---|---|---|---|---|---|---|
| 964 | 1342236236 | 2455929.21517 | 500.00 | 5.557 | 0.299 | 2.9238 | 3.0448 | -19.0 | 5.624 | 0.99 | SPIRE-SM |
| 964 | 1342236235 | 2455929.20786 | 250.00 | 21.979 | 1.184 | 2.9238 | 3.0447 | -19.0 | 21.406 | 1.03 | SPIRE-SM |
| 964 | 1342236235 | 2455929.20786 | 350.00 | 11.366 | 0.612 | 2.9238 | 3.0447 | -19.0 | 11.164 | 1.02 | SPIRE-SM |
| 964 | 1342236235 | 2455929.20786 | 500.00 | 5.559 | 0.300 | 2.9238 | 3.0447 | -19.0 | 5.627 | 0.99 | SPIRE-SM |
| 948 | 1342234931 | 2455913.98852 | 250.00 | 24.660 | 1.328 | 2.9317 | 2.8432 | -19.7 | 24.430 | 1.01 | SPIRE-SM |
| 948 | 1342234931 | 2455913.98852 | 350.00 | 12.880 | 0.694 | 2.9317 | 2.8432 | -19.7 | 12.744 | 1.01 | SPIRE-SM |
| 948 | 1342234931 | 2455913.98852 | 500.00 | 6.362 | 0.343 | 2.9317 | 2.8432 | -19.7 | 6.424 | 0.99 | SPIRE-SM |
| 775 | 1342223221 | 2455741.08499 | 250.00 | 29.967 | 1.614 | 2.9830 | 2.6717 | 20.0 | 28.338 | 1.06 | SPIRE-SM |
| 775 | 1342223221 | 2455741.08499 | 350.00 | 15.709 | 0.846 | 2.9830 | 2.6717 | 20.0 | 14.769 | 1.06 | SPIRE-SM |
| 775 | 1342223221 | 2455741.08499 | 500.00 | 7.758 | 0.418 | 2.9830 | 2.6717 | 20.0 | 7.441 | 1.04 | SPIRE-SM |
| 725 | 1342220642 | 2455690.46241 | 250.00 | 19.396 | 1.045 | 2.9836 | 3.3280 | 17.5 | 18.400 | 1.05 | SPIRE-SM |
| 725 | 1342220642 | 2455690.46241 | 350.00 | 10.123 | 0.545 | 2.9836 | 3.3280 | 17.5 | 9.587 | 1.06 | SPIRE-SM |
| 725 | 1342220642 | 2455690.46241 | 500.00 | 5.004 | 0.270 | 2.9836 | 3.3280 | 17.5 | 4.829 | 1.04 | SPIRE-SM |
| 529 | 1342207050 | 2455494.45545 | 250.00 | 19.442 | 1.047 | 2.9245 | 3.2415 | -17.8 | 18.992 | 1.02 | SPIRE-SM |
| 529 | 1342207050 | 2455494.45545 | 350.00 | 10.142 | 0.546 | 2.9245 | 3.2415 | -17.8 | 9.903 | 1.02 | SPIRE-SM |
| 529 | 1342207050 | 2455494.45545 | 500.00 | 4.954 | 0.267 | 2.9245 | 3.2415 | -17.8 | 4.991 | 0.99 | SPIRE-SM |
| 521 | 1342206682 | 2455487.09628 | 250.00 | 20.576 | 1.108 | 2.9205 | 3.1448 | -18.6 | 20.114 | 1.02 | SPIRE-SM |
| 521 | 1342206682 | 2455487.09628 | 350.00 | 10.706 | 0.577 | 2.9205 | 3.1448 | -18.6 | 10.489 | 1.02 | SPIRE-SM |
| 521 | 1342206682 | 2455487.09628 | 500.00 | 5.255 | 0.283 | 2.9205 | 3.1448 | -18.6 | 5.287 | 0.99 | SPIRE-SM |
| 515 | 1342206204 | 2455480.89981 | 250.00 | 21.708 | 1.169 | 2.9171 | 3.0604 | -19.2 | 21.188 | 1.02 | SPIRE-SM |
| 515 | 1342206204 | 2455480.89981 | 350.00 | 11.356 | 0.612 | 2.9171 | 3.0604 | -19.2 | 11.050 | 1.03 | SPIRE-SM |
| 515 | 1342206204 | 2455480.89981 | 500.00 | 5.520 | 0.297 | 2.9171 | 3.0604 | -19.2 | 5.570 | 0.99 | SPIRE-SM |
| 499 | 1342205096 | 2455465.15714 | 250.00 | 25.268 | 1.363 | 2.9081 | 2.8376 | -20.2 | 24.568 | 1.03 | SPIRE-SM |
| 499 | 1342205096 | 2455465.15714 | 350.00 | 13.206 | 0.713 | 2.9081 | 2.8376 | -20.2 | 12.814 | 1.03 | SPIRE-SM |
| 499 | 1342205096 | 2455465.15714 | 500.00 | 6.519 | 0.353 | 2.9081 | 2.8376 | -20.2 | 6.459 | 1.01 | SPIRE-SM |
| 486 | 1342204371 | 2455452.12485 | 250.00 | 29.081 | 1.566 | 2.9002 | 2.6487 | -20.4 | 28.217 | 1.03 | SPIRE-LM |
| 486 | 1342204371 | 2455452.12485 | 350.00 | 15.384 | 0.829 | 2.9002 | 2.6487 | -20.4 | 14.717 | 1.05 | SPIRE-LM |
| 486 | 1342204371 | 2455452.12485 | 500.00 | 7.376 | 0.397 | 2.9002 | 2.6487 | -20.4 | 7.418 | 0.99 | SPIRE-LM |
| 479 | 1342204061 | 2455445.08675 | 250.00 | 31.222 | 1.681 | 2.8958 | 2.5467 | -20.2 | 30.601 | 1.02 | SPIRE-SM |
| 479 | 1342204061 | 2455445.08675 | 350.00 | 16.217 | 0.873 | 2.8958 | 2.5467 | -20.2 | 15.959 | 1.02 | SPIRE-SM |
| 479 | 1342204061 | 2455445.08675 | 500.00 | 8.005 | 0.431 | 2.8958 | 2.5467 | -20.2 | 8.044 | 1.00 | SPIRE-SM |
| 326 | 1342193790 | 2455291.64229 | 250.00 | 39.011 | 2.101 | 2.7829 | 2.3859 | 20.7 | 36.808 | 1.06 | SPIRE-LM |
| 326 | 1342193790 | 2455291.64229 | 350.00 | 20.240 | 1.090 | 2.7829 | 2.3859 | 20.7 | 19.159 | 1.06 | SPIRE-LM |
| 326 | 1342193790 | 2455291.64229 | 500.00 | 10.115 | 0.545 | 2.7829 | 2.3859 | 20.7 | 9.643 | 1.05 | SPIRE-LM |
| 326 | 1342193788 | 2455291.61907 | 250.00 | 38.602 | 2.079 | 2.7829 | 2.3863 | 20.7 | 36.792 | 1.05 | SPIRE-SM |
| 326 | 1342193788 | 2455291.61907 | 350.00 | 20.372 | 1.098 | 2.7829 | 2.3863 | 20.7 | 19.151 | 1.06 | SPIRE-SM |
| 326 | 1342193788 | 2455291.61907 | 500.00 | 10.064 | 0.543 | 2.7829 | 2.3863 | 20.7 | 9.639 | 1.04 | SPIRE-SM |
| 287 | 1342191193 | 2455253.20392 | 250.00 | 27.183 | 1.464 | 2.7515 | 2.8833 | 20.2 | 25.420 | 1.07 | SPIRE-LM |
| 287 | 1342191193 | 2455253.20392 | 350.00 | 14.243 | 0.767 | 2.7515 | 2.8833 | 20.2 | 13.228 | 1.08 | SPIRE-LM |
| 287 | 1342191193 | 2455253.20392 | 500.00 | 6.936 | 0.374 | 2.7515 | 2.8833 | 20.2 | 6.656 | 1.04 | SPIRE-LM |
| 275 | 1342190670 | 2455240.99403 | 250.00 | 24.514 | 1.320 | 2.7415 | 3.0311 | 19.0 | 23.147 | 1.06 | SPIRE-SM |
| 275 | 1342190670 | 2455240.99403 | 350.00 | 12.756 | 0.687 | 2.7415 | 3.0311 | 19.0 | 12.042 | 1.06 | SPIRE-SM |
| 275 | 1342190670 | 2455240.99403 | 500.00 | 6.298 | 0.339 | 2.7415 | 3.0311 | 19.0 | 6.059 | 1.04 | SPIRE-SM |
| 275 | 1342190669 | 2455240.97800 | 250.00 | 24.588 | 1.324 | 2.7414 | 3.0312 | 19.0 | 23.149 | 1.06 | SPIRE-LM |
| 275 | 1342190669 | 2455240.97800 | 350.00 | 12.926 | 0.696 | 2.7414 | 3.0312 | 19.0 | 12.043 | 1.07 | SPIRE-LM |
| 275 | 1342190669 | 2455240.97800 | 500.00 | 6.294 | 0.339 | 2.7414 | 3.0312 | 19.0 | 6.059 | 1.04 | SPIRE-LM |
| 923 | 1342232694 | 2455889.00330 | 530.70 | 7.240 | 0.650 | 2.9436 | 2.5108 | -19.1 | 7.347 | 0.99 | HIFI |
| 1247 | 1342253122 | 2456212.37674 | 530.70 | 8.710 | 1.160 | 2.7161 | 2.2520 | 20.8 | 9.778 | 0.89 | HIFI |
| 1260 | 1342254428 | 2456225.38605 | 530.70 | 11.480 | 0.720 | 2.7056 | 2.0809 | 19.1 | 11.541 | 0.99 | HIFI |
| 1392 | 1342266018 | | | | | | | | | | |
| 1392 | ...19/20/21 | 2456357.83605 | 544.60 | 8.610 | 0.620 | 2.6095 | 2.3030 | -22.4 | 8.737 | 0.99 | HIFI |

Table 17: Photometric Herschel data of (2) Pallas.

| OD | OBSID | mid-time [JD] | $\lambda$ [$\mu$m] | FD [Jy] | $\sigma$ [Jy] | r [AU] | $\Delta$ [AU] | $\alpha$ [°] | TPM [Jy] | FD/TPM | Instr./Mode |
|---|---|---|---|---|---|---|---|---|---|---|---|
| 1295 | 1342256236 | 2456260.76741 | 70.00 | 115.167 | 5.873 | 2.8097 | 2.3896 | -20.1 | 119.153 | 0.97 | PACS-SM |
| 1295 | 1342256237 | 2456260.77145 | 70.00 | 115.263 | 5.878 | 2.8097 | 2.3897 | -20.1 | 118.967 | 0.97 | PACS-SM |
| 1139 | 1342247436 | 2456104.37881 | 70.00 | 67.342 | 3.434 | 3.1345 | 3.0368 | 19.1 | 70.565 | 0.95 | PACS-SM |
| 1139 | 1342247437 | 2456104.38285 | 70.00 | 67.727 | 3.454 | 3.1345 | 3.0367 | 19.1 | 70.799 | 0.96 | PACS-SM |
| 889 | 1342231264 | 2455854.68071 | 70.00 | 52.862 | 2.696 | 3.4014 | 3.2150 | -17.2 | 52.456 | 1.01 | PACS-SM |
| 889 | 1342231265 | 2455854.68475 | 70.00 | 52.788 | 2.692 | 3.4014 | 3.2151 | -17.2 | 52.462 | 1.01 | PACS-SM |
| 720 | 1342220588 | 2455685.97934 | 70.00 | 47.622 | 2.428 | 3.3789 | 3.2213 | 17.6 | 46.733 | 1.02 | PACS-SM |
| 720 | 1342220589 | 2455685.98338 | 70.00 | 47.920 | 2.444 | 3.3789 | 3.2213 | 17.6 | 46.816 | 1.02 | PACS-SM |
| 686 | 1342217781 | 2455652.04640 | 70.00 | 43.063 | 2.196 | 3.3543 | 3.6021 | 16.2 | 43.658 | 0.99 | PACS-SM |
| 686 | 1342217782 | 2455652.05044 | 70.00 | 43.136 | 2.200 | 3.3543 | 3.6021 | 16.2 | 43.643 | 0.99 | PACS-SM |
| 446 | 1342202076 | 2455411.26149 | 70.00 | 82.093 | 4.186 | 2.9997 | 2.8399 | -19.9 | 82.860 | 0.99 | PACS-SM |
| 446 | 1342202077 | 2455411.26553 | 70.00 | 82.240 | 4.194 | 2.9997 | 2.8399 | -19.9 | 82.713 | 0.99 | PACS-SM |
| 245 | 1342189264 | 2455210.82409 | 70.00 | 109.808 | 5.599 | 2.5313 | 2.6530 | 21.9 | 109.941 | 1.00 | PACS-SM |
| 245 | 1342189265 | 2455210.82775 | 70.00 | 109.962 | 5.607 | 2.5313 | 2.6529 | 21.9 | 109.942 | 1.00 | PACS-SM |
| 1295 | 1342256233 | 2456260.75672 | 100.00 | 66.457 | 3.389 | 2.8097 | 2.3895 | -20.1 | 68.852 | 0.97 | PACS-SM |
| 1295 | 1342256234 | 2456260.76076 | 100.00 | 65.948 | 3.363 | 2.8097 | 2.3895 | -20.1 | 68.654 | 0.96 | PACS-SM |
| 1139 | 1342247433 | 2456104.36813 | 100.00 | 38.779 | 1.977 | 3.1345 | 3.0369 | 19.1 | 40.661 | 0.95 | PACS-SM |
| 1139 | 1342247434 | 2456104.37216 | 100.00 | 38.889 | 1.983 | 3.1345 | 3.0369 | 19.1 | 40.830 | 0.95 | PACS-SM |
| 889 | 1342231267 | 2455854.69139 | 100.00 | 30.892 | 1.575 | 3.4014 | 3.2152 | -17.2 | 30.780 | 1.00 | PACS-SM |
| 889 | 1342231268 | 2455854.69543 | 100.00 | 30.711 | 1.566 | 3.4014 | 3.2152 | -17.2 | 30.721 | 1.00 | PACS-SM |
| 720 | 1342220590 | 2455685.98742 | 100.00 | 28.362 | 1.446 | 3.3789 | 3.2212 | 17.6 | 27.713 | 1.02 | PACS-SM |
| 720 | 1342220591 | 2455685.99146 | 100.00 | 28.394 | 1.448 | 3.3789 | 3.2212 | 17.6 | 27.853 | 1.02 | PACS-SM |
| 686 | 1342217784 | 2455652.05708 | 100.00 | 25.245 | 1.287 | 3.3543 | 3.6020 | 16.2 | 25.476 | 0.99 | PACS-SM |
| 686 | 1342217785 | 2455652.06112 | 100.00 | 25.031 | 1.276 | 3.3543 | 3.6019 | 16.2 | 25.373 | 0.99 | PACS-SM |
| 446 | 1342202079 | 2455411.27218 | 100.00 | 47.333 | 2.414 | 2.9998 | 2.8400 | -19.9 | 47.788 | 0.99 | PACS-SM |
| 446 | 1342202080 | 2455411.27622 | 100.00 | 47.081 | 2.401 | 2.9998 | 2.8401 | -19.9 | 47.706 | 0.99 | PACS-SM |
| 245 | 1342189266 | 2455210.83142 | 100.00 | 61.788 | 3.151 | 2.5313 | 2.6529 | 21.9 | 62.617 | 0.99 | PACS-SM |
| 245 | 1342189267 | 2455210.83509 | 100.00 | 61.420 | 3.132 | 2.5313 | 2.6529 | 21.9 | 62.613 | 0.98 | PACS-SM |
| 1295 | 1342256233 | 2456260.75672 | 160.00 | 28.975 | 1.478 | 2.8097 | 2.3895 | -20.1 | 29.398 | 0.99 | PACS-SM |
| 1295 | 1342256234 | 2456260.76076 | 160.00 | 28.794 | 1.473 | 2.8097 | 2.3895 | -20.1 | 29.311 | 0.98 | PACS-SM |
| 1295 | 1342256236 | 2456260.76741 | 160.00 | 28.786 | 1.469 | 2.8097 | 2.3896 | -20.1 | 29.177 | 0.99 | PACS-SM |
| 1295 | 1342256237 | 2456260.77145 | 160.00 | 28.701 | 1.464 | 2.8097 | 2.3897 | -20.1 | 29.130 | 0.99 | PACS-SM |
| 1139 | 1342247433 | 2456104.36813 | 160.00 | 16.989 | 0.869 | 3.1345 | 3.0369 | 19.1 | 17.566 | 0.97 | PACS-SM |
| 1139 | 1342247434 | 2456104.37216 | 160.00 | 17.029 | 0.870 | 3.1345 | 3.0369 | 19.1 | 17.636 | 0.97 | PACS-SM |
| 1139 | 1342247436 | 2456104.37881 | 160.00 | 17.293 | 0.883 | 3.1345 | 3.0368 | 19.1 | 17.735 | 0.98 | PACS-SM |
| 1139 | 1342247437 | 2456104.38285 | 160.00 | 17.199 | 0.880 | 3.1345 | 3.0367 | 19.1 | 17.789 | 0.97 | PACS-SM |
| 889 | 1342231264 | 2455854.68071 | 160.00 | 13.649 | 0.697 | 3.4014 | 3.2150 | -17.2 | 13.440 | 1.02 | PACS-SM |
| 889 | 1342231265 | 2455854.68475 | 160.00 | 13.564 | 0.693 | 3.4014 | 3.2151 | -17.2 | 13.436 | 1.01 | PACS-SM |
| 889 | 1342231267 | 2455854.69139 | 160.00 | 13.520 | 0.690 | 3.4014 | 3.2152 | -17.2 | 13.402 | 1.01 | PACS-SM |
| 889 | 1342231268 | 2455854.69543 | 160.00 | 13.443 | 0.687 | 3.4014 | 3.2152 | -17.2 | 13.377 | 1.00 | PACS-SM |
| 720 | 1342220588 | 2455685.97934 | 160.00 | 12.312 | 0.628 | 3.3789 | 3.2213 | 17.6 | 12.016 | 1.02 | PACS-SM |
| 720 | 1342220589 | 2455685.98338 | 160.00 | 12.294 | 0.629 | 3.3789 | 3.2213 | 17.6 | 12.043 | 1.02 | PACS-SM |
| 720 | 1342220590 | 2455685.98742 | 160.00 | 12.372 | 0.632 | 3.3789 | 3.2212 | 17.6 | 12.085 | 1.02 | PACS-SM |
| 720 | 1342220591 | 2455685.99146 | 160.00 | 12.402 | 0.633 | 3.3789 | 3.2212 | 17.6 | 12.149 | 1.02 | PACS-SM |
| 686 | 1342217781 | 2455652.04640 | 160.00 | 11.037 | 0.564 | 3.3543 | 3.6021 | 16.2 | 11.094 | 0.99 | PACS-SM |
| 686 | 1342217782 | 2455652.05044 | 160.00 | 10.975 | 0.560 | 3.3543 | 3.6021 | 16.2 | 11.086 | 0.99 | PACS-SM |
| 686 | 1342217784 | 2455652.05708 | 160.00 | 10.997 | 0.562 | 3.3543 | 3.6020 | 16.2 | 11.050 | 1.00 | PACS-SM |
| 686 | 1342217785 | 2455652.06112 | 160.00 | 10.927 | 0.557 | 3.3543 | 3.6019 | 16.2 | 11.006 | 0.99 | PACS-SM |
| 446 | 1342202076 | 2455411.26149 | 160.00 | 20.825 | 1.064 | 2.9997 | 2.8399 | -19.9 | 20.632 | 1.01 | PACS-SM |
| 446 | 1342202077 | 2455411.26553 | 160.00 | 20.792 | 1.061 | 2.9997 | 2.8399 | -19.9 | 20.600 | 1.01 | PACS-SM |
| 446 | 1342202079 | 2455411.27218 | 160.00 | 20.843 | 1.064 | 2.9998 | 2.8400 | -19.9 | 20.545 | 1.01 | PACS-SM |
| 446 | 1342202080 | 2455411.27622 | 160.00 | 20.748 | 1.058 | 2.9998 | 2.8401 | -19.9 | 20.510 | 1.01 | PACS-SM |
| 245 | 1342189264 | 2455210.82409 | 160.00 | 26.771 | 1.367 | 2.5313 | 2.6530 | 21.9 | 26.560 | 1.01 | PACS-SM |

*continued on next page*

Table 17: *continued*

| OD | OBSID | mid-time [JD] | $\lambda$ [$\mu$m] | FD [Jy] | $\sigma$ [Jy] | r [AU] | $\Delta$ [AU] | $\alpha$ [°] | TPM [Jy] | FD/TPM | Instr./Mode |
|---|---|---|---|---|---|---|---|---|---|---|---|
| 245 | 1342189265 | 2455210.82775 | 160.00 | 26.774 | 1.366 | 2.5313 | 2.6529 | 21.9 | 26.559 | 1.01 | PACS-SM |
| 245 | 1342189266 | 2455210.83142 | 160.00 | 26.748 | 1.364 | 2.5313 | 2.6529 | 21.9 | 26.557 | 1.01 | PACS-SM |
| 245 | 1342189267 | 2455210.83509 | 160.00 | 26.755 | 1.364 | 2.5313 | 2.6529 | 21.9 | 26.556 | 1.01 | PACS-SM |
| 245 | 1342189262 | 2455210.81910 | 70.00 | 109.681 | 5.595 | 2.5313 | 2.6530 | 21.9 | 109.936 | 1.00 | PACS-CN |
| 245 | 1342189262 | 2455210.81910 | 160.00 | 26.141 | 1.382 | 2.5313 | 2.6530 | 21.9 | 26.560 | 0.98 | PACS-CN |
| 245 | 1342189263 | 2455210.82170 | 100.00 | 61.250 | 3.126 | 2.5313 | 2.6530 | 21.9 | 62.623 | 0.98 | PACS-CN |
| 245 | 1342189263 | 2455210.82170 | 160.00 | 26.117 | 1.390 | 2.5313 | 2.6530 | 21.9 | 26.560 | 0.98 | PACS-CN |
| 446 | 1342202078 | 2455411.26979 | 100.00 | 46.463 | 2.371 | 2.9998 | 2.8400 | -19.9 | 47.835 | 0.97 | PACS-CN |
| 446 | 1342202078 | 2455411.26979 | 160.00 | 20.230 | 1.074 | 2.9998 | 2.8400 | -19.9 | 20.565 | 0.98 | PACS-CN |
| 446 | 1342202075 | 2455411.25911 | 70.00 | 82.115 | 4.189 | 2.9997 | 2.8398 | -19.9 | 82.942 | 0.99 | PACS-CN |
| 446 | 1342202075 | 2455411.25911 | 160.00 | 20.337 | 1.075 | 2.9997 | 2.8398 | -19.9 | 20.649 | 0.98 | PACS-CN |
| 1295 | 1342256232 | 2456260.75434 | 100.00 | 65.818 | 3.359 | 2.8098 | 2.3895 | -20.1 | 69.000 | 0.95 | PACS-CN |
| 1295 | 1342256232 | 2456260.75434 | 160.00 | 28.695 | 1.519 | 2.8098 | 2.3895 | -20.1 | 29.463 | 0.97 | PACS-CN |
| 1295 | 1342256235 | 2456260.76502 | 70.00 | 116.244 | 5.930 | 2.8097 | 2.3896 | -20.1 | 119.300 | 0.97 | PACS-CN |
| 1295 | 1342256235 | 2456260.76502 | 160.00 | 28.554 | 1.504 | 2.8097 | 2.3896 | -20.1 | 29.214 | 0.98 | PACS-CN |
| 686 | 1342217783 | 2455652.05470 | 100.00 | 25.339 | 1.293 | 3.3543 | 3.6020 | 16.2 | 25.514 | 0.99 | PACS-CN |
| 686 | 1342217783 | 2455652.05470 | 160.00 | 10.861 | 0.566 | 3.3543 | 3.6020 | 16.2 | 11.067 | 0.98 | PACS-CN |
| 686 | 1342217780 | 2455652.04402 | 70.00 | 43.842 | 2.237 | 3.3543 | 3.6021 | 16.2 | 43.633 | 1.00 | PACS-CN |
| 686 | 1342217780 | 2455652.04402 | 160.00 | 10.888 | 0.569 | 3.3543 | 3.6021 | 16.2 | 11.089 | 0.98 | PACS-CN |
| 889 | 1342231266 | 2455854.68900 | 100.00 | 31.301 | 1.597 | 3.4014 | 3.2151 | -17.2 | 30.831 | 1.02 | PACS-CN |
| 889 | 1342231266 | 2455854.68900 | 160.00 | 13.555 | 0.722 | 3.4014 | 3.2151 | -17.2 | 13.423 | 1.01 | PACS-CN |
| 889 | 1342231263 | 2455854.67832 | 70.00 | 53.636 | 2.736 | 3.4014 | 3.2150 | -17.2 | 52.391 | 1.02 | PACS-CN |
| 889 | 1342231263 | 2455854.67832 | 160.00 | 13.571 | 0.715 | 3.4014 | 3.2150 | -17.2 | 13.428 | 1.01 | PACS-CN |
| 1139 | 1342247435 | 2456104.37642 | 70.00 | 67.809 | 3.460 | 3.1345 | 3.0368 | 19.1 | 70.427 | 0.96 | PACS-CN |
| 1139 | 1342247435 | 2456104.37642 | 160.00 | 16.941 | 0.897 | 3.1345 | 3.0368 | 19.1 | 17.703 | 0.96 | PACS-CN |
| 1139 | 1342247432 | 2456104.36574 | 100.00 | 37.960 | 1.938 | 3.1345 | 3.0370 | 19.1 | 40.548 | 0.94 | PACS-CN |
| 1139 | 1342247432 | 2456104.36574 | 160.00 | 16.720 | 0.893 | 3.1345 | 3.0370 | 19.1 | 17.519 | 0.95 | PACS-CN |
| 1348 | 1342261597 | 2456313.20672 | 250.00 | 8.488 | 0.457 | 2.6837 | 2.9769 | -19.3 | 8.397 | 1.01 | SPIRE-SM |
| 1348 | 1342261597 | 2456313.20672 | 350.00 | 4.454 | 0.240 | 2.6837 | 2.9769 | -19.3 | 4.364 | 1.02 | SPIRE-SM |
| 1348 | 1342261597 | 2456313.20672 | 500.00 | 2.228 | 0.120 | 2.6837 | 2.9769 | -19.3 | 2.193 | 1.02 | SPIRE-SM |
| 1330 | 1342258378 | 2456295.65890 | 250.00 | 9.481 | 0.511 | 2.7264 | 2.7947 | -20.7 | 9.365 | 1.01 | SPIRE-SM |
| 1330 | 1342258378 | 2456295.65890 | 350.00 | 4.965 | 0.267 | 2.7264 | 2.7947 | -20.7 | 4.869 | 1.02 | SPIRE-SM |
| 1330 | 1342258378 | 2456295.65890 | 500.00 | 2.453 | 0.132 | 2.7264 | 2.7947 | -20.7 | 2.448 | 1.00 | SPIRE-SM |
| 1314 | 1342257361 | 2456279.28441 | 250.00 | 10.926 | 0.588 | 2.7658 | 2.6072 | -21.1 | 10.758 | 1.02 | SPIRE-SM |
| 1314 | 1342257361 | 2456279.28441 | 350.00 | 5.715 | 0.308 | 2.7658 | 2.6072 | -21.1 | 5.598 | 1.02 | SPIRE-SM |
| 1314 | 1342257361 | 2456279.28441 | 500.00 | 2.853 | 0.154 | 2.7658 | 2.6072 | -21.1 | 2.816 | 1.01 | SPIRE-SM |
| 1156 | 1342247987 | 2456121.38941 | 250.00 | 9.082 | 0.489 | 3.1042 | 2.7596 | 19.0 | 8.967 | 1.01 | SPIRE-SM |
| 1156 | 1342247987 | 2456121.38941 | 350.00 | 4.803 | 0.259 | 3.1042 | 2.7596 | 19.0 | 4.678 | 1.03 | SPIRE-SM |
| 1156 | 1342247987 | 2456121.38941 | 500.00 | 2.405 | 0.130 | 3.1042 | 2.7596 | 19.0 | 2.358 | 1.02 | SPIRE-SM |
| 1116 | 1342246576 | 2456081.35549 | 250.00 | 5.712 | 0.308 | 3.1732 | 3.3999 | 17.5 | 5.749 | 0.99 | SPIRE-SM |
| 1116 | 1342246576 | 2456081.35549 | 350.00 | 3.007 | 0.162 | 3.1732 | 3.3999 | 17.5 | 3.001 | 1.00 | SPIRE-SM |
| 1116 | 1342246576 | 2456081.35549 | 500.00 | 1.510 | 0.081 | 3.1732 | 3.3999 | 17.5 | 1.513 | 1.00 | SPIRE-SM |
| 880 | 1342230881 | 2455846.05779 | 250.00 | 6.455 | 0.348 | 3.4043 | 3.1021 | -17.0 | 6.200 | 1.04 | SPIRE-SM |
| 880 | 1342230881 | 2455846.05779 | 350.00 | 3.393 | 0.183 | 3.4043 | 3.1021 | -17.0 | 3.245 | 1.05 | SPIRE-SM |
| 880 | 1342230881 | 2455846.05779 | 500.00 | 1.673 | 0.090 | 3.4043 | 3.1021 | -17.0 | 1.640 | 1.02 | SPIRE-SM |
| 718 | 1342219819 | 2455684.42266 | 250.00 | 5.795 | 0.312 | 3.3779 | 3.2392 | 17.5 | 5.544 | 1.05 | SPIRE-LM |
| 718 | 1342219819 | 2455684.42266 | 350.00 | 3.106 | 0.167 | 3.3779 | 3.2392 | 17.5 | 2.901 | 1.07 | SPIRE-LM |
| 718 | 1342219819 | 2455684.42266 | 500.00 | 1.525 | 0.082 | 3.3779 | 3.2392 | 17.5 | 1.466 | 1.04 | SPIRE-LM |
| 683 | 1342216957 | 2455649.46441 | 250.00 | 4.677 | 0.252 | 3.3522 | 3.6288 | 16.0 | 4.574 | 1.02 | SPIRE-SM |
| 683 | 1342216957 | 2455649.46441 | 350.00 | 2.463 | 0.133 | 3.3522 | 3.6288 | 16.0 | 2.390 | 1.03 | SPIRE-SM |
| 683 | 1342216957 | 2455649.46441 | 500.00 | 1.226 | 0.066 | 3.3522 | 3.6288 | 16.0 | 1.207 | 1.02 | SPIRE-SM |
| 467 | 1342203584 | 2455432.33449 | 250.00 | 7.549 | 0.407 | 3.0422 | 3.1155 | -19.0 | 7.285 | 1.04 | SPIRE-SM |
| 467 | 1342203584 | 2455432.33449 | 350.00 | 3.963 | 0.213 | 3.0422 | 3.1155 | -19.0 | 3.798 | 1.04 | SPIRE-SM |

*continued on next page*

Table 17: *continued*

| OD | OBSID | mid-time [JD] | $\lambda$ [$\mu$m] | FD [Jy] | $\sigma$ [Jy] | r [AU] | $\Delta$ [AU] | $\alpha$ [°] | TPM [Jy] | FD/TPM | Instr./Mode |
|---|---|---|---|---|---|---|---|---|---|---|---|
| 467 | 1342203584 | 2455432.33449 | 500.00 | 1.989 | 0.107 | 3.0422 | 3.1155 | -19.0 | 1.913 | 1.04 | SPIRE-SM |
| 458 | 1342203076 | 2455424.05120 | 250.00 | 8.030 | 0.432 | 3.0258 | 3.0078 | -19.5 | 7.586 | 1.06 | SPIRE-SM |
| 458 | 1342203076 | 2455424.05120 | 350.00 | 4.240 | 0.228 | 3.0258 | 3.0078 | -19.5 | 3.956 | 1.07 | SPIRE-SM |
| 458 | 1342203076 | 2455424.05120 | 500.00 | 2.094 | 0.113 | 3.0258 | 3.0078 | -19.5 | 1.994 | 1.05 | SPIRE-SM |
| 447 | 1342202207 | 2455412.99738 | 250.00 | 9.040 | 0.487 | 3.0033 | 2.8629 | -19.9 | 8.490 | 1.06 | SPIRE-LM |
| 447 | 1342202207 | 2455412.99738 | 350.00 | 4.804 | 0.259 | 3.0033 | 2.8629 | -19.9 | 4.427 | 1.09 | SPIRE-LM |
| 447 | 1342202207 | 2455412.99738 | 500.00 | 2.366 | 0.127 | 3.0033 | 2.8629 | -19.9 | 2.231 | 1.06 | SPIRE-LM |
| 423 | 1342200202 | 2455388.80251 | 250.00 | 11.245 | 0.606 | 2.9524 | 2.5509 | -19.8 | 10.833 | 1.04 | SPIRE-LM |
| 423 | 1342200202 | 2455388.80251 | 350.00 | 5.984 | 0.322 | 2.9524 | 2.5509 | -19.8 | 5.644 | 1.06 | SPIRE-LM |
| 423 | 1342200202 | 2455388.80251 | 500.00 | 2.955 | 0.159 | 2.9524 | 2.5509 | -19.8 | 2.843 | 1.04 | SPIRE-LM |
| 417 | 1342199784 | 2455382.98106 | 250.00 | 11.891 | 0.640 | 2.9398 | 2.4794 | -19.6 | 11.357 | 1.05 | SPIRE-LM |
| 417 | 1342199784 | 2455382.98106 | 350.00 | 6.343 | 0.342 | 2.9398 | 2.4794 | -19.6 | 5.917 | 1.07 | SPIRE-LM |
| 417 | 1342199784 | 2455382.98106 | 500.00 | 3.089 | 0.166 | 2.9398 | 2.4794 | -19.6 | 2.980 | 1.04 | SPIRE-LM |

Table 18: Photometric Herschel data of (4) Vesta.

| OD | OBSID | mid-time [JD] | $\lambda$ [$\mu$m] | FD [Jy] | $\sigma$ [Jy] | r [AU] | $\Delta$ [AU] | $\alpha$ [°] | TPM [Jy] | FD/TPM | Instr./Mode |
|---|---|---|---|---|---|---|---|---|---|---|---|
| 1377 | 1342263924 | 2456342.87696 | 70.00 | 116.565 | 5.944 | 2.5563 | 2.1799 | -22.5 | 116.717 | 1.00 | PACS-SM |
| 1377 | 1342263925 | 2456342.88100 | 70.00 | 117.414 | 5.987 | 2.5563 | 2.1800 | -22.5 | 116.794 | 1.01 | PACS-SM |
| 1202 | 1342250298 | 2456167.66639 | 70.00 | 91.754 | 4.679 | 2.5560 | 2.5584 | 23.0 | 91.318 | 1.00 | PACS-SM |
| 1202 | 1342250299 | 2456167.67043 | 70.00 | 91.668 | 4.674 | 2.5560 | 2.5583 | 23.0 | 90.840 | 1.01 | PACS-SM |
| 900 | 1342231689 | 2455865.63354 | 70.00 | 158.580 | 8.087 | 2.3223 | 2.0156 | -25.5 | 158.553 | 1.00 | PACS-SM |
| 900 | 1342231690 | 2455865.63758 | 70.00 | 157.717 | 8.042 | 2.3223 | 2.0157 | -25.5 | 158.297 | 1.00 | PACS-SM |
| 743 | 1342221724 | 2455708.58932 | 70.00 | 276.330 | 14.091 | 2.1890 | 1.6460 | 26.5 | 259.573 | 1.06 | PACS-SM |
| 743 | 1342221725 | 2455708.59336 | 70.00 | 276.764 | 14.113 | 2.1890 | 1.6460 | 26.5 | 259.100 | 1.07 | PACS-SM |
| 726 | 1342220287 | 2455691.58957 | 70.00 | 215.624 | 10.995 | 2.1794 | 1.8280 | 27.8 | 206.579 | 1.04 | PACS-SM |
| 726 | 1342220288 | 2455691.59361 | 70.00 | 215.392 | 10.983 | 2.1794 | 1.8280 | 27.8 | 206.104 | 1.05 | PACS-SM |
| 720 | 1342220583 | 2455685.95713 | 70.00 | 206.611 | 10.535 | 2.1765 | 1.8900 | 27.9 | 197.115 | 1.05 | PACS-SM |
| 720 | 1342220584 | 2455685.96117 | 70.00 | 207.588 | 10.585 | 2.1765 | 1.8900 | 27.9 | 197.456 | 1.05 | PACS-SM |
| 703 | 1342218744 | 2455669.08336 | 70.00 | 168.821 | 8.608 | 2.1688 | 2.0770 | 27.5 | 164.326 | 1.03 | PACS-SM |
| 703 | 1342218745 | 2455669.08740 | 70.00 | 169.162 | 8.626 | 2.1688 | 2.0769 | 27.5 | 163.512 | 1.03 | PACS-SM |
| 686 | 1342217778 | 2455652.03242 | 70.00 | 143.699 | 7.327 | 2.1624 | 2.2633 | 26.2 | 138.529 | 1.04 | PACS-SM |
| 686 | 1342217779 | 2455652.03646 | 70.00 | 144.625 | 7.375 | 2.1624 | 2.2632 | 26.2 | 138.387 | 1.05 | PACS-SM |
| 677 | 1342216610 | 2455642.92424 | 70.00 | 118.582 | 6.047 | 2.1597 | 2.3600 | 25.2 | 126.596 | 0.94 | PACS-SM |
| 677 | 1342216611 | 2455642.93718 | 70.00 | 130.812 | 6.671 | 2.1597 | 2.3598 | 25.2 | 125.608 | 1.04 | PACS-SM |
| 677 | 1342216608 | 2455642.91616 | 70.00 | 132.078 | 6.735 | 2.1597 | 2.3600 | 25.2 | 127.223 | 1.04 | PACS-SM |
| 677 | 1342216609 | 2455642.92020 | 70.00 | 131.624 | 6.712 | 2.1597 | 2.3600 | 25.2 | 126.915 | 1.04 | PACS-SM |
| 348 | 1342195624 | 2455313.63307 | 70.00 | 193.322 | 9.858 | 2.3284 | 1.8378 | -24.9 | 188.418 | 1.03 | PACS-SM |
| 348 | 1342195625 | 2455313.63699 | 70.00 | 192.251 | 9.804 | 2.3284 | 1.8378 | -24.9 | 188.257 | 1.02 | PACS-SM |
| 345 | 1342195470 | 2455310.51046 | 70.00 | 202.929 | 10.348 | 2.3315 | 1.8047 | -24.4 | 195.865 | 1.04 | PACS-SM |
| 345 | 1342195471 | 2455310.51933 | 70.00 | 200.257 | 10.212 | 2.3315 | 1.8048 | -24.4 | 195.622 | 1.02 | PACS-SM |
| 345 | 1342195472 | 2455310.52819 | 70.00 | 193.816 | 9.884 | 2.3315 | 1.8049 | -24.4 | 194.723 | 1.00 | PACS-SM |
| 345 | 1342195473 | 2455310.53750 | 70.00 | 194.582 | 9.922 | 2.3315 | 1.8050 | -24.4 | 192.832 | 1.01 | PACS-SM |
| 160 | 1342186135 | 2455125.58284 | 70.00 | 93.395 | 4.762 | 2.4984 | 2.7129 | 21.7 | 88.365 | 1.06 | PACS-SM |
| 160 | 1342186136 | 2455125.59777 | 70.00 | 94.994 | 4.844 | 2.4984 | 2.7127 | 21.7 | 88.724 | 1.07 | PACS-SM |
| 160 | 1342186137 | 2455125.60851 | 70.00 | 95.968 | 4.894 | 2.4984 | 2.7125 | 21.7 | 89.183 | 1.08 | PACS-SM |
| 1377 | 1342263921 | 2456342.86627 | 100.00 | 64.052 | 3.266 | 2.5563 | 2.1798 | -22.5 | 67.804 | 0.94 | PACS-SM |
| 1377 | 1342263922 | 2456342.87031 | 100.00 | 63.734 | 3.250 | 2.5563 | 2.1798 | -22.5 | 67.523 | 0.94 | PACS-SM |
| 900 | 1342231692 | 2455865.64422 | 100.00 | 85.552 | 4.362 | 2.3223 | 2.0158 | -25.5 | 90.141 | 0.95 | PACS-SM |
| 900 | 1342231693 | 2455865.64826 | 100.00 | 84.922 | 4.330 | 2.3223 | 2.0158 | -25.5 | 89.565 | 0.95 | PACS-SM |
| 743 | 1342221727 | 2455708.60000 | 100.00 | 150.596 | 7.679 | 2.1890 | 1.6459 | 26.5 | 146.877 | 1.03 | PACS-SM |
| 743 | 1342221728 | 2455708.60404 | 100.00 | 149.658 | 7.631 | 2.1890 | 1.6459 | 26.4 | 146.551 | 1.02 | PACS-SM |
| 726 | 1342220290 | 2455691.60025 | 100.00 | 117.084 | 5.970 | 2.1794 | 1.8279 | 27.8 | 117.231 | 1.00 | PACS-SM |
| 726 | 1342220291 | 2455691.60429 | 100.00 | 116.798 | 5.956 | 2.1794 | 1.8278 | 27.8 | 117.162 | 1.00 | PACS-SM |
| 720 | 1342220586 | 2455685.96781 | 100.00 | 113.144 | 5.769 | 2.1765 | 1.8899 | 27.9 | 112.752 | 1.00 | PACS-SM |
| 720 | 1342220587 | 2455685.97185 | 100.00 | 112.400 | 5.731 | 2.1765 | 1.8898 | 27.9 | 113.067 | 0.99 | PACS-SM |
| 703 | 1342218747 | 2455669.09404 | 100.00 | 91.262 | 4.653 | 2.1688 | 2.0769 | 27.5 | 92.294 | 0.99 | PACS-SM |
| 703 | 1342218748 | 2455669.09808 | 100.00 | 90.485 | 4.614 | 2.1688 | 2.0768 | 27.5 | 91.872 | 0.98 | PACS-SM |
| 677 | 1342216612 | 2455642.95012 | 100.00 | 70.831 | 3.612 | 2.1597 | 2.3597 | 25.2 | 71.210 | 0.99 | PACS-SM |
| 677 | 1342216613 | 2455642.96306 | 100.00 | 70.676 | 3.604 | 2.1597 | 2.3596 | 25.2 | 71.535 | 0.99 | PACS-SM |
| 348 | 1342195627 | 2455313.64352 | 100.00 | 103.752 | 5.290 | 2.3284 | 1.8379 | -24.9 | 107.504 | 0.97 | PACS-SM |
| 348 | 1342195628 | 2455313.64744 | 100.00 | 102.945 | 5.249 | 2.3284 | 1.8379 | -24.9 | 107.136 | 0.96 | PACS-SM |
| 348 | 1342195622 | 2455313.58429 | 100.00 | 105.135 | 5.361 | 2.3285 | 1.8372 | -24.8 | 107.951 | 0.97 | PACS-SM |
| 345 | 1342195474 | 2455310.54681 | 100.00 | 107.226 | 5.468 | 2.3315 | 1.8051 | -24.4 | 109.397 | 0.98 | PACS-SM |
| 345 | 1342195475 | 2455310.55567 | 100.00 | 107.573 | 5.485 | 2.3315 | 1.8052 | -24.4 | 108.931 | 0.99 | PACS-SM |
| 345 | 1342195476 | 2455310.56454 | 100.00 | 108.382 | 5.526 | 2.3315 | 1.8052 | -24.4 | 109.282 | 0.99 | PACS-SM |
| 345 | 1342195477 | 2455310.57384 | 100.00 | 108.339 | 5.524 | 2.3315 | 1.8053 | -24.4 | 110.083 | 0.98 | PACS-SM |
| 160 | 1342186132 | 2455125.54682 | 100.00 | 51.085 | 2.605 | 2.4984 | 2.7133 | 21.7 | 51.635 | 0.99 | PACS-SM |
| 160 | 1342186133 | 2455125.56175 | 100.00 | 50.999 | 2.601 | 2.4984 | 2.7131 | 21.7 | 51.125 | 1.00 | PACS-SM |
| 160 | 1342186134 | 2455125.57249 | 100.00 | 51.702 | 2.636 | 2.4984 | 2.7130 | 21.7 | 50.708 | 1.02 | PACS-SM |

*continued on next page*

Table 18: *continued*

| OD | OBSID | mid-time [JD] | $\lambda$ [$\mu$m] | FD [Jy] | $\sigma$ [Jy] | r [AU] | $\Delta$ [AU] | $\alpha$ [°] | TPM [Jy] | FD/TPM | Instr./Mode |
|---|---|---|---|---|---|---|---|---|---|---|---|
| 1377 | 1342263921 | 2456342.86627 | 160.00 | 27.116 | 1.384 | 2.5563 | 2.1798 | -22.5 | 28.625 | 0.95 | PACS-SM |
| 1377 | 1342263922 | 2456342.87031 | 160.00 | 27.177 | 1.387 | 2.5563 | 2.1798 | -22.5 | 28.518 | 0.95 | PACS-SM |
| 1377 | 1342263924 | 2456342.87696 | 160.00 | 27.434 | 1.400 | 2.5563 | 2.1799 | -22.5 | 28.486 | 0.96 | PACS-SM |
| 1377 | 1342263925 | 2456342.88100 | 160.00 | 27.578 | 1.408 | 2.5563 | 2.1800 | -22.5 | 28.527 | 0.97 | PACS-SM |
| 1202 | 1342250298 | 2456167.66639 | 160.00 | 21.610 | 1.103 | 2.5560 | 2.5584 | 23.0 | 22.228 | 0.97 | PACS-SM |
| 1202 | 1342250299 | 2456167.67043 | 160.00 | 21.463 | 1.095 | 2.5560 | 2.5583 | 23.0 | 22.114 | 0.97 | PACS-SM |
| 900 | 1342231689 | 2455865.63354 | 160.00 | 36.283 | 1.851 | 2.3223 | 2.0156 | -25.5 | 38.137 | 0.95 | PACS-SM |
| 900 | 1342231690 | 2455865.63758 | 160.00 | 35.952 | 1.835 | 2.3223 | 2.0157 | -25.5 | 38.063 | 0.94 | PACS-SM |
| 900 | 1342231692 | 2455865.64422 | 160.00 | 35.656 | 1.819 | 2.3223 | 2.0158 | -25.5 | 37.813 | 0.94 | PACS-SM |
| 900 | 1342231693 | 2455865.64826 | 160.00 | 35.440 | 1.810 | 2.3223 | 2.0158 | -25.5 | 37.573 | 0.94 | PACS-SM |
| 743 | 1342221724 | 2455708.58932 | 160.00 | 64.068 | 3.267 | 2.1890 | 1.6460 | 26.5 | 61.553 | 1.04 | PACS-SM |
| 743 | 1342221725 | 2455708.59336 | 160.00 | 63.969 | 3.264 | 2.1890 | 1.6460 | 26.5 | 61.461 | 1.04 | PACS-SM |
| 743 | 1342221727 | 2455708.60000 | 160.00 | 63.779 | 3.252 | 2.1890 | 1.6459 | 26.5 | 61.259 | 1.04 | PACS-SM |
| 743 | 1342221728 | 2455708.60404 | 160.00 | 63.571 | 3.243 | 2.1890 | 1.6459 | 26.4 | 61.124 | 1.04 | PACS-SM |
| 726 | 1342220287 | 2455691.58957 | 160.00 | 49.397 | 2.519 | 2.1794 | 1.8280 | 27.8 | 49.147 | 1.01 | PACS-SM |
| 726 | 1342220288 | 2455691.59361 | 160.00 | 49.105 | 2.504 | 2.1794 | 1.8280 | 27.8 | 49.028 | 1.00 | PACS-SM |
| 726 | 1342220290 | 2455691.60025 | 160.00 | 49.250 | 2.512 | 2.1794 | 1.8279 | 27.8 | 48.920 | 1.01 | PACS-SM |
| 726 | 1342220291 | 2455691.60429 | 160.00 | 49.161 | 2.508 | 2.1794 | 1.8278 | 27.8 | 48.886 | 1.01 | PACS-SM |
| 720 | 1342220583 | 2455685.95713 | 160.00 | 47.438 | 2.420 | 2.1765 | 1.8900 | 27.9 | 46.799 | 1.01 | PACS-SM |
| 720 | 1342220584 | 2455685.96117 | 160.00 | 47.412 | 2.419 | 2.1765 | 1.8900 | 27.9 | 46.875 | 1.01 | PACS-SM |
| 720 | 1342220586 | 2455685.96781 | 160.00 | 47.495 | 2.422 | 2.1765 | 1.8899 | 27.9 | 47.031 | 1.01 | PACS-SM |
| 720 | 1342220587 | 2455685.97185 | 160.00 | 47.172 | 2.406 | 2.1765 | 1.8898 | 27.9 | 47.159 | 1.00 | PACS-SM |
| 703 | 1342218744 | 2455669.08336 | 160.00 | 38.461 | 1.962 | 2.1688 | 2.0770 | 27.5 | 39.037 | 0.99 | PACS-SM |
| 703 | 1342218745 | 2455669.08740 | 160.00 | 38.190 | 1.950 | 2.1688 | 2.0769 | 27.5 | 38.863 | 0.98 | PACS-SM |
| 703 | 1342218747 | 2455669.09404 | 160.00 | 38.017 | 1.939 | 2.1688 | 2.0769 | 27.5 | 38.531 | 0.99 | PACS-SM |
| 703 | 1342218748 | 2455669.09808 | 160.00 | 37.672 | 1.922 | 2.1688 | 2.0768 | 27.5 | 38.355 | 0.98 | PACS-SM |
| 686 | 1342217778 | 2455652.03242 | 160.00 | 32.920 | 1.680 | 2.1624 | 2.2633 | 26.2 | 32.819 | 1.00 | PACS-SM |
| 686 | 1342217779 | 2455652.03646 | 160.00 | 32.807 | 1.674 | 2.1624 | 2.2632 | 26.2 | 32.785 | 1.00 | PACS-SM |
| 677 | 1342216610 | 2455642.92424 | 160.00 | 29.065 | 1.515 | 2.1597 | 2.3600 | 25.2 | 29.998 | 0.97 | PACS-SM |
| 677 | 1342216611 | 2455642.93718 | 160.00 | 30.297 | 1.548 | 2.1597 | 2.3598 | 25.2 | 29.773 | 1.02 | PACS-SM |
| 677 | 1342216612 | 2455642.95012 | 160.00 | 29.973 | 1.529 | 2.1597 | 2.3597 | 25.2 | 29.672 | 1.01 | PACS-SM |
| 677 | 1342216613 | 2455642.96306 | 160.00 | 29.970 | 1.528 | 2.1597 | 2.3596 | 25.2 | 29.806 | 1.01 | PACS-SM |
| 677 | 1342216608 | 2455642.91616 | 160.00 | 30.328 | 1.547 | 2.1597 | 2.3600 | 25.2 | 30.126 | 1.01 | PACS-SM |
| 677 | 1342216609 | 2455642.92020 | 160.00 | 30.138 | 1.537 | 2.1597 | 2.3600 | 25.2 | 30.063 | 1.00 | PACS-SM |
| 348 | 1342195624 | 2455313.63307 | 160.00 | 44.240 | 2.257 | 2.3284 | 1.8378 | -24.9 | 45.365 | 0.98 | PACS-SM |
| 348 | 1342195625 | 2455313.63699 | 160.00 | 43.826 | 2.235 | 2.3284 | 1.8378 | -24.9 | 45.304 | 0.97 | PACS-SM |
| 348 | 1342195627 | 2455313.64352 | 160.00 | 43.496 | 2.218 | 2.3284 | 1.8379 | -24.9 | 45.133 | 0.96 | PACS-SM |
| 348 | 1342195628 | 2455313.64744 | 160.00 | 43.267 | 2.207 | 2.3284 | 1.8379 | -24.9 | 44.975 | 0.96 | PACS-SM |
| 348 | 1342195622 | 2455313.58429 | 160.00 | 43.976 | 2.243 | 2.3285 | 1.8372 | -24.8 | 45.359 | 0.97 | PACS-SM |
| 345 | 1342195470 | 2455310.51046 | 160.00 | 45.466 | 2.319 | 2.3315 | 1.8047 | -24.4 | 47.166 | 0.96 | PACS-SM |
| 345 | 1342195471 | 2455310.51933 | 160.00 | 45.071 | 2.298 | 2.3315 | 1.8048 | -24.4 | 47.063 | 0.96 | PACS-SM |
| 345 | 1342195474 | 2455310.54681 | 160.00 | 44.840 | 2.287 | 2.3315 | 1.8051 | -24.4 | 45.942 | 0.98 | PACS-SM |
| 345 | 1342195475 | 2455310.55567 | 160.00 | 45.339 | 2.312 | 2.3315 | 1.8052 | -24.4 | 45.778 | 0.99 | PACS-SM |
| 345 | 1342195472 | 2455310.52819 | 160.00 | 44.769 | 2.283 | 2.3315 | 1.8049 | -24.4 | 46.808 | 0.96 | PACS-SM |
| 345 | 1342195473 | 2455310.53750 | 160.00 | 44.775 | 2.283 | 2.3315 | 1.8050 | -24.4 | 46.354 | 0.97 | PACS-SM |
| 345 | 1342195476 | 2455310.56454 | 160.00 | 45.839 | 2.338 | 2.3315 | 1.8052 | -24.4 | 45.938 | 1.00 | PACS-SM |
| 345 | 1342195477 | 2455310.57384 | 160.00 | 45.937 | 2.343 | 2.3315 | 1.8053 | -24.4 | 46.274 | 0.99 | PACS-SM |
| 160 | 1342186132 | 2455125.54682 | 160.00 | 21.544 | 1.099 | 2.4984 | 2.7133 | 21.7 | 21.682 | 0.99 | PACS-SM |
| 160 | 1342186135 | 2455125.58284 | 160.00 | 21.997 | 1.122 | 2.4984 | 2.7129 | 21.7 | 21.272 | 1.03 | PACS-SM |
| 160 | 1342186133 | 2455125.56175 | 160.00 | 21.456 | 1.095 | 2.4984 | 2.7131 | 21.7 | 21.472 | 1.00 | PACS-SM |
| 160 | 1342186136 | 2455125.59777 | 160.00 | 22.211 | 1.133 | 2.4984 | 2.7127 | 21.7 | 21.355 | 1.04 | PACS-SM |
| 160 | 1342186134 | 2455125.57249 | 160.00 | 21.761 | 1.110 | 2.4984 | 2.7130 | 21.7 | 21.297 | 1.02 | PACS-SM |
| 160 | 1342186137 | 2455125.60851 | 160.00 | 21.943 | 1.119 | 2.4984 | 2.7125 | 21.7 | 21.464 | 1.02 | PACS-SM |

*continued on next page*

Table 18: *continued*

| OD | OBSID | mid-time [JD] | $\lambda$ [$\mu$m] | FD [Jy] | $\sigma$ [Jy] | r [AU] | $\Delta$ [AU] | $\alpha$ [°] | TPM [Jy] | FD/TPM | Instr./Mode |
|---|---|---|---|---|---|---|---|---|---|---|---|
| 348 | 1342195623 | 2455313.63068 | 70.00 | 188.286 | 9.605 | 2.3284 | 1.8377 | -24.9 | 188.493 | 1.00 | PACS-CN |
| 348 | 1342195623 | 2455313.63068 | 160.00 | 43.230 | 2.289 | 2.3284 | 1.8377 | -24.9 | 45.395 | 0.95 | PACS-CN |
| 348 | 1342195626 | 2455313.64113 | 100.00 | 102.348 | 5.224 | 2.3284 | 1.8379 | -24.9 | 107.666 | 0.95 | PACS-CN |
| 348 | 1342195626 | 2455313.64113 | 160.00 | 42.787 | 2.277 | 2.3284 | 1.8379 | -24.9 | 45.205 | 0.95 | PACS-CN |
| 677 | 1342216607 | 2455642.91377 | 70.00 | 125.064 | 6.380 | 2.1597 | 2.3601 | 25.2 | 127.336 | 0.98 | PACS-CN |
| 677 | 1342216607 | 2455642.91377 | 160.00 | 29.649 | 1.567 | 2.1597 | 2.3601 | 25.2 | 30.147 | 0.98 | PACS-CN |
| 686 | 1342217777 | 2455652.03003 | 70.00 | 146.266 | 7.466 | 2.1624 | 2.2633 | 26.2 | 138.521 | 1.06 | PACS-CN |
| 686 | 1342217777 | 2455652.03003 | 160.00 | 32.604 | 1.701 | 2.1624 | 2.2633 | 26.2 | 32.819 | 0.99 | PACS-CN |
| 703 | 1342218746 | 2455669.09166 | 100.00 | 91.008 | 4.644 | 2.1688 | 2.0769 | 27.5 | 92.577 | 0.98 | PACS-CN |
| 703 | 1342218746 | 2455669.09166 | 160.00 | 37.926 | 1.995 | 2.1688 | 2.0769 | 27.5 | 38.647 | 0.98 | PACS-CN |
| 703 | 1342218743 | 2455669.08097 | 70.00 | 170.015 | 8.674 | 2.1688 | 2.0770 | 27.5 | 164.767 | 1.03 | PACS-CN |
| 703 | 1342218743 | 2455669.08097 | 160.00 | 38.333 | 2.018 | 2.1688 | 2.0770 | 27.5 | 39.131 | 0.98 | PACS-CN |
| 743 | 1342221726 | 2455708.59762 | 100.00 | 148.870 | 7.596 | 2.1890 | 1.6459 | 26.5 | 147.039 | 1.01 | PACS-CN |
| 743 | 1342221726 | 2455708.59762 | 160.00 | 63.044 | 3.294 | 2.1890 | 1.6459 | 26.5 | 61.325 | 1.03 | PACS-CN |
| 743 | 1342221723 | 2455708.58693 | 70.00 | 275.629 | 14.062 | 2.1890 | 1.6461 | 26.5 | 259.825 | 1.06 | PACS-CN |
| 743 | 1342221723 | 2455708.58693 | 160.00 | 63.173 | 3.311 | 2.1890 | 1.6461 | 26.5 | 61.603 | 1.03 | PACS-CN |
| 726 | 1342220289 | 2455691.59787 | 100.00 | 115.638 | 5.900 | 2.1794 | 1.8279 | 27.8 | 117.283 | 0.99 | PACS-CN |
| 726 | 1342220289 | 2455691.59787 | 160.00 | 48.637 | 2.564 | 2.1794 | 1.8279 | 27.8 | 48.946 | 0.99 | PACS-CN |
| 726 | 1342220286 | 2455691.58719 | 70.00 | 214.163 | 10.926 | 2.1794 | 1.8280 | 27.8 | 206.952 | 1.03 | PACS-CN |
| 726 | 1342220286 | 2455691.58719 | 160.00 | 49.079 | 2.577 | 2.1794 | 1.8280 | 27.8 | 49.237 | 1.00 | PACS-CN |
| 720 | 1342220585 | 2455685.96543 | 100.00 | 111.369 | 5.683 | 2.1765 | 1.8899 | 27.9 | 112.599 | 0.99 | PACS-CN |
| 720 | 1342220585 | 2455685.96543 | 160.00 | 47.085 | 2.471 | 2.1765 | 1.8899 | 27.9 | 46.968 | 1.00 | PACS-CN |
| 720 | 1342220582 | 2455685.95475 | 70.00 | 204.079 | 10.410 | 2.1765 | 1.8900 | 27.9 | 196.897 | 1.04 | PACS-CN |
| 720 | 1342220582 | 2455685.95475 | 160.00 | 46.909 | 2.471 | 2.1765 | 1.8900 | 27.9 | 46.751 | 1.00 | PACS-CN |
| 900 | 1342231688 | 2455865.63116 | 70.00 | 160.240 | 8.175 | 2.3223 | 2.0156 | -25.5 | 158.575 | 1.01 | PACS-CN |
| 900 | 1342231688 | 2455865.63116 | 160.00 | 35.876 | 1.878 | 2.3223 | 2.0156 | -25.5 | 38.154 | 0.94 | PACS-CN |
| 900 | 1342231691 | 2455865.64184 | 100.00 | 85.598 | 4.367 | 2.3223 | 2.0157 | -25.5 | 90.392 | 0.95 | PACS-CN |
| 900 | 1342231691 | 2455865.64184 | 160.00 | 35.410 | 1.865 | 2.3223 | 2.0157 | -25.5 | 37.919 | 0.93 | PACS-CN |
| 1181 | 1342249192 | 2456146.62035 | 100.00 | 42.930 | 2.191 | 2.5479 | 2.8132 | 21.2 | 43.936 | 0.98 | PACS-CN |
| 1181 | 1342249192 | 2456146.62035 | 160.00 | 17.909 | 0.942 | 2.5479 | 2.8132 | 21.2 | 18.509 | 0.97 | PACS-CN |
| 1181 | 1342249193 | 2456146.62295 | 70.00 | 78.925 | 4.026 | 2.5479 | 2.8132 | 21.2 | 76.103 | 1.04 | PACS-CN |
| 1181 | 1342249193 | 2456146.62295 | 160.00 | 17.795 | 0.939 | 2.5479 | 2.8132 | 21.2 | 18.476 | 0.96 | PACS-CN |
| 1202 | 1342250297 | 2456167.66400 | 70.00 | 90.450 | 4.615 | 2.5560 | 2.5584 | 23.0 | 91.542 | 0.99 | PACS-CN |
| 1202 | 1342250297 | 2456167.66400 | 160.00 | 21.496 | 1.137 | 2.5560 | 2.5584 | 23.0 | 22.279 | 0.96 | PACS-CN |
| 1377 | 1342263920 | 2456342.86389 | 100.00 | 63.413 | 3.236 | 2.5563 | 2.1798 | -22.5 | 67.992 | 0.93 | PACS-CN |
| 1377 | 1342263920 | 2456342.86389 | 160.00 | 27.137 | 1.450 | 2.5563 | 2.1798 | -22.5 | 28.698 | 0.95 | PACS-CN |
| 1377 | 1342263923 | 2456342.87457 | 70.00 | 116.738 | 5.956 | 2.5563 | 2.1799 | -22.5 | 116.721 | 1.00 | PACS-CN |
| 1377 | 1342263923 | 2456342.87457 | 160.00 | 27.244 | 1.467 | 2.5563 | 2.1799 | -22.5 | 28.474 | 0.96 | PACS-CN |
| 1403 | 1342267747 | 2456368.70388 | 250.00 | 8.732 | 0.470 | 2.5462 | 2.5201 | -22.8 | 8.654 | 1.01 | SPIRE-SM |
| 1403 | 1342267747 | 2456368.70388 | 350.00 | 4.314 | 0.232 | 2.5462 | 2.5201 | -22.8 | 4.279 | 1.01 | SPIRE-SM |
| 1403 | 1342267747 | 2456368.70388 | 500.00 | 2.061 | 0.111 | 2.5462 | 2.5201 | -22.8 | 2.055 | 1.00 | SPIRE-SM |
| 1388 | 1342265385 | 2456353.78877 | 250.00 | 10.206 | 0.550 | 2.5523 | 2.3244 | -23.0 | 10.087 | 1.01 | SPIRE-SM |
| 1388 | 1342265385 | 2456353.78877 | 350.00 | 5.042 | 0.272 | 2.5523 | 2.3244 | -23.0 | 4.988 | 1.01 | SPIRE-SM |
| 1388 | 1342265385 | 2456353.78877 | 500.00 | 2.423 | 0.131 | 2.5523 | 2.3244 | -23.0 | 2.396 | 1.01 | SPIRE-SM |
| 1375 | 1342263811 | 2456340.51600 | 250.00 | 11.703 | 0.630 | 2.5571 | 2.1490 | -22.3 | 11.998 | 0.98 | SPIRE-SM |
| 1375 | 1342263811 | 2456340.51600 | 350.00 | 5.735 | 0.309 | 2.5571 | 2.1490 | -22.3 | 5.930 | 0.97 | SPIRE-SM |
| 1375 | 1342263811 | 2456340.51600 | 500.00 | 2.722 | 0.147 | 2.5571 | 2.1490 | -22.3 | 2.847 | 0.96 | SPIRE-SM |
| 1201 | 1342250324 | 2456166.19958 | 250.00 | 9.073 | 0.489 | 2.5555 | 2.5768 | 22.9 | 8.867 | 1.02 | SPIRE-SM |
| 1201 | 1342250324 | 2456166.19958 | 350.00 | 4.447 | 0.240 | 2.5555 | 2.5768 | 22.9 | 4.381 | 1.02 | SPIRE-SM |
| 1201 | 1342250324 | 2456166.19958 | 500.00 | 2.147 | 0.116 | 2.5555 | 2.5768 | 22.9 | 2.102 | 1.02 | SPIRE-SM |
| 1179 | 1342249090 | 2456145.01874 | 250.00 | 7.585 | 0.408 | 2.5473 | 2.8314 | 21.1 | 7.252 | 1.05 | SPIRE-SM |
| 1179 | 1342249090 | 2456145.01874 | 350.00 | 3.751 | 0.202 | 2.5473 | 2.8314 | 21.1 | 3.581 | 1.05 | SPIRE-SM |
| 1179 | 1342249090 | 2456145.01874 | 500.00 | 1.796 | 0.097 | 2.5473 | 2.8314 | 21.1 | 1.718 | 1.05 | SPIRE-SM |

*continued on next page*

Table 18: *continued*

| OD | OBSID | mid-time [JD] | $\lambda$ [$\mu$m] | FD [Jy] | $\sigma$ [Jy] | r [AU] | $\Delta$ [AU] | $\alpha$ [°] | TPM [Jy] | FD/TPM | Instr./Mode |
|---|---|---|---|---|---|---|---|---|---|---|---|
| 916 | 1342232369 | 2455882.00303 | 250.00 | 12.440 | 0.670 | 2.3385 | 2.2340 | -25.1 | 12.203 | 1.02 | SPIRE-SM |
| 916 | 1342232369 | 2455882.00303 | 350.00 | 6.177 | 0.333 | 2.3385 | 2.2340 | -25.1 | 6.021 | 1.03 | SPIRE-SM |
| 916 | 1342232369 | 2455882.00303 | 500.00 | 2.972 | 0.160 | 2.3385 | 2.2340 | -25.1 | 2.887 | 1.03 | SPIRE-SM |
| 892 | 1342231347 | 2455858.07191 | 250.00 | 16.451 | 0.886 | 2.3148 | 1.9159 | -25.3 | 16.811 | 0.98 | SPIRE-SM |
| 892 | 1342231347 | 2455858.07191 | 350.00 | 8.087 | 0.436 | 2.3148 | 1.9159 | -25.3 | 8.290 | 0.98 | SPIRE-SM |
| 892 | 1342231347 | 2455858.07191 | 500.00 | 3.897 | 0.210 | 2.3148 | 1.9159 | -25.3 | 3.974 | 0.98 | SPIRE-SM |
| 702 | 1342218688 | 2455667.55980 | 250.00 | 15.521 | 0.836 | 2.1682 | 2.0937 | 27.4 | 14.873 | 1.04 | SPIRE-SM |
| 702 | 1342218688 | 2455667.55980 | 350.00 | 7.676 | 0.413 | 2.1682 | 2.0937 | 27.4 | 7.323 | 1.05 | SPIRE-SM |
| 702 | 1342218688 | 2455667.55980 | 500.00 | 3.695 | 0.199 | 2.1682 | 2.0937 | 27.4 | 3.506 | 1.05 | SPIRE-SM |
| 669 | 1342215994 | 2455634.38330 | 250.00 | 11.246 | 0.606 | 2.1575 | 2.4480 | 24.1 | 10.902 | 1.03 | SPIRE-SM |
| 669 | 1342215994 | 2455634.38330 | 350.00 | 5.579 | 0.300 | 2.1575 | 2.4480 | 24.1 | 5.366 | 1.04 | SPIRE-SM |
| 669 | 1342215994 | 2455634.38330 | 500.00 | 2.648 | 0.143 | 2.1575 | 2.4480 | 24.1 | 2.568 | 1.03 | SPIRE-SM |
| 402 | 1342198575 | 2455367.16860 | 250.00 | 10.810 | 0.582 | 2.2764 | 2.4131 | -25.1 | 10.538 | 1.03 | SPIRE-LM |
| 402 | 1342198575 | 2455367.16860 | 350.00 | 5.367 | 0.289 | 2.2764 | 2.4131 | -25.1 | 5.202 | 1.03 | SPIRE-LM |
| 402 | 1342198575 | 2455367.16860 | 500.00 | 2.545 | 0.137 | 2.2764 | 2.4131 | -25.1 | 2.495 | 1.02 | SPIRE-LM |
| 393 | 1342198142 | 2455358.16957 | 250.00 | 11.444 | 0.616 | 2.2849 | 2.3205 | -25.7 | 11.367 | 1.01 | SPIRE-LM |
| 393 | 1342198142 | 2455358.16957 | 350.00 | 5.680 | 0.306 | 2.2849 | 2.3205 | -25.7 | 5.613 | 1.01 | SPIRE-LM |
| 393 | 1342198142 | 2455358.16957 | 500.00 | 2.681 | 0.144 | 2.2849 | 2.3205 | -25.7 | 2.693 | 1.00 | SPIRE-LM |
| 381 | 1342197317 | 2455347.15618 | 250.00 | 11.610 | 0.625 | 2.2955 | 2.2034 | -26.2 | 12.383 | 0.94 | SPIRE-LM |
| 381 | 1342197317 | 2455347.15618 | 350.00 | 5.996 | 0.323 | 2.2955 | 2.2034 | -26.2 | 6.114 | 0.98 | SPIRE-LM |
| 381 | 1342197317 | 2455347.15618 | 500.00 | 2.884 | 0.155 | 2.2955 | 2.2034 | -26.2 | 2.933 | 0.98 | SPIRE-LM |
| 381 | 1342197316 | 2455347.14027 | 250.00 | 12.285 | 0.662 | 2.2955 | 2.2033 | -26.2 | 12.496 | 0.98 | SPIRE-LM |
| 381 | 1342197316 | 2455347.14027 | 350.00 | 6.265 | 0.337 | 2.2955 | 2.2033 | -26.2 | 6.170 | 1.02 | SPIRE-LM |
| 381 | 1342197316 | 2455347.14027 | 500.00 | 2.996 | 0.161 | 2.2955 | 2.2033 | -26.2 | 2.960 | 1.01 | SPIRE-LM |
| 369 | 1342196667 | 2455335.10704 | 250.00 | 14.413 | 0.776 | 2.3072 | 2.0721 | -26.3 | 14.160 | 1.02 | SPIRE-LM |
| 369 | 1342196667 | 2455335.10704 | 350.00 | 7.121 | 0.383 | 2.3072 | 2.0721 | -26.3 | 6.993 | 1.02 | SPIRE-LM |
| 369 | 1342196667 | 2455335.10704 | 500.00 | 3.402 | 0.183 | 2.3072 | 2.0721 | -26.3 | 3.355 | 1.01 | SPIRE-LM |
| 354 | 1342195750 | 2455319.94391 | 250.00 | 16.889 | 0.910 | 2.3222 | 1.9059 | -25.5 | 16.796 | 1.01 | SPIRE-LM |
| 354 | 1342195750 | 2455319.94391 | 350.00 | 8.487 | 0.457 | 2.3222 | 1.9059 | -25.5 | 8.294 | 1.02 | SPIRE-LM |
| 354 | 1342195750 | 2455319.94391 | 500.00 | 4.161 | 0.224 | 2.3222 | 1.9059 | -25.5 | 3.979 | 1.05 | SPIRE-LM |

Table 19: Photometric Herschel data of (21) Lutetia.

| OD | OBSID | mid-time [JD] | $\lambda$ [$\mu$m] | FD [Jy] | $\sigma$ [Jy] | r [AU] | $\Delta$ [AU] | $\alpha$ [°] | TPM [Jy] | FD/TPM | Instr./Mode |
|---|---|---|---|---|---|---|---|---|---|---|---|
| 1399 | 1342267264 | 2456364.59671 | 70.00 | 4.399 | 0.224 | 2.6964 | 2.4294 | -21.8 | 4.482 | 0.98 | PACS-SM |
| 1399 | 1342267265 | 2456364.60075 | 70.00 | 4.382 | 0.224 | 2.6964 | 2.4295 | -21.8 | 4.490 | 0.98 | PACS-SM |
| 1198 | 1342250107 | 2456163.45010 | 70.00 | 4.337 | 0.221 | 2.3743 | 2.5914 | 23.2 | 4.476 | 0.97 | PACS-SM |
| 1198 | 1342250108 | 2456163.45414 | 70.00 | 4.352 | 0.222 | 2.3743 | 2.5914 | 23.2 | 4.484 | 0.97 | PACS-SM |
| 859 | 1342228947 | 2455824.37826 | 70.00 | 11.167 | 0.569 | 2.0611 | 1.5764 | -28.6 | 11.065 | 1.01 | PACS-SM |
| 859 | 1342228948 | 2455824.38230 | 70.00 | 11.279 | 0.575 | 2.0611 | 1.5765 | -28.6 | 11.109 | 1.02 | PACS-SM |
| 684 | 1342217411 | 2455650.36816 | 70.00 | 7.082 | 0.361 | 2.2998 | 2.0525 | 26.0 | 7.335 | 0.97 | PACS-SM |
| 684 | 1342217412 | 2455650.37220 | 70.00 | 7.100 | 0.363 | 2.2998 | 2.0525 | 26.0 | 7.354 | 0.97 | PACS-SM |
| 400 | 1342198494 | 2455365.22184 | 70.00 | 2.689 | 0.137 | 2.7441 | 2.7847 | -21.4 | 2.678 | 1.00 | PACS-SM |
| 400 | 1342198495 | 2455365.22588 | 70.00 | 2.676 | 0.136 | 2.7441 | 2.7847 | -21.4 | 2.645 | 1.01 | PACS-SM |
| 1399 | 1342267261 | 2456364.58603 | 100.00 | 2.506 | 0.128 | 2.6963 | 2.4293 | -21.8 | 2.571 | 0.97 | PACS-SM |
| 1399 | 1342267262 | 2456364.59007 | 100.00 | 2.504 | 0.128 | 2.6963 | 2.4293 | -21.8 | 2.576 | 0.97 | PACS-SM |
| 1198 | 1342250104 | 2456163.43942 | 100.00 | 2.453 | 0.125 | 2.3743 | 2.5915 | 23.2 | 2.523 | 0.97 | PACS-SM |
| 1198 | 1342250105 | 2456163.44346 | 100.00 | 2.426 | 0.124 | 2.3743 | 2.5915 | 23.2 | 2.525 | 0.96 | PACS-SM |
| 859 | 1342228950 | 2455824.38895 | 100.00 | 6.486 | 0.331 | 2.0611 | 1.5765 | -28.6 | 6.391 | 1.01 | PACS-SM |
| 859 | 1342228951 | 2455824.39299 | 100.00 | 6.497 | 0.331 | 2.0611 | 1.5766 | -28.6 | 6.432 | 1.01 | PACS-SM |
| 684 | 1342217414 | 2455650.37884 | 100.00 | 4.022 | 0.205 | 2.2998 | 2.0524 | 26.0 | 4.172 | 0.96 | PACS-SM |
| 684 | 1342217415 | 2455650.38288 | 100.00 | 4.001 | 0.204 | 2.2998 | 2.0523 | 26.0 | 4.178 | 0.96 | PACS-SM |
| 400 | 1342198492 | 2455365.21376 | 100.00 | 1.591 | 0.082 | 2.7441 | 2.7846 | -21.4 | 1.592 | 1.00 | PACS-SM |
| 400 | 1342198493 | 2455365.21780 | 100.00 | 1.554 | 0.079 | 2.7441 | 2.7846 | -21.4 | 1.568 | 0.99 | PACS-SM |
| 221 | 1342188334 | 2455186.57887 | 100.00 | 1.802 | 0.093 | 2.8326 | 2.5069 | 20.3 | 1.751 | 1.03 | PACS-SM |
| 221 | 1342188335 | 2455186.58253 | 100.00 | 1.819 | 0.093 | 2.8326 | 2.5069 | 20.3 | 1.754 | 1.04 | PACS-SM |
| 221 | 1342188336 | 2455186.58620 | 100.00 | 1.829 | 0.094 | 2.8326 | 2.5068 | 20.3 | 1.765 | 1.04 | PACS-SM |
| 221 | 1342188337 | 2455186.58987 | 100.00 | 1.814 | 0.093 | 2.8326 | 2.5068 | 20.3 | 1.784 | 1.02 | PACS-SM |
| 1399 | 1342267261 | 2456364.58603 | 160.00 | 1.083 | 0.096 | 2.6963 | 2.4293 | -21.8 | 1.101 | 0.98 | PACS-SM |
| 1399 | 1342267262 | 2456364.59007 | 160.00 | 1.009 | 0.074 | 2.6963 | 2.4293 | -21.8 | 1.103 | 0.91 | PACS-SM |
| 1399 | 1342267264 | 2456364.59671 | 160.00 | 1.058 | 0.073 | 2.6964 | 2.4294 | -21.8 | 1.105 | 0.96 | PACS-SM |
| 1399 | 1342267265 | 2456364.60075 | 160.00 | 1.072 | 0.078 | 2.6964 | 2.4295 | -21.8 | 1.107 | 0.97 | PACS-SM |
| 1198 | 1342250104 | 2456163.43942 | 160.00 | 1.052 | 0.060 | 2.3743 | 2.5915 | 23.2 | 1.064 | 0.99 | PACS-SM |
| 1198 | 1342250105 | 2456163.44346 | 160.00 | 1.026 | 0.056 | 2.3743 | 2.5915 | 23.2 | 1.065 | 0.96 | PACS-SM |
| 1198 | 1342250107 | 2456163.45010 | 160.00 | 1.032 | 0.068 | 2.3743 | 2.5914 | 23.2 | 1.067 | 0.97 | PACS-SM |
| 1198 | 1342250108 | 2456163.45414 | 160.00 | 1.085 | 0.057 | 2.3743 | 2.5914 | 23.2 | 1.069 | 1.01 | PACS-SM |
| 859 | 1342228947 | 2455824.37826 | 160.00 | 2.707 | 0.158 | 2.0611 | 1.5764 | -28.6 | 2.681 | 1.01 | PACS-SM |
| 859 | 1342228948 | 2455824.38230 | 160.00 | 2.710 | 0.146 | 2.0611 | 1.5765 | -28.6 | 2.691 | 1.01 | PACS-SM |
| 859 | 1342228950 | 2455824.38895 | 160.00 | 2.802 | 0.152 | 2.0611 | 1.5765 | -28.6 | 2.715 | 1.03 | PACS-SM |
| 859 | 1342228951 | 2455824.39299 | 160.00 | 2.819 | 0.148 | 2.0611 | 1.5766 | -28.6 | 2.732 | 1.03 | PACS-SM |
| 684 | 1342217411 | 2455650.36816 | 160.00 | 1.597 | 0.092 | 2.2998 | 2.0525 | 26.0 | 1.751 | 0.91 | PACS-SM |
| 684 | 1342217412 | 2455650.37220 | 160.00 | 1.667 | 0.096 | 2.2998 | 2.0525 | 26.0 | 1.754 | 0.95 | PACS-SM |
| 684 | 1342217414 | 2455650.37884 | 160.00 | 1.718 | 0.097 | 2.2998 | 2.0524 | 26.0 | 1.758 | 0.98 | PACS-SM |
| 684 | 1342217415 | 2455650.38288 | 160.00 | 1.709 | 0.097 | 2.2998 | 2.0523 | 26.0 | 1.761 | 0.97 | PACS-SM |
| 400 | 1342198492 | 2455365.21376 | 160.00 | 0.708 | 0.041 | 2.7441 | 2.7846 | -21.4 | 0.680 | 1.04 | PACS-SM |
| 400 | 1342198493 | 2455365.21780 | 160.00 | 0.696 | 0.037 | 2.7441 | 2.7846 | -21.4 | 0.670 | 1.04 | PACS-SM |
| 400 | 1342198494 | 2455365.22184 | 160.00 | 0.688 | 0.043 | 2.7441 | 2.7847 | -21.4 | 0.661 | 1.04 | PACS-SM |
| 400 | 1342198495 | 2455365.22588 | 160.00 | 0.654 | 0.040 | 2.7441 | 2.7847 | -21.4 | 0.652 | 1.00 | PACS-SM |
| 221 | 1342188334 | 2455186.57887 | 160.00 | 0.781 | 0.048 | 2.8326 | 2.5069 | 20.3 | 0.756 | 1.03 | PACS-SM |
| 221 | 1342188335 | 2455186.58253 | 160.00 | 0.812 | 0.048 | 2.8326 | 2.5069 | 20.3 | 0.758 | 1.07 | PACS-SM |
| 221 | 1342188336 | 2455186.58620 | 160.00 | 0.869 | 0.048 | 2.8326 | 2.5068 | 20.3 | 0.763 | 1.14 | PACS-SM |
| 221 | 1342188337 | 2455186.58987 | 160.00 | 0.834 | 0.049 | 2.8326 | 2.5068 | 20.3 | 0.771 | 1.08 | PACS-SM |
| 221 | 1342188333 | 2455186.57648 | 70.00 | 3.180 | 0.166 | 2.8326 | 2.5070 | 20.3 | 3.008 | 1.06 | PACS-CN |
| 221 | 1342188333 | 2455186.57648 | 160.00 | 0.784 | 0.092 | 2.8326 | 2.5070 | 20.3 | 0.756 | 1.04 | PACS-CN |
| 221 | 1342188332 | 2455186.57388 | 100.00 | 1.831 | 0.098 | 2.8326 | 2.5070 | 20.3 | 1.754 | 1.04 | PACS-CN |
| 221 | 1342188332 | 2455186.57388 | 160.00 | 0.766 | 0.097 | 2.8326 | 2.5070 | 20.3 | 0.757 | 1.01 | PACS-CN |
| 684 | 1342217410 | 2455650.36578 | 70.00 | 7.101 | 0.364 | 2.2998 | 2.0525 | 26.0 | 7.321 | 0.97 | PACS-CN |

*continued on next page*

Table 19: *continued*

| OD | OBSID | mid-time [JD] | $\lambda$ [$\mu$m] | FD [Jy] | $\sigma$ [Jy] | r [AU] | $\Delta$ [AU] | $\alpha$ [°] | TPM [Jy] | FD/TPM | Instr./Mode |
|---|---|---|---|---|---|---|---|---|---|---|---|
| 684 | 1342217410 | 2455650.36578 | 160.00 | 1.661 | 0.120 | 2.2998 | 2.0525 | 26.0 | 1.748 | 0.95 | PACS-CN |
| 684 | 1342217413 | 2455650.37646 | 100.00 | 3.984 | 0.205 | 2.2998 | 2.0524 | 26.0 | 4.168 | 0.96 | PACS-CN |
| 684 | 1342217413 | 2455650.37646 | 160.00 | 1.781 | 0.118 | 2.2998 | 2.0524 | 26.0 | 1.757 | 1.01 | PACS-CN |
| 859 | 1342228949 | 2455824.38656 | 100.00 | 6.440 | 0.330 | 2.0611 | 1.5765 | -28.6 | 6.370 | 1.01 | PACS-CN |
| 859 | 1342228949 | 2455824.38656 | 160.00 | 2.735 | 0.171 | 2.0611 | 1.5765 | -28.6 | 2.706 | 1.01 | PACS-CN |
| 859 | 1342228946 | 2455824.37588 | 70.00 | 11.183 | 0.572 | 2.0611 | 1.5764 | -28.6 | 11.034 | 1.01 | PACS-CN |
| 859 | 1342228946 | 2455824.37588 | 160.00 | 2.695 | 0.164 | 2.0611 | 1.5764 | -28.6 | 2.673 | 1.01 | PACS-CN |
| 1198 | 1342250103 | 2456163.43704 | 100.00 | 2.489 | 0.129 | 2.3743 | 2.5915 | 23.2 | 2.523 | 0.99 | PACS-CN |
| 1198 | 1342250103 | 2456163.43704 | 160.00 | 1.118 | 0.092 | 2.3743 | 2.5915 | 23.2 | 1.064 | 1.05 | PACS-CN |
| 1198 | 1342250106 | 2456163.44772 | 70.00 | 4.345 | 0.225 | 2.3743 | 2.5914 | 23.2 | 4.471 | 0.97 | PACS-CN |
| 1198 | 1342250106 | 2456163.44772 | 160.00 | 1.057 | 0.091 | 2.3743 | 2.5914 | 23.2 | 1.067 | 0.99 | PACS-CN |
| 1399 | 1342267263 | 2456364.59433 | 70.00 | 4.447 | 0.229 | 2.6964 | 2.4294 | -21.8 | 4.479 | 0.99 | PACS-CN |
| 1399 | 1342267263 | 2456364.59433 | 160.00 | 1.025 | 0.093 | 2.6964 | 2.4294 | -21.8 | 1.104 | 0.93 | PACS-CN |
| 1399 | 1342267260 | 2456364.58365 | 100.00 | 2.523 | 0.131 | 2.6963 | 2.4292 | -21.8 | 2.568 | 0.98 | PACS-CN |
| 1399 | 1342267260 | 2456364.58365 | 160.00 | 0.999 | 0.112 | 2.6963 | 2.4292 | -21.8 | 1.100 | 0.91 | PACS-CN |
| 1434 | 1342270326 | 2456399.98378 | 250.00 | 0.305 | 0.017 | 2.7365 | 2.9446 | -20.2 | 0.305 | 1.00 | SPIRE-SM |
| 1434 | 1342270326 | 2456399.98378 | 350.00 | 0.157 | 0.009 | 2.7365 | 2.9446 | -20.2 | 0.159 | 0.99 | SPIRE-SM |
| 1434 | 1342270326 | 2456399.98378 | 500.00 | 0.074 | 0.007 | 2.7365 | 2.9446 | -20.2 | 0.080 | 0.93 | SPIRE-SM |
| 1411 | 1342268345 | 2456376.62531 | 250.00 | 0.424 | 0.023 | 2.7107 | 2.6090 | -21.7 | 0.417 | 1.02 | SPIRE-SM |
| 1411 | 1342268345 | 2456376.62531 | 350.00 | 0.247 | 0.014 | 2.7107 | 2.6090 | -21.7 | 0.217 | 1.14 | SPIRE-SM |
| 1411 | 1342268345 | 2456376.62531 | 500.00 | 0.180 | 0.010 | 2.7107 | 2.6090 | -21.7 | 0.109 | 1.65 | SPIRE-SM |
| 1402 | 1342267716 | 2456367.67595 | 250.00 | 0.442 | 0.024 | 2.7001 | 2.4755 | -21.8 | 0.449 | 0.99 | SPIRE-SM |
| 1402 | 1342267716 | 2456367.67595 | 350.00 | 0.222 | 0.013 | 2.7001 | 2.4755 | -21.8 | 0.234 | 0.95 | SPIRE-SM |
| 1402 | 1342267716 | 2456367.67595 | 500.00 | 0.108 | 0.008 | 2.7001 | 2.4755 | -21.8 | 0.118 | 0.92 | SPIRE-SM |
| 1388 | 1342265386 | 2456353.79785 | 250.00 | 0.520 | 0.028 | 2.6829 | 2.2690 | -21.2 | 0.545 | 0.95 | SPIRE-SM |
| 1388 | 1342265386 | 2456353.79785 | 350.00 | 0.257 | 0.015 | 2.6829 | 2.2690 | -21.2 | 0.284 | 0.90 | SPIRE-SM |
| 1388 | 1342265386 | 2456353.79785 | 500.00 | 0.103 | 0.013 | 2.6829 | 2.2690 | -21.2 | 0.143 | 0.72 | SPIRE-SM |
| 1215 | 1342250802 | 2456181.02598 | 250.00 | 0.520 | 0.028 | 2.4062 | 2.4086 | 24.3 | 0.536 | 0.97 | SPIRE-SM |
| 1215 | 1342250802 | 2456181.02598 | 350.00 | 0.261 | 0.015 | 2.4062 | 2.4086 | 24.3 | 0.278 | 0.94 | SPIRE-SM |
| 1215 | 1342250802 | 2456181.02598 | 500.00 | 0.124 | 0.010 | 2.4062 | 2.4086 | 24.3 | 0.140 | 0.89 | SPIRE-SM |
| 1196 | 1342250637 | 2456162.04058 | 250.00 | 0.452 | 0.025 | 2.3717 | 2.6052 | 23.0 | 0.445 | 1.02 | SPIRE-SM |
| 1196 | 1342250637 | 2456162.04058 | 350.00 | 0.232 | 0.013 | 2.3717 | 2.6052 | 23.0 | 0.231 | 1.01 | SPIRE-SM |
| 1196 | 1342250637 | 2456162.04058 | 500.00 | 0.110 | 0.008 | 2.3717 | 2.6052 | 23.0 | 0.116 | 0.95 | SPIRE-SM |
| 892 | 1342231344 | 2455858.04713 | 250.00 | 0.669 | 0.036 | 2.0438 | 1.9298 | -29.1 | 0.634 | 1.06 | SPIRE-SM |
| 892 | 1342231344 | 2455858.04713 | 350.00 | 0.342 | 0.019 | 2.0438 | 1.9298 | -29.1 | 0.330 | 1.04 | SPIRE-SM |
| 892 | 1342231344 | 2455858.04713 | 500.00 | 0.156 | 0.010 | 2.0438 | 1.9298 | -29.1 | 0.166 | 0.94 | SPIRE-SM |
| 861 | 1342229193 | 2455826.85575 | 250.00 | 1.168 | 0.063 | 2.0594 | 1.6018 | -28.8 | 1.143 | 1.02 | SPIRE-SM |
| 861 | 1342229193 | 2455826.85575 | 350.00 | 0.595 | 0.032 | 2.0594 | 1.6018 | -28.8 | 0.593 | 1.00 | SPIRE-SM |
| 861 | 1342229193 | 2455826.85575 | 500.00 | 0.289 | 0.016 | 2.0594 | 1.6018 | -28.8 | 0.298 | 0.97 | SPIRE-SM |
| 423 | 1342200204 | 2455388.83050 | 250.00 | 0.272 | 0.016 | 2.7189 | 3.0543 | -19.4 | 0.281 | 0.97 | SPIRE-SM |
| 423 | 1342200204 | 2455388.83050 | 350.00 | 0.144 | 0.010 | 2.7189 | 3.0543 | -19.4 | 0.146 | 0.99 | SPIRE-SM |
| 423 | 1342200204 | 2455388.83050 | 500.00 | 0.065 | 0.009 | 2.7189 | 3.0543 | -19.4 | 0.073 | 0.89 | SPIRE-SM |